Title
Alterations of Thalamostriatal and Corticostriatal Projections in Mouse Models of Huntington's Disease

Author
Parievsky, Anna

Publication Date
2015

Peer reviewed|Thesis/dissertation

UNIVERSITY OF CALIFORNIA

Los Angeles

Alterations of Thalamostriatal and Corticostriatal Projections in Mouse Models of Huntington's Disease

A dissertation submitted in partial satisfaction of the requirements for the degree Doctor of Philosophy in Neuroscience

by

Anna Parievsky

2015

ABSTRACT OF THE DISSERATION

Alterations of Thalamostriatal and Corticostriatal Projections in Mouse Models of Huntington's Disease

by

Anna Parievsky

Doctor of Philosophy in Neuroscience

University of California, Los Angeles, 2015

Professor Michael S. Levine, Chair

Huntington's disease (HD) is a fatal, autosomal dominant, genetic disorder characterized by cell death of medium-sized spiny neurons (MSNs) in the striatum. Striatal cell death has been traditionally attributed to excessive excitatory inputs, or more recently to disrupted balance of excitatory, inhibitory, and modulatory signaling. Therefore, understanding of altered synaptic signaling at striatal inputs is essential for the development and design of HD treatments. MSNs receive excitatory glutamatergic projections from the cortex and thalamus. HD induced functional changes in corticostriatal projections have been studied extensively in mouse models. However, although thalamic atrophy is correlated with cognitive impairments in HD patients and the centromedian-parafascicular (CMPf) nuclear complex (the primary origin of thalamostriatal projections) undergoes a 55% neuronal loss in HD patients, functional alterations of

thalamostriatal projections have not been electrophysiology investigated. An adeno-associated virus (AAV) expressing channelrhodopsin-2 (ChR2) under the calcium/calmodulin-dependent protein kinase type II alpha subunit (CaMKIIa) promoter was injected into the CMPf or the sensorimotor cortex of HD model mice to allow for selective activation of thalamostriatal or corticostriatal projections respectively. Pharmacological and holding potential manipulations were used to isolate AMPA and NMDA receptor-mediated currents. In the symptomatic R6/2 fragment mouse model, thalamostriatal synapses displayed increased decay times of both AMPA and NMDA receptor-mediated currents, alterations in glutamate reuptake, and increased probability of glutamate release. These findings suggest functional evidence consistent with early degeneration of thalamostriatal projections observed in the Q140 mouse model previously published. These effects were more prominent at synapses between thalamic inputs and direct pathway projecting MSNs rather than indirect pathway projecting MSNs. Corticostriatal synapses showed much more discrete changes than thalamostriatal. The differences in kinetics of AMPA and NMDA receptor-mediated currents were contrasting, changes in glutamate reuptake were smaller than those at thalamostriatal projections, and no change in the probability of glutamate release was detected. No significant changes were observed in presymptomatic or symptomatic YAC128 full length mouse models. Perhaps, a more severe and later disease state should be examined in this slowly progressing HD model.

The dissertation of Anna Parievsky is approved.

Dean Buonomano

Marie-Francoise Chesselet

Joseph B. Watson

Michael S. Levine, Committee Chair

University of California, Los Angeles

2015

This is for you, mom and dad. For your unconditional love, support, hard work, patience, and more patience. For being my biggest cheerleaders and always being on my side, even when I was wrong…although that probably never happened.

And for my grandparents, who for some reason think I'm the smartest, hardest working, most beautiful, flawless, and unspoiled (well…maybe a little spoiled) granddaughter in the world. I'm not…but shhh…

~ Dr. Nura

Table of Contents

List of Figures, Tables, Acronyms

Figures

Tables

Acronyms

- µl Microliter
- µm Micrometer
- µm Micrometer
- µM Micromollar
- AAV Adeno-associated virus

- Ach — Acetylcholine
- AMPA — α-amino-3-hydroxy-5-methyl-4-isoxazolepropionic acid
- ANOVA — Analysis of variance
- BAC — Bacterial artificial chromosomes
- BDNF — Brain derived neurotrophic factor
- BIC — Bicuculline
- CaMKIIa — calcium/calmodulin-dependent protein kinase type II alpha subunit
- cAMP — Cyclic adenosine monophosphate
- CB1 — Cannabinoid receptor type 1
- ChR2 — Channelrhodopsin-2
- C_m — Membrane capacitance
- CMPf — Centromedian-parafascicular complex
- DA — Dopamine
- DIC — Differential interference contrast
- DNA — Deoxyribonucleic acid
- DV — Dorsoventral
- EAAC — Excitatory amino acid carrier
- EAAT — Excitatory amino acid transporter
- EPSC — Excitatory postsynaptic current
- eYFP — Enhanced yellow fluorescent protein
- FSI — Fast spiking interneuron
- GABA — γ-aminobutyric acid
- GLAST — Glutamate aspartate transporter
- GLT1 — Glutamate transporter 1
- HD — Huntington’s disease
- Hdh — Mouse Huntington's disease gene homolog
- Htt — Huntingtin gene (mouse)
- *HTT* — Huntingtin gene (human)
- HTT — Huntingtin protein
- Hz — Hertz
- IPSC — Inhibitory postsynaptic current
- IR — Infrared
- IT — Intratelencephalic
- LCI — Large cholinergic interneuron
- LED — Light-emitting diode
- mHTT — Mutant huntingtin protein
- ML — Mediolateral
- mRNA — Messenger ribonucleic acid

- ms — Millisecond
- MSN — Medium-sized spiny neurons mV
- NBQX — 2,3-dihydroxy-6-nitro-7-sulfamoyl-benzo[f]quinoxaline-2,3-dione
- Nm — Nanometer
- NMDA — N-methyl-D-aspartate
- pA — Picoamp
- PBS — Phosphate buffered saline
- PCR — Polymerase chain reaction
- PFA — Paraformaldehyde
- PLTS — Persistent low-threshold spiking
- PPD — Paired-pulse depression
- PPF — Paired-pulse facilitation
- PPR — Paired-pulse ratio
- PT — Pyramidal tract
- PV — Parvalbumin
- R_m — Membrane resistance
- SE — Standard error
- sEPSC — Spontaneous excitatory postsynaptic current
- sIPSC — Spontaneous inhibitory postsynaptic current
- SOM — Somatostatin
- Tau — Time constant
- TBZ — Tetrabenazine
- TetO — Tetracycline resistance operon
- Trk — Tyrosine kinase
- TTX — Tetrodotoxin
- VGLUT — Vesicular glutamate trasnporter
- WT — Wild-type
- YAC — Yeast artificial chromosomes

Acknowledgments

It takes a village to raise a graduate student, this grad student took a few villages. And I want to thank them all.

To begin, I would like to thank Dr. Michael Levine for his direction, support, constructive (and sometimes harsh, because I needed a lot of that too) motivation, and tolerance and acceptance of who I am as a student, a scientists, a lab member, and a person. I'm extremely grateful to him for believing in me, even when I didn't think I'd ever have enough data, let alone a dissertation. I thank Carlos for making me the electrophysiologist I am today, teaching me the ropes, always encouraging me to get that "one more cell" at the end of the day, and proofreading every one of my abstracts and papers one too many times. I must thank ALL my lab mates because I really consider them my lab family, and if it wasn't for them, my lab life would really just have been sitting in a tiny dark closet alone for days at a time. Thank you all for keeping me awake at 9am meetings, making every SfN 4 days of Fireballs and awful inside jokes, and teaching me the ropes of surviving life as a grad student. Thank you Laurie for being my partner in crime, and Christmas chair races, Sandra for your direction, Josh for being my favorite solution buddy eva, and Jane for being the bestest office roomie in the world and letting me steal all your nail polish. Jan, I'm sorry for always requesting mice last minute and thank you for putting up with my endless colonies of YACs. And if it wasn't for Veró who showed me how to perform surgeries and set up my optogenetics experiments, I'd probably still be trying to figure out how to plug in the mercury lamp.

Everything I am today, I am because of my family. This PhD is as much mine as it is theirs. I owe a huge part of it to my Babulya who taught me how to read and write, how to keep my butt in a chair and study, brought me snacks every 15 minutes while I was doing homework

(or only every 20 if I wasn't hungry), and most importantly, for always being proud of me. Thank you to Dedulya for picking me up from school for what felt like 50 years and letting me be your granddaughter. And thank you to my dedushka Yasha and babushka Klara for supporting and encouraging me. My Munches, thank you for laughing at my awful science puns and sending me endless nubba pictures when I missed everyone and wanted to run away from school and go home. I'm grateful for my aunts and uncles, but a special shout out to my Tetya for always fighting for me, being in my corner, and inspiring me. And for my cousin Julia, for surviving grad school with me and timing it just right so we could graduate together. Coopa, thank you for never eating my homework and being excited for at most 3 minutes when I come home and then showing me your pretty "scary" zubi for 3 days. Mom and dad, you deserve a thank you on every page of this dissertation. Dad, thank you for loading and unloading my boxes and shoe rack to move to and from LA about a million times, teaching me not to give up on a goal (like only a real Raiders fan can), always having sirochki ready when I come home, and being proud of me. Mom, thank you for being my best friend, going through airport security with chicken, trusting me with my decisions, over 20 years of vstrochs, panicking when I don't respond after one phone call and one text, and making me feel assured that no matter how old I get, I will always have a home. Thank you both for giving me the world.

I would also like to thank my funding sources: the NIH, HDF, and CHDI, for continuous financial support and making the experiments realizable and possible. Chapter 2 contains work and figures from "Enhanced GABAergic Inputs Contribute to Functional Alterations of Cholinergic Interneurons in the R6/2 Mouse Model of Huntington's" published by eNeuro 0008-14.2015 in 2015 and coauthored by Holley SM, Joshi PR, myself, Huynh MN, Cepeda C, Levine MS, Galvan L, Chen JY, Fisher YE. Figures 2.17, 2.18, and Table 2.2 are from this work.

CURRICULUM VITAE

Anna Parievsky

EDUCATION

Bachelor of Science, Psychobiology: **12/2005**
University of California, Los Angeles; major GPA 4.0

RESEARCH EXPERIENCE

University of California, Los Angeles **9/2009 – Expected 9/2015**
Advisor: Dr. Michael S. Levine
• Thesis: Alterations of thalamostriatal and corticostriatal projections in mouse models of Huntington's disease.

- Designed, managed, and conducted all experiments from beginning to end.
- Organized, analyzed, synthesized, and presented large quantities of data.
- Conducted whole cell patch clamp recordings in slice and analysis of electrophysiology data.
- Performed stereotaxic surgery for viral delivery of optogenetic constructs, use of channel rhodopsin to control neuronal activity in slice.

Stanford Memory Lab, Stanford University **5/2008 - 8/2009**
Research Assistant
Advisor: Dr. Anthony Wanger
• Worked as part of a research team on the construction, implementation, and data analysis of a memory experiment using functional imaging (fMRI) to determine how specific medial temporal lobe sub-regions respond to previously encountered vs. novel stimuli, based on subject's mnemonic goal during incidental encoding.
• Operated 1.5T and 3T scanners, carried out fMRI data preprocessing using SPM, preformed behavioral data analysis, generated/administered experiments using MATLAB and Psychtoobox.

Roche Palo Alto LLC, Palo Alto, CA **4/2006 - 10/2008**
Research Associate
• Conducted complete *in vivo* microdialysis studies including:

- Cannula brain implantation surgery in rats followed by and probe placement verification.
- High Pressure Liquid Chromotography (HPLC) for analysis of catecholamines and amino acids.

• Proficient in various animal dosing techniques (i.p., p.o., and i.v.), cardiac punctures, brain extraction.

University of California, Los Angeles **3/2004 - 6/2005**
Laboratory Assistant
Advisor: Dr. Michael Fanselow
• Assisted on a fear conditioning study in mice using Skinner Boxes.
• Performed an operant conditioning study in mice using the Radial Arm Maze.

HONORS/AWARDS

BRI/Semel Institute Neuroscience Graduate Travel Award **5/2013, 5/2014**
ARCS Foundation Scholar **9/2011 - 6/2015**
Cota Robles Fellowship **9/2009 - 6/2012**

SELECT PUBLICATIONS

- A. Parievsky, C. Cepeda, M. S. Levine. Alterations of Synaptic Function in Huntington's Disease. Handbook of Basal Ganglia Structure and Function, 2nd edition, submitted 4/2015.
- S. M. Holley, P. Joshi, A. Parievsky, L. Galvan, J. Chen, Y. Fisher, M. Huynh, C. Cepeda, M. S. Levine. Enhanced GABAergic inputs contribute to functional alterations of cholinergic interneurons in the R6/2 mouse model of Huntington's disease. eNeuro 0008-14.2015.
- A. Parievsky, S. M. Holley, P. Joshi, J. Y. Chen, C. Cepeda, M. S. Levine. Electrophysiological alterations of striatal cholinergic interneurons in the R6/2 mouse model of Huntington's disease. Poster session presented at the Society for Neuroscience Conference, Washington DC. November 2014.
- A. Parievsky, D. Litvak, C. Cepeda, M. S. Levine. Thalamostriatal and corticostriatal synapses exhibit differential alterations in the R6/2 mouse model of Huntigton's disease. Poster session presented at the Society for Neuroscience Conference, San Diego, CA. November 2013.
- A. Parievsky, C. Cepeda, M. S. Levine. September 2012. Abnormal brain metabolism as a biomarker for evaluating therapeutic approaches in Huntington's disease. Future Neurology 7(5), 527-530.

TALKS

- "Thalamostriatal and corticostriatal synapses exhibit differential alterations in the R6/2 mouse model of Huntington's disease," CAG Triple Repeat Disorders Gordon Research Conference, Waterville Valley, NH. June 2013.
- "Assessing alterations of thalamostriatal projections in the R6/2 mouse model of Huntington's disease using optogenetics," HD2012 Conference, Cambridge, MA. August 2012.

LEADERSHIP/SERVICE

- Assisted in organizing events for the Los Angeles chapter of Pint of Science; 2015.
- Volunteered as a counselor for the Neuroguide program designed to help undergraduate students interested in neuroscience plan for graduate school; 2014-2015 school year.
- Participated in the Blondes vs. Brunettes annual flag football game to help raise money and awareness for the Alzheimer's Foundation; 2014.
- Served as the TA for Neuroscience 101A course "From Molecules to Mind - Cellular and Systems Neuroscience"; Fall 2013.
- Served as a member on the Neuroscience Program Retreat Committee to help organize the yearly retreat; 2010.

Chapter 1

Huntington's Disease

1.1 Huntington's disease

Huntington's disease (HD) is a progressive, genetic, neurodegenerative, and fatal disorder. HD is estimated to occur in 5 to 10 people per 100,000. Familial cases of HD are documented worldwide but it's most prevalent in Europe and North America (Borrell-Pagès et al., 2006). Most commonly, symptoms begin to appear during middle age (around 45 years old). However juvenile cases (age of onset <20 years old) account for 5-10% of all cases. Late onset cases (>50 years of old) account for 20% of all cases (Brinkman et al., 1997). Patients suffer from motor symptoms such as chorea (involuntary dance-like movements) in early stages of the disease, akinesia (slowing or loss of voluntary movements) in later stages of the disease, dystonia, difficulty with production of speech or swallowing (Bird, 1980; Harper, 1996; Bonelli and Hofmann, 2007). Patients also experience cognitive disturbances which can precede a clinical diagnosis of motor onset by up to 15 years (Bates et al., 2015) and may include learning impairments and difficulty focusing, as well as psychiatric changes which may include depression, fatigue, and insomnia (Bird, 1980; Harper, 1996; Bonelli and Hofmann, 2007). Disease progression occurs over 15-20 years and results in death (Walker, 2007). Children with HD often develop bradykinesia (slowed movement), rigidity, dystonia, learning disabilities, and epileptic seizures (Rasmussen et al., 2000; Seneca et al., 2004). Interestingly, choreic movements are often absent in children who develop juvenile HD but are more common in children who have an age of onset of 15 years or older (Byers and Dodge, 1967).

There is currently no cure for HD and no treatment to stop, hinder, or prevent its onset. The only medications available to HD patients solely manage symptoms (Novak and Tabrizi, 2010). Tetrabenazine (TBZ) is the only FDA drug approved specifically for HD and is

administered to reduce chorea. However, like most drugs prescribed for HD, it only treats one of a large array of symptoms associated with the disease and has many unfavorable side effects (Ross and Tabrizi, 2011). The development of novel therapies which target HD symptoms more specifically, and therefore produce fewer adverse side effects, is imperative. Therefore, a more thorough understanding of HD pathology and more specific targets is needed.

HD is inherited in an autosomal dominant manner and is caused by an unstable expansion of a CAG repeat within exon 1 of the Huntington gene (*HTT*, initially termed IT15) which results in an elongated polyglutamine stretch (CAG >40) near the N terminal of the huntingtin (HTT) protein (The Huntington's Disease Collaborative Research Group, 1993). Severity of symptoms is said to be directly correlated, while age of onset is inversely correlated, with number of CAG repeats (Brinkman et al., 1997; Harper and Jones, 2002). Individuals with 35 repeats or less are considered not to have the mutation or not to be at risk for HD, those with 36-39 carry the incomplete/reduced penetrance allele and may experience symptoms later in adult life (70% will be symptomatic at 75 years or older), while those with 40 or more repeats carry the full penetrant allele and will develop HD within their lifetime (Andrew et al., 1993; Walker, 2007). Juvenile onset HD can present when longer (CAG>50) polyglutamine stretches are present.

The number of CAG repeats in the *HTT* gene is determined by the number of repeats in the gene inherited from the parents. If the number of repeats in the parents' gene is in the normal range (<36), the number of repeats inherited remains stable. However, disease alleles are altered in length (they may increase or decrease) for 70–80% of intergenerational transmissions (MacDonald et al., 1993; Zühlke et al., 1993; Telenius et al., 1994). Interestingly, the change in repeat length is dependent on the sex of the transmitting parent. Repeat length expansions are

most often associated with paternal transmission (MacDonald et al., 1993; Zühlke et al., 1993; Leeflang et al., 1995; Nørremølle et al., 1995; Telenius et al., 1995; Wheeler et al., 2007). Repeat lengths are shown to expand for male children and contract for female children with maternal transmission (Wheeler et al., 2007).

HTT is a large cytoplasmic protein of ~350 kDa. The increased number of CAG repeats results in an abnormally long polyglutamine region in the HTT protein. This polyglutamine expansion results in an extra-long protein which causes mutant (m)HTT to misfold and form amyloid-like intracellular aggregates (Scherzinger et al., 1999). Immunostaining of HD mouse model brains for glutamine expansions reveals dense, circular, intraneuronal inclusions in the striatum, cerebral cortex, cerebellum, and spinal cord (Davies et al., 1997). Similarly, immunostaining also shows inclusion bodies in the cortex and striatum of HD patient brains (DiFiglia et al., 1997; Becher et al., 1998). Notably, the number of CAG repeats of *HTT* or similarly, the length of the glutamine stretch of HTT, is positively correlated with the extent of HTT accumulation (DiFiglia et al., 1997; Becher et al., 1998). Immunostaining with antibodies for ubiquitin detect increased amounts of this pro-degradation protein in HD patient brains, consistent with the hypothesis that mHTT is targeted for proteolysis but is resistant to removal (DiFiglia et al., 1997; Becher et al., 1998). Nuclear inclusions are found in neurons before any overt behavioral symptoms are observed (Ordway et al., 1997; Davies et al., 1997), however, whether these inclusions are toxic, incidental, or part of a beneficial coping mechanism, remains controversial.

The role of HTT is still unclear but it is critical for development as knockout of *Htt* is lethal in mice (Nasir et al., 1995). HTT upregulates the expression of brain derived neurotrophic factor (BDNF) (Zuccato et al., 2001), and has numerous binding proteins which help predict its

function in the brain and body. Among its partners are proteins with roles in transcriptional regulation, intracellular trafficking, cytoskeletal organization, endocytosis, and exocytosis (Velier et al., 1998; Waelter et al., 2001; Li et al., 2003a). Immunohistochemical, electron microscopy, and subcellular fractionation studies agree that HTT is a cytoplasmic protein primarily associated with vesicles and microtubules (DiFiglia et al., 1995; Hoffner et al., 2002) and has a distribution very similar to that of synaptophysin (Wood et al., 1996). Similarly, the ubiquitous cytoplasmic distribution of HTT in neurons and its association with vesicles reinforce the idea that HTT may have a role in vesicle trafficking, exocytosis, and endocytosis (DiFiglia et al., 1995; Caviston and Holzbaur, 2009). Thus, it is probable that the mutation in *HTT* may be responsible for abnormal synaptic transmission (Smith et al., 2005).

1.2 Striatal circuit

The most apparent neuropathology in HD is neurodegeneration in the cortical and basal ganglia circuit (Vonsattel et al., 1985), although other regions undergo neurodegeneration as well. For example, the thalamus shows severe degeneration as described later in this chapter (Heinsen et al., 1996; Kassubek et al., 2004a, 2004b). In addition, levels of neuropeptides derived from the hypothalamic-pituitary axis, as well as hypothalamically-mediated behaviors including sleep, circadian rhythms, and metabolism, also are altered in HD (Kirkwood et al., 2001; Morton et al., 2005; Goodman et al., 2008).

The striatum is responsible for planning, executing, and modulating movement. Hence neurodegeneration of the striatum is consistent with the extensive presence of motor symptoms observed in HD patients. To understand deficits in synaptic transmission caused by mHTT, the striatal circuit should first be understood. The striatum is part of the complex cortico-basal ganglia-thalamo-cortical loop. It receives two major types of afferents, excitatory glutamatergic

projections from the cortex and thalamus, and modulatory dopamine (DA) projections from the substantia nigra pars compacta. It has two inhibitory γ-aminobutyric acid (GABA) output pathways which converge onto the ventral anterior and ventral lateral nuclei of the thalamus, either *via* the substantia nigra pars reticulata and internal segment of the globus pallidus (Albin et al., 1989; Gerfen et al., 1990) or *via* the external segment of the globus pallidus, subthalamic nucleus, and substantia nigra pars reticulata (Albin et al., 1989; Kawaguchi et al., 1990). The thalamic nuclei then project back onto discrete cortical regions, segregated onto areas with distinct cognitive, motor and psychiatric functions, completing the cortical-basal ganglia-thalamo-cortical loop (Alexander et al., 1986; Smith et al., 2004).

In the striatum, medium-sized spiny neurons (MSNs) are the main neurons affected. These cells make up 90-95% of the striatal neuronal population, utilize GABA as their principal neurotransmitter, and receive abundant inputs from both outside and within the striatum (Kita and Kitai, 1988). MSNs are segregated into two subpopulations based on their projections (Penney and Young, 1983; Alexander and Crutcher, 1990), as well as DA receptor and neuropeptide expression (Gerfen, 1992; Bolam et al., 2000). MSNs expressing the D1 DA receptor (Gerfen et al., 1990), substance P (Haber and Nauta, 1983), and dynorphin (Vincent et al., 1982) project to the substantia nigra pars reticulata and internal segment of the globus pallidus (Albin et al., 1989; Gerfen et al., 1990) *via* the direct pathway. Those expressing the D2 DA receptor (Gerfen et al., 1990) and met-enkephalin (Haber and Nauta, 1983; Steiner and Gerfen, 1999) project to the external segment of the globus pallidus (Albin et al., 1989; Kawaguchi et al., 1990) *via* the indirect pathway. The direct pathway is often termed the "Go" pathway while the indirect pathway is called the "No-Go" pathway, suggesting proper gating and balance of activity in these two pathways is necessary to initiate a desired action and inhibit an

undesired action (Albin et al., 1989; Alexander and Crutcher, 1990; Mink, 1996). Therefore, HD-induced alterations which affect the two pathways differently will offset this intrinsic equilibrium and result in either undesired movement (chorea) or inability to move (akinesia) (Galvan et al., 2012). It is believed that indirect pathway MSNs projecting to the external globus pallidus are more susceptible to degeneration than direct pathway MSNs projecting to the internal segment of the globus pallidus (Reiner et al., 1988; Albin et al., 1992; Deng et al., 2004).

In addition to the MSNs, the striatum contains several types of interneurons. Inhibitory interneurons represent less than 5% of the striatal cell population but are critical in controlling MSN output. GABAergic interneurons consist of several subtypes. These include the parvalbumin- (PV) expressing fast-spiking (FS) interneurons, somatostatin- (SOM), neuropeptide Y-, and nitric oxide synthase-expressing persistent low-threshold spiking (PLTS) interneurons and calretinin-expressing interneurons (Kreitzer, 2009; Tepper et al., 2010). Large cholinergic interneurons (LCIs) account for the remainder of striatal neurons. LCIs represent 1-2% of striatal neurons and have been implicated in motor control, as well as associated with plasticity and reward-dependent learning (Exley and Cragg, 2008; Shuen et al., 2008).

Glial cells also represent a major part of the striatal cellular population. The human striatum contains 3.35 glia cells for every one neuron (Heinsen et al., 1994). A much higher glia to neuron ratio has been described in rats (Gomide et al., 2005). Astrocytes perform many essential functions in the striatum including glutamine synthesis (a glutamate precursor) (Schousboe et al., 2011), glutamate release (Bezzi et al., 2004; Hamilton and Attwell, 2010), glycogen storage (an energy precursor that supports high levels of neuronal activity) (Fernandez-Fernandez et al., 2012), supply of the precursor for gluthathione (an antioxidant) (Fernandez-Fernandez et al., 2012), and glutamate reuptake (Hertz, 1979). Besides glutamate release and

glutamate reuptake, astrocytes have also been shown to express glutamate receptors (Palygin et al., 2010).

A. Corticostriatal projections

Cortical projections into the striatum arise from the entire neocortex, including major projections from the primary motor and somatosensory cortices (Flaherty and Graybiel, 1994). Activation of corticostriatal inputs brings the MSNs from a hyperpolarized (down) to a depolarized (up) state inducing action potentials (Wilson, 1993). Corticostriatal projections have been further subdivided into two classes which are believed to synapse differentially onto direct and indirect pathway MSNs (Reiner et al., 2003). Intratelencephalic (IT) pyramidal neurons project bilaterally to the striatum but preferentially onto direct pathway MSNs. Collaterals of pyramidal tract (PT) neurons project ipsilaterally but preferentially onto indirect pathway MSNs. Furthermore, axon terminals making asymmetric axospinous synapses with direct pathway MSNs are significantly smaller than those making connections with indirect pathway MSNs (Lei et al., 2004). Such a difference in synapse morphology suggests that indirect pathway MSNs may be subject to increased glutamate release from corticostriatal projections (Reiner et al., 2003). However, more recent findings using electrophysiological recordings and antidromic activation of cortical neurons in rats (Ballion et al., 2008) or optogenetic activation of IT and PT axons in mice (Kress et al., 2013), failed to provide evidence to support the hypothesis that these different types of cortical projections innervate specific subpopulations of striatal MSNs. Additional electron microscopy studies have aimed to clarify this discrepancy (Deng et al., 2015). These studies suggest that direct pathway projecting MSNs receive twice as many axospinous projections from IT neurons than they do from PT neurons. Indirect pathway projecting MSNs receive 1.5 times as many axospinous terminals from PT as IT neurons. Conversely, axodendritic

inputs from PT neurons synapse preferentially onto direct MSNs while axodendritic inputs from IT neurons are very slight to both types of MSNs (Deng et al., 2015).

B. Thalamostriatal projections

The majority of thalamostriatal projections originate in the intralaminar thalamic nuclei, although substantial inputs from midline and specific relay nuclei have been described in rats, cats, and monkeys (Macchi et al., 1984; Smith et al., 2004). The principle source of thalamic projections to the dorsolateral striatum in rodents is the centromedian-parafascicular (CMPf) complex (Berendse and Groenewegen, 1990; Smith et al., 2004). *In vivo* single unit recordings in monkeys suggest the CMPf participates in the processes of attention and arousal elicited by salient sensory events (Matsumoto et al., 2001; Minamimoto and Kimura, 2002; Kimura et al., 2004). Based on slice whole-cell recordings in mice, thalamostriatal synapses display a high probability of release to an initial stimulus which rapidly declines with successive stimulation, which is fitting for the role of transmitting precisely timed sporadic signals (Ding et al., 2008). A positron emission tomographic study in humans supports these results as the CMPf complex shows activation when participants switch from a relaxed to an attention requiring reaction-time task (Kinomura et al., 1996).

Anatomical studies show that thalamostriatal projections constitute 40% of glutamatergic synapses onto striatal MSNs while corticostriatal make up the other 60% (Smith et al., 2004). However, unlike corticostriatal projections which synapse predominantly on dendritic spines (Smith and Bolam, 1990), thalamostriatal projections have been shown to preferentially terminate on dendritic shafts in rats and monkeys (Smith and Bolam, 1990; Sadikot et al., 1992; Smith et al., 1994; Sidibé and Smith, 1996). In rats, more positive reversal potentials and slow decay kinetics of N-methyl-D-aspartate (NMDA) receptor mediated currents at thalamostriatal

than corticostriatal projections is consistent with thalamic input synapses being located more distally on the dendritic arbor (Smeal et al., 2008). Excitatory thalamic terminals use the vesicular glutamate transporter (VGLUT) 2 for packaging glutamate in synaptic vesicles, while excitatory cortical terminals use VGLUT1 (Fremeau et al., 2001, 2004; Herzog et al., 2001; Fujiyama et al., 2004; Lei et al., 2013). Mouse studies immunolabeling for VGLUT2 and VGLUT1 find that thalamostriatal axospinous terminals account for 35% of all terminals, thalamostriatal axodendritic for 9%, corticostriatal axospinous for 52%, and corticostriatal axodendritic for 4% (Deng et al., 2013).

Both the CM and Pf make direct synaptic connections with MSNs (Xu et al., 1991; Sadikot et al., 1992; Lacey et al., 2007). In primates, CM projections predominately synapse onto the direct pathways projecting MSNs while Pf projections are biased toward the indirect pathways projecting MSNs (Sidibé and Smith, 1996). In primates and rats, striatal GABAergic interneurons are preferentially innervated by the cortex and CM, while receiving very light innervation from the Pf (Zemanick et al., 1991; Berretta et al., 1997). Cholinergic striatal interneurons receive strong innervation from the entire CMPf complex, but very few inputs from cortical projections (Meredith et al., 1990; Lapper and Bolam, 1992; Thomas et al., 2000). Also, in contrast to corticostriatal projections which closely converge with, and are modulated by, DA afferents, thalamic and DA terminals do not synapse in close proximity to each other, in the primate brain (Smith et al., 1994). Striatal and thalamic activity is correlated *in vivo* (Matsumoto et al., 2001; Minamimoto and Kimura, 2002), however the effect of thalamic inputs on MSN activity is poorly understood.

Like cortical synapses onto MSNs, thalamic synapses also contain α-amino-3-hydroxy-5-methyl-4-isoxazolepropionic acid (AMPA), NMDA, and kainate receptors (Bernard et al., 1997;

Kieval et al., 2001; Smith et al., 2004). However, the contribution of glutamatergic receptors at thalamostriatal versus corticostriatal synapses has been disputed (Ding et al., 2008; Smeal et al., 2008). Whole-cell slice recordings from mouse brains suggest that NMDA receptors mediate larger currents than AMPA receptors at corticostriatal projections, while NMDA receptor-mediated currents are smaller than AMPA receptor-mediated currents at thalamostriatal projections. In other words, NMDA/AMPA ratios are greater for corticostriatal than thalamostriatal projections (Ding et al., 2008). On the other hand, whole-cell slice recordings from rat brains suggest the opposite. In these experiments, the NMDA/AMPA ratio was greater for responses evoked from thalamostriatal projections than for those evoked from the corticostriatal projections (Smeal et al., 2008).

1.3 Human HD

A. Neuropathology

Postmortem assessment of brains of HD patients indicates a 30% reduction in total brain volume (De La Monte et al., 1988). Most prominently, there is a marked decrease in striatal volume and enlargement of the lateral ventricles. The cortex and thalamus also are affected. The cross-sectional areas of gray and white matter are reduced in the frontal, temporal, insular, and parietal cortical areas (Mann and South, 1993; Halliday et al., 1998). A 30% reduction in the number of cortical pyramidal neurons in cortical layers III, V, and VI occurs (Cudkowicz and Kowall, 1990; Hedreen et al., 1991; Sotrel et al., 1991; Heinsen et al., 1994). The CMPf nuclear complex of the thalamus undergoes a 55% neuronal loss, as well as a significant glial cell loss (Heinsen et al., 1996). Interestingly, thalamic atrophy measured by 3D magnetic resonance imaging is correlated with cognitive impairments in HD patients (Kassubek et al., 2004a, 2004b).

B. Glutamate neurotransmission

Since the cortex and CMPf complex provide the bulk of glutamatergic excitatory input into the striatum, neurotransmission mediated by these inputs is affected. Postmortem striatal tissue from HD patients exhibits reduced binding of glutamate to NMDA receptors, suggesting loss of this type of receptor (Young et al., 1988; Albin et al., 1990). Membrane preparations from postmortem brains exhibit reduced mRNA levels of the glutamate transporter 1 (GLT-1), which may result in glutamate spillover and aberrant receptor activation (Arzberger et al., 1997). Postmortem measurements also reveal decreased glutamate content in cerebrospinal fluid and frontal cortex of HD patients (Wong, 1985).

C. GABA neurotransmission

Studies examining inhibitory neurotransmission in HD patients have resulted in conflicting findings. Older publications report reductions in GABA, as well as glutamic acid decarboxylase (GAD), the enzyme responsible for the synthesis of GABA from glutamate (Perry et al., 1973; Bird and Iversen, 1974; Manyam et al., 1978; Spokes et al., 1980). Similarly, in the cerebral cortex there is evidence that GABA is decreased (Pearson and Reynolds, 1994). In contrast, other findings provide evidence suggesting HD patients do not undergo alterations in GABAergic indices (Perry et al., 1982). From an anatomical perspective, early studies of the cortex indicated the GABA releasing PV, calretinin-, and calbindin- expressing interneurons were normally distributed without evident morphological changes (Macdonald and Halliday, 2002), although more recent observations provide evidence for significant alterations in GABAergic interneurons in striatum and cortex. In striatum, a decrease in PV expressing interneurons occurs with advancing disease grade (Reiner et al., 2013). In cingulate cortex, all three major classes of GABA interneurons are reduced in HD with a dominant mood phenotype, whereas in motor cortex the loss is specific to calbindin-expressing interneurons in HD dominated by motor symptoms (Kim et al., 2014). Alterations in GABA receptors are seen in the

striatum, cerebral cortex, and cerebellum (Lloyd et al., 1977; Lloyd and Davidson, 1979; Reisine et al., 1980; Walker et al., 1984). In addition, positron emission tomography findings suggest up regulation of $GABA_A$ receptors (Kunig et al., 2000).

D. Dopamine neurotransmission

Biphasic progression of movement symptoms in HD patients has been attributed to parallel biphasic changes in DA neurotransmission. Increased DA release early in the progression of the disease induces chorea (Garrett and Soares-da-Silva, 1992). Decreasing DA concentration with TBZ alleviates chorea symptoms in HD patients (Huntington Study Group, 2006). TBZ acts by blocking vesicular uptake of DA and ultimately depletes DA stores (Pettibone et al., 1984). TBZ is the only drug approved by the FDA for the treatment of chorea. Conversely, a reduction in DA during the later stages of HD leads to akinesia (Bird, 1980; Spokes, 1980). Consistently, late-stage HD patients show decreased levels of DA and homovanillic acid (a major DA metabolite) in the caudate nucleus (Bernheimer et al., 1973; Kish et al., 1987). Both D1 and D2 DA receptors, and DA reuptake sites, are reduced in symptomatic HD patients (Sedvall et al., 1994; Antonini et al., 1996; Ginovart et al., 1997). Interestingly, D1 and D2 DA receptors are reduced in presymptomatic HD patients (Antonini et al., 1996; Weeks et al., 1996).

1.4 HD animals models

Animal models have been instrumental in our understanding of the mechanisms leading to neuropathology of HD. The first HD models, prior to discovery of the *HTT* gene, relied on neurotoxin-induced striatal lesions (McGeer and McGeer, 1976; Schwarcz et al., 1984; Beal et al., 1986). Glutamate receptor agonists, such as ibotenic and kainic acid were injected into the striatum to cause MSN death and mimic the neuropathology of HD. In later models, quinolinic acid, which is more selective for NMDA receptors, was used as it relatively spared striatal

interneurons which were believed to be unaffected in HD (Coyle and Schwarcz, 1976; McGeer and McGeer, 1976; Beal et al., 1986, 1991; Ferrante et al., 1993). The brains of animals after the excitotoxic lesions closely resembled the neuropathological and neurochemical alterations observed in HD (Coyle, 1979; Schwarcz et al., 1984; Beal et al., 1986; Choi, 1988; DiFiglia, 1990; Bordelon and Chesselet, 1999). Therefore, theories have proposed that in HD, MSNs are hypersensitive to glutamate released from cortical and thalamic inputs, due to changes in their postsynaptic receptors. However, these models were limited because they did not replicate the slow progression of HD or dysfunction and degeneration in extrastriatal areas, especially the cortex.

Subsequent to the discovery and sequencing of the gene mutation, genetic animal models of HD were developed. As with all animal models of human disease, none replicate the human condition completely. Over the years, a variety of HD models have been developed including drosophila melanogaster (Jackson et al., 1998), C. elegans (Faber et al., 2002), sheep (Jacobsen et al., 2010; Morton and Avanzo, 2011), pig (Yang et al., 2010), nonhuman primate (Yang et al., 2008), rat (Von Horsten et al., 2003), and mouse models. This chapter focuses on, and therefore presents a summary of, some of the most commonly used HD mouse models. Each model has unique advantages and has contributed to our current understanding of the pathophysiology of the disease (Levine et al., 2004; Pouladi et al., 2013). There are several types of genetic rodent models, differing in the way the gene mutation is expressed. These include transgenic models, knock-in models, conditional models and viral models. There are two types of transgenic models, those expressing fragments of the human HD gene and those expressing the full-length gene. Generally, knock-in models more faithfully represent the mutation carried by HD patients as they do not express an additional exogenous copy of the gene, but instead an expanded polyglutamine

tract is placed within the appropriate context of the rodent HD gene. In conditional models, the mutation is tissue-specific, expressed only in select brain regions or by specific neuronal populations, and sometimes can be temporally controlled. Viral models are generated by injecting viral vectors into specific brain regions to produce overexpression of mHTT.

A. Fragment models

The first fragment models generated were the R6/2 and R6/1 lines of transgenic mice (Mangiarini et al., 1996). R6/2 mice express exon 1 of the gene with ~150 CAG repeats and present with a very aggressively and rapidly progressing phenotype. These mice begin to show behavioral abnormalities at 5-7 weeks and die at approximately 15 weeks of age. They exhibit numerous neuropathological changes including neuronal intranuclear inclusions (Davies et al., 1997) and alterations in receptors and signaling mechanisms (Bibb et al., 2000; Luthi-Carter et al., 2000; Menalled et al., 2000). These mice also develop late onset neurodegeneration within a number of areas (Turmaine et al., 2000). Death of neurons has been attributed to the presence of neuronal intranuclear inclusions, condensation of both the cytoplasm and nucleus, and ruffling of the plasma membrane (Turmaine et al., 2000). The rapid progression of the disease in R6/2 mice makes them a valuable model for studies using electrophysiology, as well as for drug screening, primarily because experiments can be completed more quickly (Gil and Rego, 2008). Due to the early onset of phenotypic changes, as well as the occurrence of seizures, (Mangiarini et al., 1996; Cummings et al., 2009), these mice have been considered a model of juvenile onset HD (Gambardella et al., 2001; Seneca et al., 2004; Wojaczyńska-Stanek et al., 2006). However, if strain and length of CAG repeats are controlled, phenotypes of fragment and knock-in models develop similarly, which provides validity for the R6/2 as a model of adult onset HD (Woodman et al., 2007). R6/1 mice express exon 1 of *HTT* but with ~110 CAG repeats and display

alterations similar to those of R6/2 mice but with a longer time course. Because the progression is slower in the R6/1, some of the alterations can be separated temporally. For example, R6/1 mice display abnormal hippocampal synaptic plasticity, which occurs prior to the formation of nuclear aggregates (Milnerwood et al., 2006). This suggests HTT aggregates may not be necessary for the development of synaptic alterations.

Phenotype severity in the R6/2 mouse model of HD fluctuates with CAG repeat-length (Cummings et al., 2012). More specifically, electrophysiological properties of MSNs, motor activity, inclusion formation, and protein expression show an inverted "U-shaped" relationship between CAG repeat length and phenotype. Mice with 160 CAG repeats show a more severe phenotype than those with 110 repeats, whereas mice with 310 CAG repeats show a greatly ameliorated phenotype compared to mice with 210 repeats (Cummings et al., 2012). Similarly, mice with 450 CAG repeats showed delayed onset of the behavioral phenotype, prolonged survival, and delayed appearance of neuronal intranuclear inclusions than mice with 170 repeats (Morton et al., 2009). Spontaneous elongation to ≥335 repeats, increased the lifespan of mice up to >20 weeks, compared to ~12 weeks in mice with 150 repeats, as well as reduced the amount of intranuclear aggregates, diminished mutant protein production, and slowed symptom development (Dragatsis et al., 2009).

B. Full length models

Yeast artificial chromosomes (YAC) are used to express the full length human *HTT* gene in mice with various numbers of CAG repeats (18, 46, 72 and 128) (Hodgson et al., 1999; Slow et al., 2003). YAC18 mice are typically used as controls as they do not appear to develop a phenotype. Disease phenotypes develop slower in these models than in the fragment models like the R6/1 and R6/2. YAC128 mice display the most severe alterations when compared to YAC46

and 72 models. Typically the behavioral phenotype begins at about 2-3 months of age and progresses over a year. Neuropathological changes at 2 months include EM48-reactive mHTT in the nucleus (Van Raamsdonk et al., 2005). These mice display ~10% striatal atrophy and neuronal loss in the striatum and cortex, and sparing of the cerebellum and hippocampus at 12 months (Van Raamsdonk et al., 2005). Neurodegeneration can be present in the absence of aggregates in YAC mice, indicating that aggregates may not be essential to initiate neuronal death (Hodgson et al., 1999).

Bacterial artificial chromosomes (BAC) also are used to express the full length human HD gene. BACHD mice express 97 CAG repeats and exhibit progressive motor deficits beginning at approximately 2 months of age, neuronal synaptic dysfunction, and late-onset selective neuropathology (Gray et al., 2008). Neuronal dysfunction is evident by 6 months and precedes neurodegeneration. By 12 months, large nuclear inclusions are present in the cortex and small aggregates in the striatum. Interestingly, in BACHD mice, selective pathogeneses can occur without diffuse nuclear accumulation of mHTT. Instead, a relatively steady-state level of mHTT and a small amount of N-terminal fragments are sufficient to elicit the degeneration (Gray et al., 2008).

C. Knock-in models

Several knock-in models have been generated, mainly differing in the number of polyglutamine repeats expressed. Knock-in models include the Hdh^{neoq50} and Hdh^{Q50} (White et al., 1997), CAG71 and CAG94 (Levine et al., 1999), Hdh4/Q80 and Hdh6/Q72 (Shelbourne et al., 1999), Hdh^{Q92} and Hdh^{Q111} (Wheeler et al., 2000), $Hdh^{(CAG)80}$ and $Hdh^{(CAG)150}$ (Lin et al., 2001), CAG140 (Menalled et al., 2003), and Q175 (Menalled et al., 2012) mice. In general the progression of the phenotype positively correlates with the number of CAG repeats. Models with

shorter repeat lengths display more subtle alterations that tend to occur in older mice. Behavioral changes often occur before any neuropathology, and there is good evidence that cellular dysfunction is responsible for the initial symptoms (Hickey and Chesselet, 2003). Knock-in models also exhibit a gene-dose effect where homozygous animals express more severe phenotypes, and generally earlier than heterozygous animals. Some of the models present behavioral abnormalities as early as 1-2 months of age (Menalled and Chesselet, 2002; Menalled et al., 2003). Behavioral symptoms are biphasic and can mirror the progression of motor symptoms in HD (Harper, 1996; Kirkwood et al., 2001). At 2-6 months, there is evidence that these models display nuclear staining and mHTT microaggregates, preferentially in the striosomes (Menalled and Chesselet, 2002), an area initially targeted in brains of HD patients (Hedreen and Folstein, 1995). Nuclear inclusions are observed in the cerebellum and olfactory bulbs as early as 4 months, and in the striatum and cortex by 6 months (Menalled et al., 2003).

Knock-in models have provided noteworthy evidence regarding CAG repeat instability in *Htt* gene transmission. As previously mentioned and observed in humans (MacDonald et al., 1993; Zühlke et al., 1993; Telenius et al., 1994), mice with a low number of repeats (48-90) reveal almost no or very minimal changes in repeat lengths, suggesting mechanisms responsible for repeat length instability operate at higher number of CAG repeats. However, when the repeats are lengthened to 109, the mutation frequency increased to >70%. Instability is more apparent in maternal transmission, with contractions typically resulting through maternal transmission and expansions through paternal transmission (Wheeler et al., 1998).

D. Conditional models

The first conditional model was a tet-regulatable mouse which expressed exon 1 of the HD gene with 94 CAG repeats in conjunction with a tetracycline resistance operon **(**TetO).

Transcription of mHTT was activated in the forebrain by elimination of doxycycline from the drinking water (Yamamoto et al., 2000). These mice developed progressive motor alterations and neuropathology, which was ameliorated when the expression of mHTT was turned off by reintroduction of doxycycline.

The Cre/LoxP system has also been utilized to target mHTT expression. Cre/LoxP HD mice were originally designed to test the cell-autonomous versus cell-cell interaction HD hypothesis (Gu et al., 2005). These animals expressed exon 1 of mHTT with 103 CAG repeats in either the entire brain or just in cortical pyramidal neurons. Restricting mHTT expression to cortical pyramidal neurons is sufficient to produce nuclear accumulation and aggregate formation but no other HD-associated neuropathology or locomotor deficits (Gu et al., 2005). However, NMDA currents recorded from acutely dissociated MSNs are altered when mHTT is expressed in all neurons or only in striatal neurons, but not when expressed just in cortical neurons. In other words, the presence of mHTT in cortical pyramidal neurons alone is not sufficient to impair NMDA receptor-mediated currents (Gu et al., 2007). These studies support the "two-hit" hypothesis suggesting that both cell-autonomous and cell-cell interactions contribute to HD pathology.

In the D9-N171-98Q mouse model, the first 171 amino acids of the human *HTT* gene with 98 CAG repeats are expressed only in striatal MSNs (Thomas et al., 2011). These mice exhibited intranuclear inclusion bodies, failure to gain weight, and motor deficits. They provide evidence that cell-autonomous alterations cause a number of the deficits in HD. Taken together, the conclusions from these studies indicate that both cell-autonomous and cell-cell interactions contribute to the pathophysiology of HD.

1.5 Alterations of neurotransmission HD animal models

A leading theory of the cause of MSN death in HD is the excitotoxicity hypothesis which proposes that striatal neurons are degenerating and dying due to increased excitation caused by glutamate (DiFiglia, 1990; Freese et al., 1990; Beal et al., 1993; Ferrante et al., 2000). Therefore, alterations in glutamate release and in glutamatergic receptor function, as well as deficits in inhibition, and abnormalities in modulation, have been examined extensively in various HD models.

A. Biphasic alterations in glutamate neurotransmission

There is now considerable evidence that alterations in glutamatergic neurotransmission are not linear throughout the progression of the HD phenotype but are biphasic, characterized by increased neurotransmission followed by decreased neurotransmission. These changes correlate roughly with the behavioral alterations of hyperactivity followed by hypoactivity. In the R6/2, YAC128, and BACHD models, glutamatergic inputs begin to show alterations very early on. In R6/2 mice, the frequency of large amplitude spontaneous excitatory postsynaptic currents (sEPSCs) recorded in MSNs is increased as early as 5-7 weeks, the age at which behavioral symptoms begin to emerge (Cepeda et al., 2003). These events decrease markedly after 7 weeks. At 5-7 weeks the frequency of lower amplitude sEPSCs starts to decrease and continues to decrease as the phenotype progresses. Firing of striatal neurons is increased in R6/2 mice at 6-9 weeks (Rebec et al., 2006). These alterations appear to be caused by changes in presynaptic cortical inputs as recordings from cortical pyramidal neurons in layers II/III are characterized by increased frequencies of sEPSCs, as well as increased amplitudes of evoked EPSCs in 40 and 80 day-old R6/2 mice (Cummings et al., 2009). In addition, there is evidence for dysregulation of modulation of glutamate release of the presynaptic cortical inputs by DA and endocannabinoids which would cause increased release (André et al., 2010).

In YAC128 mice, frequency of sEPSCs in MSNs is increased at 1-1.5 months of age, and this increase is more evident in direct versus indirect pathway projecting MSNs (Joshi et al., 2009; André et al., 2011). Direct pathway MSNs in 1-2 month YAC128 mice and BACHD mice also display decreased paired-pulse ratios, suggesting increased glutamate release (André et al., 2011). Increased glutamate release onto direct, but not indirect pathway MSNs alters the inherent balance of the circuit, resulting in increased activity in the "Go" pathway compared to the "No-Go" pathway. Amplified activity of the "Go" pathway predicts chorea symptoms of HD patients (Albin et al., 1989; Alexander and Crutcher, 1990; Mink, 1996).

In contrast, MSNs from 7 month-old YAC128 mice show reduced evoked glutamate currents compared to age-matched controls, and even more significant progressive reductions at 12 months (Joshi et al., 2009). Similarly, sEPSC frequencies in MSNs are decreased at 12 months, while paired-pulse ratios are increased but only in direct pathway MSNs, consistent with decreased glutamate release from corticostriatal projections in older symptomatic mice (André et al., 2011). Thus, in the more symptomatic mice, there is decreased excitation of direct pathway MSNs of the "Go" pathway which is consistent with hypoactivity in these mice and the akinesia observed in HD patients.

Glutamatergic inputs from the thalamus have not yet been examined as extensively as those from the cortex. Light and electron microscopy studies in Q140 knock-in mice find loss of thalamostriatal axospinous terminals by 4 months and loss of corticostriatal axospinous terminals by 12 months (Deng et al., 2013). Immunolabeling for VGLUT1 (corticostriatal) and VGLUT2 (thalamostriatal) projections, in conjunction with labeling for D1 DA receptors, suggests that the loss of corticostriatal terminals at 12 months of age is preferentially for D1-expressing spines

while thalamostriatal terminal loss is analogous for D1-expressing and D1 non-expressing spines at 4 and 12 months (Deng et al., 2014).

A large proportion of glutamatergic thalamostriatal projections synapse onto LCIs. LCIs are relatively spared from degeneration in HD but show functional deficits in mouse models such as decreased acetylcholine release (Vetter et al., 2003; Smith et al., 2006; Farrar et al., 2011). The majority of excitatory glutamatergic inputs to LCIs arise from the CMPf and less from the cortex (Smith et al., 2004). Therefore, alterations in excitatory inputs to LCIs may reflect changes in thalamostriatal projections. With the use of viral transfection, the excitatory opsin, channelrhodopsin can be expressed in the CMPf, which then permits selective activation of thalamic projections in the striatum. Both thalamostriatal evoked AMPA and NMDA receptor-mediated currents are minimally affected in symptomatic R6/2s (Holley et al., 2015). Frequency of sEPSCs, mediated by AMPA receptors also is unchanged. As degeneration of MSNs has been explained by excitotoxicity, unaltered excitatory inputs to LCIs is in marked contrast to changes seen in MSNs and may partially explain the selective sparing of LCIs in HD.

Recently, the excitotoxicity hypothesis of cell death in HD has been challenged. Degeneration of glutamatergic terminals, from both the cortex and thalamus, suggests a progressive loss of glutamatergic inputs to MSNs, rather than a progressive increment of those inputs. Loss of glutamatergic synaptic inputs then favors activation of extrasynaptic receptors. Another hypothesis gaining ample attention suggests that degeneration of MSNs is due to loss of trophic factors released from the cortex onto the striatum (Zuccato and Cattaneo, 2009; Plotkin and Surmeier, 2015). BDNF is synthesized by cortical pyramidal neurons innervating the striatum and released to the striatum (Altar et al., 1997). BDNF activates tyrosine kinase (Trk) B receptors on postsynaptic membranes of MSNs and is vital for maintenance of dendritic and

synaptic function, and cell survival (Zuccato and Cattaneo, 2009; Jia et al., 2010; Nithianantharajah and Hannan, 2013). Therefore, decreased BDNF signaling may explain striatal cell death. The deficits in BDNF signaling may be due to impaired postsynaptic responses and signaling in MSNs to BDNF rather than, or in addition to, diminished release from corticostriatal projections (Brito et al., 2013; Plotkin et al., 2014). The idea that the deficit may be postsynaptic helps explain differential alterations shown in direct versus indirect pathway neurons.

In summary, changes in glutamatergic neurotransmission are extensive in mouse models of HD and reflect both alterations in synaptic inputs and receptors. The biphasic pattern observed throughout the progression of HD in genetic mouse models, as well as the dysregulation of the equilibrium between the competing direct and indirect striatal projection pathways, parallels the changes in movement patterns manifested in HD patients. An important implication for treatment of HD symptoms emanating from this conclusion is that therapies probably need to be specifically adjusted according to disease progression in patients. An additional source of the disrupted equilibrium in HD is the dissimilar pattern of alterations undergone by cortical and thalamic inputs. As noted, functional properties of thalamic inputs onto striatal MSNs are still highly disputed, while the number of studies focusing on these inputs in HD is minimal. Therefore, for my dissertation project, I focused on teasing apart alterations at corticostriatal and thalamostriatal synapses in HD.

B. Alterations in GABAergic projections

B.1 Striatal inhibition

Assessing changes in inhibitory activity in HD is important to further understand how the local circuits are altered. The striatum is highly enriched in GABA which originates from two parallel pathways, a feedback inhibitory pathway mediated by axon collaterals from MSNs and a

feedforward inhibitory pathway mediated by the GABAergic interneurons (Tepper et al., 2004, 2008).

Unlike excitatory inputs to MSNs which display a biphasic change, first increasing and then decreasing, inhibitory inputs to MSNs tend to consistently increase as the disease progresses. Evidence for this increase emanates from studies examining changes in both spontaneous inhibitory postsynaptic currents (sIPSCs) and evoked IPSCs (Cepeda et al., 2004, 2013; Centonze et al., 2005; Dvorzhak et al., 2013). The frequency of sIPSCs is increased in MSNs from 5-10 week R6/2 mice (Cepeda et al., 2004, 2013; Centonze et al., 2005; Dvorzhak et al., 2013). The increases in frequency of sIPSCs are progressive and even more prominent by the time the R6/2 mice are 9-14 weeks. These increases are abolished in tetrodotoxin (TTX), suggesting differences are due to the occurrence of action potentials and presynaptic release of GABA onto MSNs (Cepeda et al., 2004), most likely from PLTS interneurons as discussed below. In addition, local electrical stimulation produces an increased evoked IPSC (Cepeda et al., 2013), probably due to enhanced GABA release by FS interneurons, also addressed below. Acutely isolated MSNs from R6/2 mice also show increased GABA current densities indicating that possibly receptor alterations have occurred (Cepeda et al., 2004). Consistent with this finding, immunofluorescence experiments show increased expression of the ubiquitous alpha 1 subunit of $GABA_A$ receptors in MSNs from R6/2 mice (Cepeda et al., 2004). Similar to findings in the R6/2, frequency of sIPSCs is increased in older symptomatic R6/1 mice (Cepeda et al., 2004). In agreement, MSNs from 12 months old BACHD and YAC128 full length transgenic mice, and CAG140 and Q175 knock-in mice, also display increased frequencies of sIPSCs (Cepeda et al., 2010, 2013; Dvorzhak et al., 2013; Indersmitten et al., 2015). In the Q175 mice, the increase in sIPSC frequency is both time-dependent and gene dose-dependent, as it is greater

in older mice as well as homozygotic compared to heterozygotic mice (Indersmitten et al., 2015). However, although frequency of sIPSCs is increased in MSNs of Q175 mice, amplitude of evoked minimal stimulation IPSCs is reduced, which in conjunction with altered paired-pulse ratios suggests there also may be a decrease in the probability of GABA release onto MSNs (Dvorzhak et al., 2013). GABA release in these mice is asynchronous and IPSC generation delayed. These authors concluded that the increase in sIPSC frequency may be due to disinhibition of firing by altered GABAergic activity (Dvorzhak et al., 2013).

In addition to phasic GABAergic inhibition, tonic GABA signaling has been shown to occur in the striatum via extrasynaptic $GABA_A$ receptors (Brickley and Mody, 2012). Low levels of GABA present at rest in the extracellular space activate these receptors to generate persistent inhibition. Tonic GABA currents are higher in direct pathway versus indirect pathway MSNs in wild-type (WT) mice (Santhakumar et al., 2010; Cepeda et al., 2013). Tonic GABA currents are unaffected in direct pathway MSNs in R6/2s, however these currents are significantly reduced in indirect pathway MSNs in R6/2s. This effect is eliminated in TTX, suggesting it is action potential dependent (Cepeda et al., 2013). Similarly, recordings from a mixed population of MSNs from Q175 and R6/2 mice show reduced $GABA_A$ receptor-mediated tonic chloride currents (Wójtowicz et al., 2013). Furthermore, low GABA concentrations added to striatal slices result in larger responses and longer $GABA_A$ channel openings in indirect versus direct pathway projecting MSNs (Ade et al., 2008). Therefore, as GABA release is altered throughout the course of HD, this change has distinct effects on the two populations of MSNs. The HD-induced increase in frequency of sIPSCs is more evident in indirect pathway MSNs and less so in direct pathway MSNs (André et al., 2011; Cepeda et al., 2013). Thus, in addition to differences in

excitatory input to direct and indirect pathway MSNs, the increase in inhibitory inputs to indirect pathway MSNs further disrupts the finely tuned intrinsic balance of the striatal circuit.

Feedback inhibition: Electrophysiological experiments in symptomatic R6/2 and, to a lesser extent, in BACHD mice suggest that the alteration in striatal GABAergic transmission to MSNs in HD mice originates from multiple sources. Feedback inhibition appears to explain a portion of the increase. Dual patch recordings reveal that there is a significant decrease in synaptic connectivity between adjacent pairs of MSNs in R6/2 and BACHD mice compared with WT littermates across age, which is interpreted as a reduction in the feedback inhibitory pathway (Cepeda et al., 2013). However, in contrast to WT MSNs where bidirectional connectivity is rarely observed, about half of the connected pairs in symptomatic R6/2 mice show bidirectional connectivity, suggesting altered axon collateral inhibition which could potentially compensate for the reduction in overall connectivity. Interestingly, in R6/2 mice, the greatest proportion of connectivity is between direct-direct pathway pairs, while in WT mice, direct-direct pathway, indirect-direct pathway, direct-indirect pathway and indirect-indirect pathway connections are more evenly distributed (Cepeda et al., 2013). Notably, a previous study using a fluorescent reporter gene found that MSN-MSN connections are not randomly distributed but that direct pathway MSNs connect to other direct pathway MSNs but much less frequently to indirect pathway MSNs, while indirect pathway MSNs connect to other indirect pathway MSNs and to direct pathway MSNs (Taverna et al., 2008). Additional studies are needed to be able to clarify and explain connectivity between direct and indirect pathway MSNs more precisely.

Feedforward inhibition: Dual patch recordings from PLTS interneuron-MSN pairs or optogenetic activation of SOM-expressing PLTS neurons do not show differences in MSN responses in R6/2 compared to WT mice. However, current clamp recordings from PLTS

interneurons, which are spontaneously active in the slice, demonstrate increased firing in R6/2 and BACHD mice compared to WTs. Thus, PLTS interneurons are another source of increased GABA activity which may underlie the increased sIPSC frequency of MSNs. These interneurons also show a significant reduction in frequency of spontaneous IPSC inputs indicating they may be under reduced inhibitory tone (Cepeda et al., 2013). Interestingly, when response amplitudes of MSNs to activation of PV or SOM interneurons are compared using optogenetics in both WTs and R6/2s, responses to PV activation are much larger than responses to SOM activation, consistent with stronger connectivity and reliability of FS-MSN connections, which is also demonstrated by dual patch recordings (Cepeda et al., 2013).

Dual patch recordings from FS interneuron-MSN pairs demonstrate a small increase in FS-MSN connectivity and a trend for greater amplitude of postsynaptic responses in MSNs from R6/2 mice compared to WTs. Similarly, selective optogenetic stimulation of PV expressing FS interneurons in R6/2 mice induce significantly larger amplitude MSN responses, pointing to one source for the increased amplitude of evoked IPSCs. Since FS interneurons do not fire spontaneously in the slice (their resting membrane potential is very hyperpolarized, ~-75 mV), and they are under increased inhibitory tone, these cells are not likely to contribute to the increase in sIPSCs frequency observed in HD mice (Cepeda et al., 2013).

Taken together these findings provide evidence for multiple sources of the increased inhibitory input to MSNs in the HD mouse models. The increase in sIPSC frequency is due primarily to increased input from PLTS interneurons, and also may have a contribution from increased reciprocal connectivity of MSNs. The increase in the amplitude of the evoked IPSC appears to be the result of increased input from FS interneurons.

B.2 Cortical inhibition

GABAergic transmission in the cortex undergoes biphasic alterations in the R6/2 model. Cortical pyramidal neurons from 21 and 40 day-old R6/2 mice show increased frequency of sIPSCs (Cummings et al., 2009). In 21 day old R6/2s, if action potential-driven GABA release is eliminated using TTX, the differences in IPSC frequency are eliminated. These findings suggest that GABAergic alterations in cortical pyramidal neurons at 21 days are most likely due to intrinsic firing of GABAergic interneurons. However, when the animals are 80 days old and exhibit overt behavioral symptoms, the effect is reversed in the R6/2 and the frequency of sIPSCs is reduced. Interestingly, the reduced inhibition may provide a mechanistic basis for the occurrence of spontaneous seizures in R6/2 mice (Mangiarini et al., 1996; Cummings et al., 2009). At this age, changes in miniature IPSCs and evoked IPSC paired-pulse ratios suggest increased probability of GABA release onto cortical pyramidal neurons (Cummings et al., 2009). Although cortical pyramidal neurons of 6 month-old BACHD mice display a reduction in sIPSC frequencies (Spampanato et al., 2008), evidence from YAC128, CAG140 and Q175 heterozygote mice indicates that at 12 months sIPSC frequency remains increased (Cummings et al., 2009; Indersmitten et al., 2015). Thus differences in cortical GABAergic activity among models do occur and may reflect different rates of disease progression.

In summary, altered neurotransmission in HD is not only a symptom of dysregulation of glutamatergic mechanisms, but is also associated with dysregulation of GABAergic mechanisms. The changes in GABA transmission are complex and occur in multiple HD mouse models, in both striatum and cortex, in multiple cell types, and are progressive across differing disease states. These changes also directly affect glutamate neurotransmission. Increased GABA release may dampen glutamate inputs by either shunting (increase in the membrane conductance) or by activating presynaptic $GABA_B$ receptors on corticostriatal terminals which in turn reduce

glutamate release. Furthermore, one can speculate that the increase in inhibitory signaling may be the brain's attempt to compensate for the increase in excitatory signaling. In the intact organism, the two processes function in parallel and balance each other, but when this balance is disrupted, neuropathology and phenotypic symptoms result.

C. Alterations in dopaminergic projections

C. 1 Dopamine release and receptor alterations

DA neurotransmission contributes to numerous physiological processes within the brain including neuronal excitability, synaptic transmission, integration and plasticity, protein trafficking, and gene transcription. One of its main functions is modulating responses evoked by glutamate and GABA. The direction of modulation depends on a number of factors including the subtype of glutamate receptor, the location of the receptors on the neuron and the timing of release. In general, in the striatum, D1 receptor activation enhances glutamate responses, while D2 receptor activation decreases glutamate responses (Cepeda et al., 1993; Levine et al., 1996; Cepeda and Levine, 1998). Similarly, DA and D1 agonists increase sEPSC frequency in direct pathway MSNs, whereas DA and D2 agonists decrease sEPSC frequency in indirect pathway MSNs (André et al., 2010). Hence the opposing effects of DA on the two populations of MSNs is in part responsible for maintaining the critical equilibrium between the two striatal output pathways, which is disrupted in HD. Less is known about changes in DA modulation of GABA inputs onto MSNs in HD and future studies will have to address this important issue.

DA also may act as a filter for less active corticostriatal inputs (Bamford et al., 2004). For example, in the dorsal striatum, D2 receptors on presynaptic corticostriatal terminals function to decrease glutamate release (Flores-Hernández et al., 1997; Cepeda et al., 2001a). Electrophysiological recordings in cells from mice lacking D2 receptors exhibit increased

glutamate release, supporting the idea that D2 receptors may act as filters or gatekeepers in the striatum (Cepeda et al., 2001a). Presynaptic D2 receptors may also be necessary in preventing excessive excitation, and therefore may play a vital role in HD, helping to regulate the biphasic alterations in glutamate transmission associated with the disease. DA modulation is additionally influenced by the endocannabinoid system and presynaptic cannabinoid receptor type 1 (CB1) receptors (Maejima et al., 2001; Patel et al., 2003; Kreitzer and Malenka, 2005).

There are multiple changes in the DA system in mouse models of HD. In the R6/2 at 4 weeks, prior to the development of motor symptoms, a significant reduction in DA metabolites is apparent (Mochel et al., 2011). Protein levels of DA- and cyclic AMP-regulated phosphoprotein are reduced (Bibb et al., 2000). A marked reduction of DA transporter immunoreactivity is observed in the striatum as well (Stack et al., 2007). Striatal D1 and D2 receptor mRNA is reduced in R6/2 mice at 4 weeks (Augood et al., 1997; Cha et al., 1998, 1999) and striatal D1 and D2 receptor binding also is reduced early in R6/1 and R6/2 mice (Cha et al., 1998; Bibb et al., 2000; Petersén et al., 2002a; Ariano et al., 2002). Consistent with this finding, both striatal D1 and D2 receptor mRNAs are reduced in late stage YAC128 mice but symptomatic BACHD mice do not show these changes (Pouladi et al., 2012).

C.2 Alterations in dopamine neurotransmission

As observed with HD-induced changes in glutamatergic and GABAergic transmission, changes in DA transmission also exhibit biphasic patterns. D1 receptor modulation is affected differently in early versus late symptomatic YAC128 mice. Activation of D1 receptors produces no change in sEPSCs in D1 receptor-expressing direct pathway MSNs at the early symptomatic stage. However, modulation is restored by treating slices with TBZ (a DA vesicular transporter inhibitor that ultimately depletes DA). This finding suggests that D1 receptor activation may be

maximized, possibly by increased DA neurotransmission in presymptomatic or early symptomatic stages of HD as abnormally high DA neurotransmission may serve as a compensatory mechanism decreasing DA receptor function (Giros et al., 1996; Dumartin et al., 2000; Wu et al., 2007). Supporting evidence has been obtained in a transgenic rat model of HD; increased DA levels in the striatum are observed in conjunction with increased number of tyrosine hydroxylase-expressing cells in the SN pars compacta and ventral tegmental area (Jahanshahi et al., 2010) as well as the dorsal raphe nucleus (Jahanshahi et al., 2013).
In contrast, in fully symptomatic YAC128 mice, D1 receptor activation is unchanged in D1 receptor-expressing direct pathway MSNs. Activation of D2 receptors has no effect on sEPSC frequencies of D2 receptor-expressing indirect pathway MSNs in early symptomatic YAC128 mice (André et al., 2011).

Overall, there is now considerable evidence for a reduction of DA release in transgenic mouse models in the late stages of HD (Petersén et al., 2002b; Hickey et al., 2002; Johnson et al., 2006; Callahan and Abercrombie, 2011). Studies using microdialysis have shown that extracellular striatal DA concentrations are reduced in R6/2 mice. This reduction parallels age-dependent progression of motor deficits on the rotarod task. Total levels of striatal DA are depleted in tissue from 11 week R6/2 mice. Similarly, extracellular DA concentrations are reduced in the striatum of 7 month YAC128 mice (Callahan and Abercrombie, 2011). Reduced DA levels and deficits in DA release have been proposed to be caused by impaired vesicle loading or decreased number of available DA reserve pool vesicles (Ortiz et al., 2010).

The function of DA as a modulator of glutamate release also is affected in HD mice. Application of amphetamine (which induces continuous DA efflux) or a D2 receptor agonist, decreases corticostriatal glutamate release similarly in striatal slices from 1 month YAC128 and

in WT mice via a D2 receptor-dependent filter (Joshi et al., 2009). However, the effect of the D2 agonist is diminished in 12 month-old symptomatic YAC128 mice. D2 receptor stimulation, DA released via amphetamine, or DA released by direct striatal stimulation, are all less effective in modulating corticostriatal glutamate release in 12 month YAC128 mice (Joshi et al., 2009).

1.6 Conclusions

This review of the functional alterations of basal ganglia-cortical circuits in HD, based mostly on genetic rodent models, supports the idea that this disease is above all a synaptopathy. The complex interplay of the two main excitatory and inhibitory neurotransmitters, glutamate and GABA, and their modulation by DA (and to a lesser extent by acetylcholine [ACh]) are severely disrupted in HD. Synaptic alterations occur before neuronal cell death becomes evident and underlie a number of HD symptoms. It is clear that biphasic alterations in synaptic neurotransmission occur. Glutamatergic, GABAergic, and DA alterations are not linear but instead shift throughout the progression of the disease. For example, the frequency of sEPSCs in MSNs is increased early but decreased later. The frequency of sIPSCs in cortical pyramidal neurons is increased early but also decreased later in the R6/2 model. DA D1 receptor modulation of sEPSCs is absent in D1-expressing direct pathway MSNs at early stages but returns in fully symptomatic YAC128 mice. Neurodegeneration of the striatum in HD involves a complicated interplay of presynaptic and postsynaptic mechanisms. Moreover, such patterns are not surprising as they parallel biphasic behavioral symptoms of HD patients.

Alterations in the inputs to MSNs disrupt the delicate neurotransmitter equilibrium of the direct and indirect striatal output pathways as the HD phenotype progresses. Altered excitatory glutamatergic transmission from the cortex and thalamus summate with altered striatal inhibitory GABAergic transmission from feedback and feedforward pathways to produce unbalanced input

to direct and indirect pathway MSNs. These pathways have an intrinsic balance and as one pathway undergoes alterations, the entire system is impacted. To maintain this balance, as well as behavioral and cognitive flexibility, DA modulation of glutamate and GABA transmission is essential, and when it is abnormal the system is even more greatly affected (Chen et al., 2013). The system attempts to compensate but such mechanisms probably are not effective long-term and eventually take a toll on the system as well. In conclusion, synaptic alterations in HD are complex, multifaceted, multilayered, and non-linear.

Chapter 2

Alterations of Thalamostriatal and Corticostriatal Projections in the R6/2 Mouse Model of Huntington's Disease

2.1 Introduction

A prominent hypothesis explaining MSN loss in HD proposes that striatal neurons are lost due to altered excitatory glutamatergic inputs. Glutamatergic inputs to the striatum originate in two distinct brain regions, the CMPf nuclear complex of the thalamus and the cortex. A more detailed understanding of alterations of glutamatergic activity in the striatum, and the source of these alterations, is necessary to aid in our full understanding of HD.

A significant body of literature concerning cellular and synaptic changes of corticostriatal projections in mouse models of HD has been published; however, there is minimal information on functional alterations of thalamostriatal inputs. Cortical and thalamic projections are interlaced within the striatum, which has made differential stimulation of each pathway difficult in striatal *in vitro* preparations. The major body of electrophysiology literature examining glutamatergic activity in the striatum has either focused on studying spontaneous excitatory activity in MSNs, or cortically-evoked excitatory activity. Excitation of cortical efferent fibers is most often achieved by either placing a stimulating electrode a) in the corpus callosum which stimulates fibers running to/from the motor, somatosensory, visual, and prefrontal cortex (Hofer and Frahm, 2006) or b) intrastriatally which stimulates a combination of all types of fibers running throughout the striatum including not only the desired corticostriatal projections, but also thalamostriatal, GABAergic, dopaminergic, and cholinergic inputs. Isolating the effects of activating thalamic inputs onto MSNs *in vitro* has been especially challenging. Oblique horizontal slices have been used to overcome the stumbling blocks. However, studies employing this technique have yielded contradictory results, possibly due to species or procedural differences (Ding et al., 2008; Smeal et al., 2008).

To circumvent this problem, we used optogenetics to specifically and individually activate each glutamatergic pathway. Optogenetics is a technique which takes advantage of light-gated channels to control neuronal activity. Channelrhodopsin-2 (ChR2), a channel from the model organism *Chlamydomonas reinhardtii*, absorbs blue light with an action spectrum maximum at 470 nm (Nagel et al., 2003). When ChR2 absorbs a photon of the appropriate wavelength, it undergoes a conformational change from a *trans* to *cis* configuration which induces the opening of its pore. ChR2 is a nonspecific cation channel allowing the flow of H^+, Na^+, K^+, and Ca^{2+} ions down their concentration gradients. Therefore, if a cell at resting membrane potential expressing ChR2 is exposed to a pulse of blue light, the pore will open allowing cations to flow down their concentration gradient, and the cell will depolarize. With the use of optogenetics and current viral and mouse genetics, ChR2 can be expressed in specific cell types or in specific brain regions, to control activation of each pathway separately. We used an adeno-associated virus (AAV) expressing ChR2(H134R) and enhanced yellow fluorescent protein (eYFP) under the calcium/calmodulin-dependent protein kinase type II alpha subunit (CaMKIIa) promoter. The virus was injected to express ChR2 in the CMPf or motor cortex to allow specific activation of thalamostriatal or corticostriatal inputs respectively.

The goals of the experiments presented in this chapter were to examine alterations of AMPA and NMDA receptor-mediated currents at thalamostriatal and corticostriatal synapses in MSNs of R6/2 mice compared to MSNs of WT mice with the use of optogenetics. The R6/2 mouse model was selected for this aim for two reasons. First, the large amount of electrophysiological data already available in the R6/2 HD model provides valuable information to which new results can be compared to. Electrophysiological data describing changes in corticostriatal inputs of these mice is useful to validate the optogentic technique, as well as

compare and contrast previous findings which relied on corpus callosum or intrastriatal electrical stimulation. Second, the rapidly progressing and aggressive phenotype presented by R6/2 mice allows relatively rapid assessment of the differences in thalamostriatal and corticostriatal inputs in HD using optogenetics.

2.2 ChR2 viral injections and expression

AAV2-CaMKIIa-ChR2(H134R)-YFP was injected either into the CMPf or motor cortex ~4 weeks prior to experiments. A set of animals was euthanized and perfused to allow verification of injection placement and visualization of viral expression by fluorescent microscopy. Representative images from mice injected into the CMPf or cortex are shown in Figures 2.1 and 2.2, respectively.

The entire parafasicular nucleus (Pf) of the thalamus expresses YFP/ChR2 ~4 weeks post injection independent of genotype (Figure 2.1A). Faint sparse fluorescence can be seen throughout the entire striatum in brain slices from both genotypes (Figure 2.1B). Brains of mice injected into the CMPf show the needle track and some viral expression in the CA3 region of the hippocampus in both the WT and R6/2. Qualitative comparison of YFP expression at injection site and striatum revealed no apparent differences of viral spread between R6/2s (n = 6) and WTs (n = 6) injected into the CMPf.

The brains of mice which underwent ChR2 injection into the cortex show viral expression in the M2 motor cortex (Figure 2.2A). This is true of brains from both WT and R6/2 mice. Coronal striatal slices from these mice show that the majority of projections from the cortical injection expressing ChR2 are localized to fiber bundles in the dorsolateral striatum (Figure 2.2B). Qualitative comparison of YFP expression at the injection site and within in the

striatum revealed no apparent differences of viral spread between R6/2 (n = 4) and WT (n = 5) mice injected in the cortex.

For consistency of responses and to account for the heterogeneous population of striatal neurons and their diverse functions and projections, all electrophysiological recordings were restricted to the dorsolateral striatum, in animals injected into the CMPf and cortex.

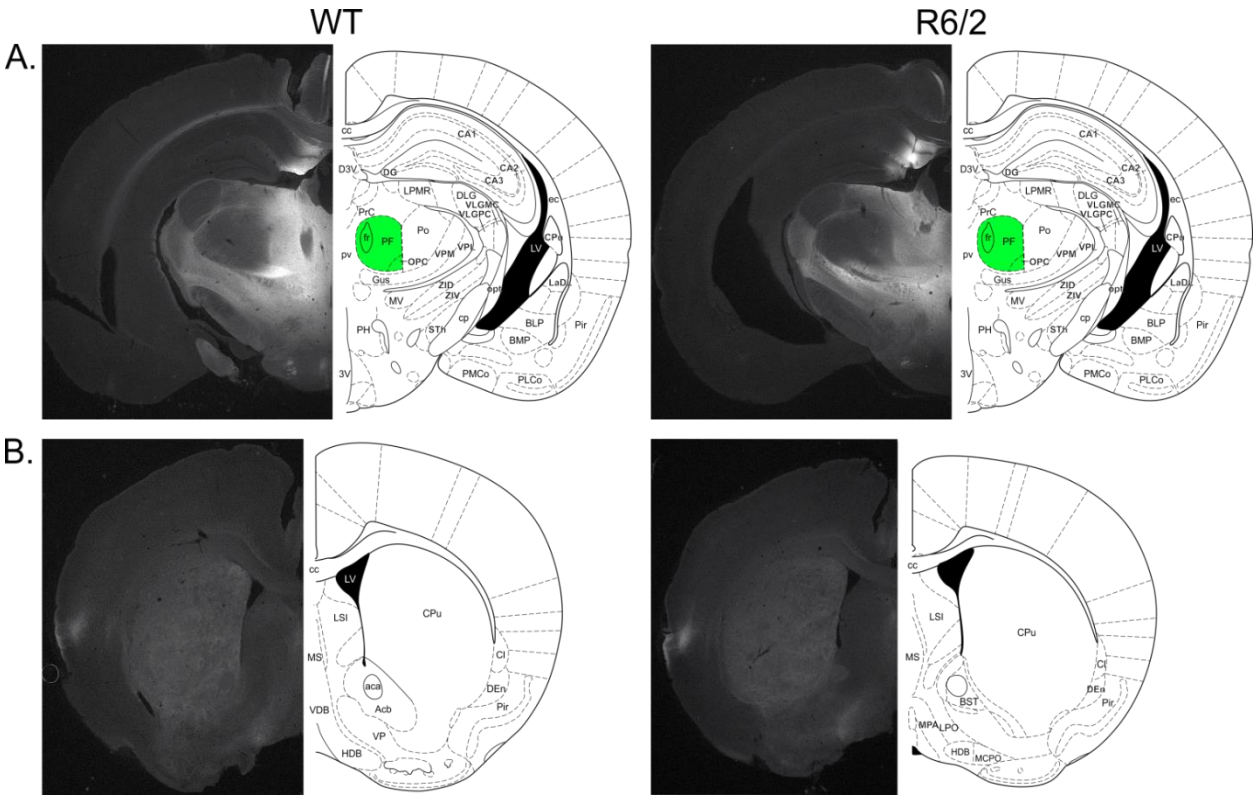

Figure 2.1. YFP expression following AAV-CaMKIIa-YFP-ChR2 injection. (A) Typical YFP expression patterns at the injection sites following AAV-CaMKIIa-YFP-ChR2 virus injections into the CMPf in thalamic slices of a WT (left) and an R6/2 (right) mouse. **(B)** Typical YFP expression patterns in the corresponding striatum of the same mice from (A).

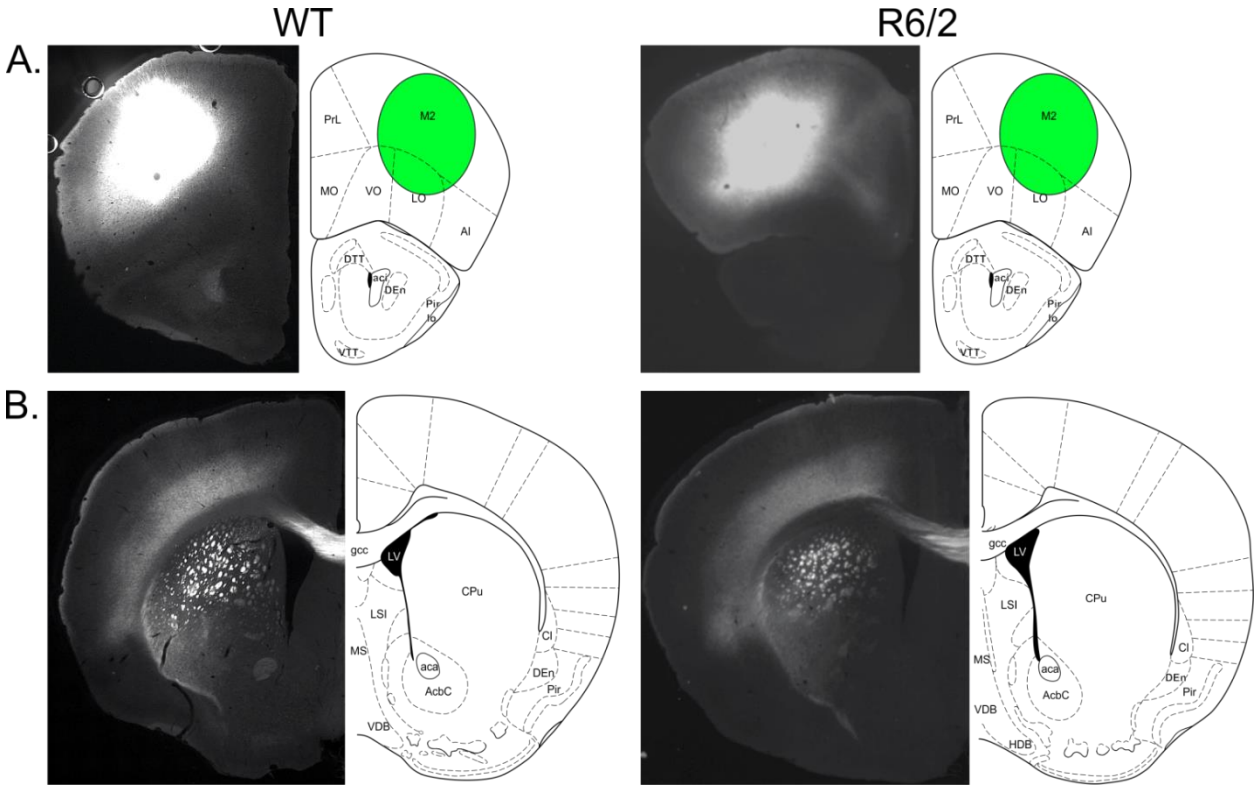

Figure 2.2. YFP expression following AAV-CaMKIIa-YFP-ChR2 injection. (A) Typical YFP expression patterns at the injection sites following AAV-CaMKIIa-YFP-ChR2 virus injections into the cortex in cortical slices of a WT (left) and an R6/2 (right) mouse. **(B)** Typical YFP expression pattern in the corresponding striatum of the same mice from (A).

2.3 MSN properties

Basic membrane properties are a useful readout to help identify neuronal type during electrophysiological recordings as MSN, LCI, FS, and PLTS neurons differ in their membrane properties. In addition, comparison of cellular membrane properties across genotype can be suggestive of the differences in neuronal size and conductance. Membrane properties were recorded for each neuron in voltage clamp mode at V_{hold} = -70 mV. The membrane capacitance (C_m), membrane input resistance (R_m), time constant (Tau), and holding current (Hold) necessary to voltage clamp the neuron at V_{hold} = -70 mV are reported in Table 2.1. MSNs recorded from mice injected into the CMPf and cortex are combined within genotype for comparison of membrane properties. MSNs from R6/2s showed significantly reduced membrane capacitance and increased membrane input resistance compared to MSNs recorded from their WT littermates. These results replicate previous findings (Klapstein et al., 2001) and suggest that MSNs from R6/2s are smaller in size and contain fewer open channels. Consistent with smaller soma size and decreased number of open channels, the average absolute holding current was also reduced in R6/2s.

Following recordings, slices were processed for biocytin and imaged using a confocal microscope equipped with lasers for visualization of fluorescence (Figure 2.3). Biocytin processing allowed observation of MSN morphology not clearly seen with infrared (IR) imaging on the electrophysiology rig. Based on qualitative observation, MSNs from R6/2s showed a decrease in spines and some dendritic fragmentation or beading. Reduced somatic size, thinning of dendrites, and reduced number of spines has been previously shown in R6/2 mice (Klapstein et al., 2001). In addition, this step allowed visualization of thalamostriatal or corticostriatal inputs expressing ChR2 in close proximity to the recorded neuron. MSNs in which a

postsynaptic response to light stimulation of thalamic or cortical inputs failed to be evoked did not have any ChR2 expression in close proximity and were excluded from the data analysis.

Table 2.1. Passive membrane properties of MSNs from WT and R6/2 mice.

	WT	R6/2
Cm (pF)	97.96 ± 3.84 (50)	77.91 ± 1.82 (62)***
Rm (MΩ)	64.52 ± 4.27 (47)	162.06 ± 9.94 (58)***
Tau (ms)	1.78 ± 0.46 (50)	1.68 ± 0.06 (62)
Hold (pA)	-91.97 ± 53.47 (50)	-41.15 ± 3.79 (62)***

Values are mean ± SE (standard error) (number of cells). * $p < 0.05$, ** $p < 0.01$, *** $p < 0.001$.

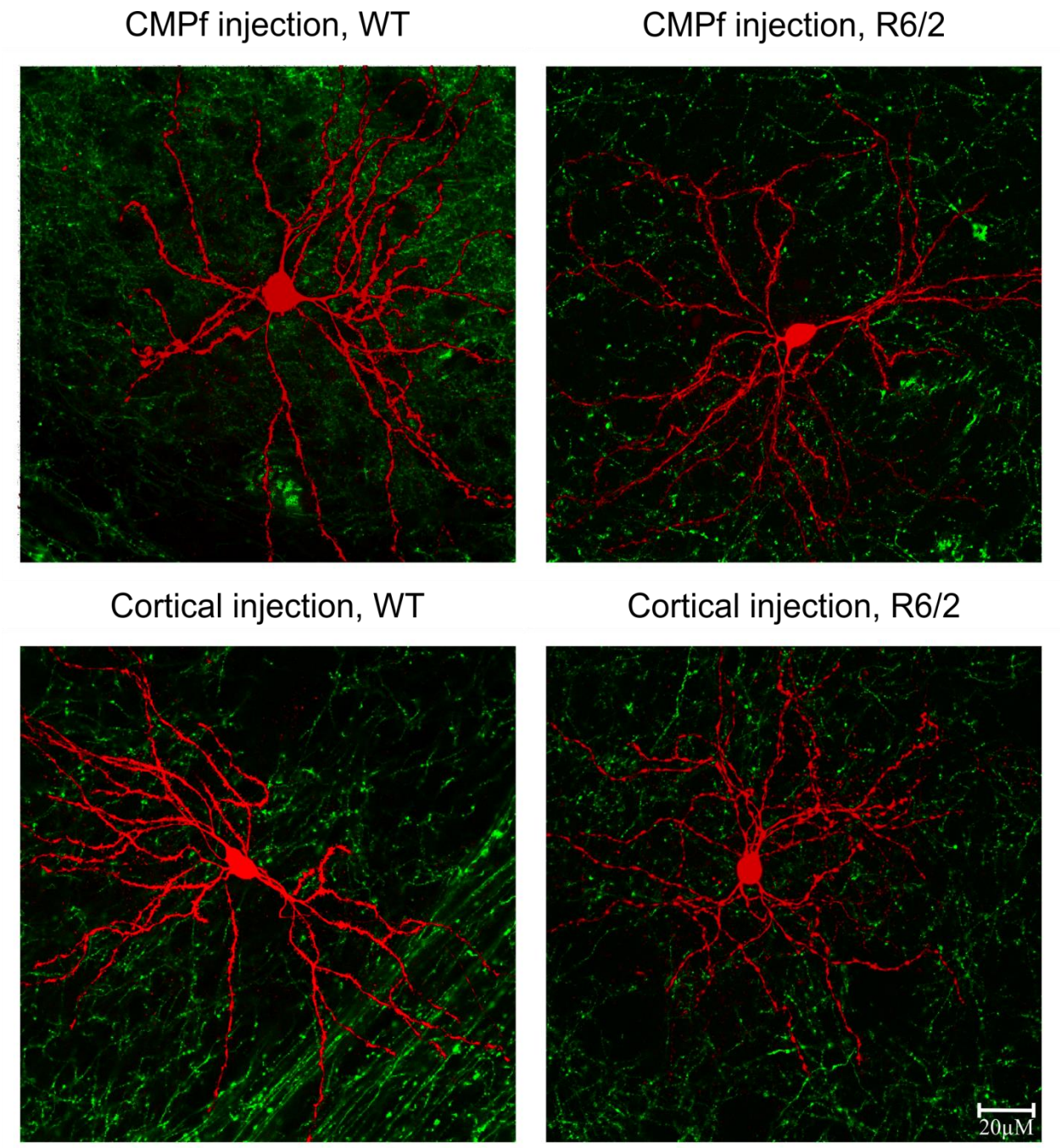

Figure 2.3. High magnification images of MSNs and striatal ChR2 expression in WT and R6/2 mice. Fluorescent confocal microscope images of ChR2 expression in thalamostriatal and corticostriatal axons (green) in the striatum and biocytin filled MSNs saved and recovered from electrophysiology experiments (red).

2.4 AMPA receptor-mediated currents

After membrane properties were recorded, the cell was maintained at V_{hold} = -70 mV and 10 μM bicuculline (BIC) was bath applied to block $GABA_A$ receptor-mediated inhibitory activity and isolate AMPA receptor-mediated currents. After approximately 4 minutes, V_{hold} was gradually stepped up to +10 mV to verify that spontaneous GABAergic activity was eliminated. The voltage holding potential was then again returned to -70 mV and the cell was given approximately a minute to equilibrate. A 2ms 470 nm light pulse was applied over 5 trials given 30 seconds apart and the evoked AMPA receptor-mediated currents were recorded. The 30 second inter-trial interval was necessary to allow full recovery of the response before the next trial (Yizhar et al., 2011).

The average amplitudes, areas, rise times, and decay times of AMPA receptor-mediated currents evoked by thalamostriatal stimulation are shown in Figure 2.4. The amplitudes of these responses were not significantly different between MSNs from WT and R6/2 mice. Similarly, the rise times were unchanged. However, AMPA currents recorded from R6/2 MSNs exhibited significantly slower decay times, i.e. took a longer time to return to baseline. These currents displayed significantly larger areas, although this difference is most likely a consequence of the longer decay times. Longer decay times may be caused by alterations in glutamate reuptake or postsynaptic changes such as alterations in AMPA receptor subunit composition.

Average measurements of AMPA receptor-mediated currents evoked by corticostriatal stimulation are shown in Figure 2.5. The average amplitude and area of AMPA receptor-mediated currents evoked by corticostriatal stimulation were unchanged in R6/2 MSNs compared to WT MSNs. Cortically-evoked responses in R6/2s displayed faster rise times than those in WTs. Unlike responses evoked by thalamostriatal stimulation, decay times of cortically-

evoked responses were unaltered. Faster rise times are often associated with alterations of postsynaptic receptors. However, changes in receptor subunit composition would most likely produce concomitant changes in other properties of the response such as altered area and decay time. In this case, because no other significant differences were observed, there is little evidence for alterations of postsynaptic AMPA receptors.

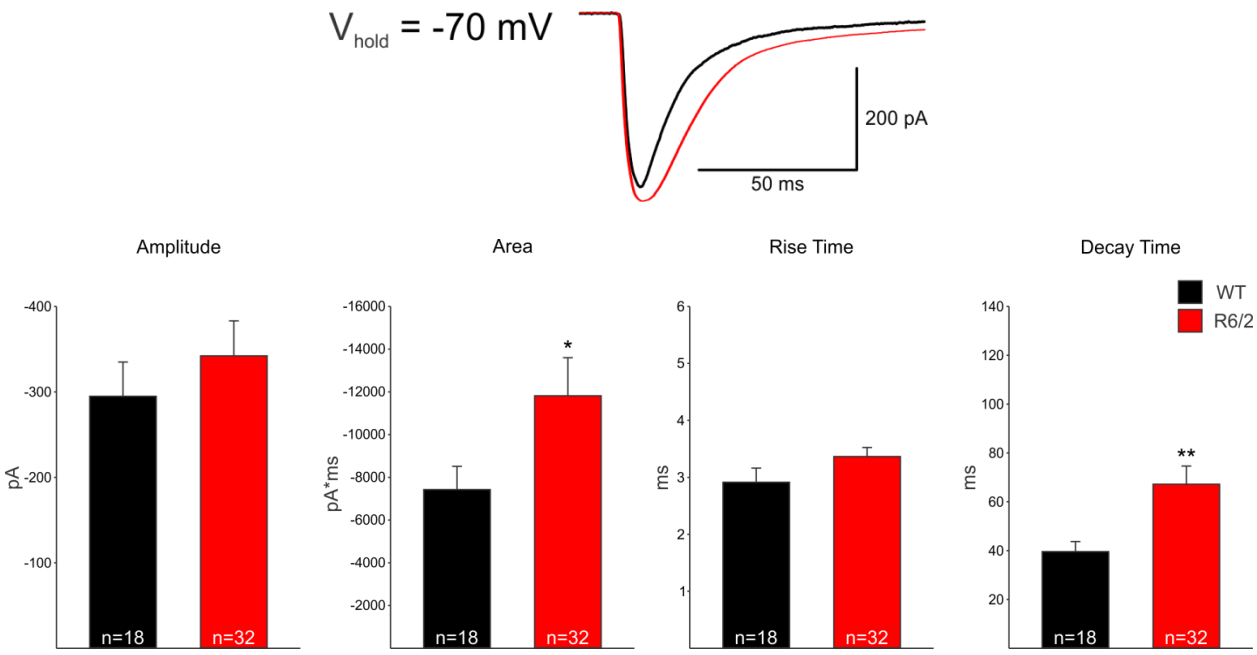

Figure 2.4. AMPA receptor-mediated currents evoked by thalamostriatal stimulation. **(Top)** Representative sample traces of AMPA receptor-mediated responses evoked by thalamostriatal stimulation, recorded in an MSN from a WT mouse (black) and R6/2 mouse (red). **(Bottom)** Average amplitudes, areas, rise times, and decay times (± SE) of AMPA receptor-mediated responses evoked by thalamostriatal stimulation. Ns are shown in each bar. * $p < 0.05$, ** $p < 0.01$, *** $p < 0.001$.

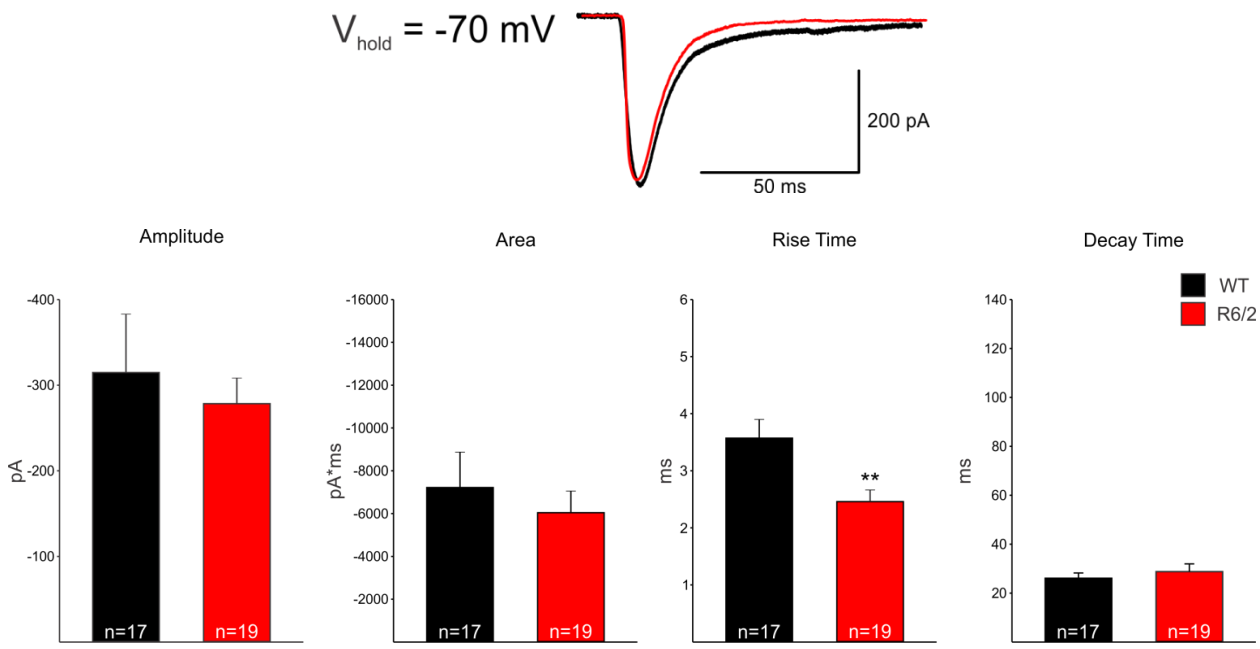

Figure 2.5. AMPA receptor-mediated currents evoked by corticostriatal stimulation. (Top) Representative sample traces of AMPA receptor-mediated responses evoked by corticostriatal stimulation, recorded in an MSN from a WT mouse (black) and R6/2 mouse (red). **(Bottom)** Average amplitudes, areas, rise times, and decay times (± SE) of AMPA receptor-mediated responses evoked by corticostriatal stimulation. Ns are shown in each bar. * $p < 0.05$, ** $p < 0.01$, *** $p < 0.001$.

2.5 NMDA receptor-mediated currents

After 5 trials of AMPA receptor-mediated currents were recorded, 10 μM 2,3-dihydroxy-6-nitro-7-sulfamoyl-benzo[f]quinoxaline-2,3-dione (NBQX, AMPA receptor antagonist) was bath applied to the slices to block AMPA channels. After ~4-6 minutes, a 2ms 470 nm pulse was given at V_{hold} = -70 mV to verify blockade of AMPA channels. The protocol for recording of NMDA receptor-mediated currents was administered after AMPA receptor-mediated currents were maximally blocked. To record NMDA currents, the voltage holding potential was stepped up to +40 mV to eliminate the Mg^{2+} block in NMDA receptors normally seen at rest, and the 2ms 470 nm pulse was applied 3 times, 30 seconds apart.

Figure 2.6 shows average amplitudes, areas, rise times, and decay times of NMDA receptor-mediated currents evoked by thalamostriatal stimulation in MSNs from R6/2 and WT mice. The amplitudes, areas, and rise times were unchanged in the R6/2 mice compared to their WT littermates. Consistent with longer decay times of AMPA currents, NMDA currents of MSNs from R6/2 mice also displayed significantly longer decay times.

As for NMDA currents evoked by thalamostriatal stimulation, amplitudes, areas, and rise times of NMDA currents evoked by corticostriatal stimulation were also not found to be different between MSNs of R6/2 and control mice (Figure 2.7). However, unlike thalamically evoked NMDA currents which showed slower decay kinetics, decay times of cortically-evoked NMDA currents were significantly faster in MSNs from R6/2s than those from WTs.

Decay time of the NMDA receptor-mediated current from each R6/2 MSN was compared to average decay time of all NMDA receptor-mediated currents for WT MSNs and is reported as percent change in Figure 2.8. Decay times of NMDA currents evoked by thalamostriatal stimulation were altered to a significantly greater extent than those evoked by corticostriatal

stimulation [23.43% ± 7.36 (thalamostriatal, n=34) vs. -15.96 ± 4.05 (corticostriatal, n=28), $p<0.001$]. Thalamostriatal and corticostriatal projections synapse onto different regions of the MSN, with thalamic inputs projecting more often onto dendritic shafts and cortical inputs projecting more often onto spines (Smith and Bolam, 1990; Sadikot et al., 1992; Smith et al., 1994; Sidibé and Smith, 1996). The spines and dendritic shafts of MSNs may undergo differential alterations in R6/2 mice which would then result in differential changes of AMPA and NMDA receptor-mediated currents evoked by thalamic versus cortical inputs. Conversely, postsynaptic changes in receptor subunit composition would be expected to result in unique changes to AMPA versus NMDA receptor-mediated currents. Since both AMPA and NMDA receptor-mediated currents evoked by thalamostriatal stimulation display longer decay times, the change in decay times observed at thalamostriatal projections is less likely to occur due to alterations in receptor subunit composition. Therefore, we hypothesize the observed increase in decay times is occurring as a result of presynaptic changes.

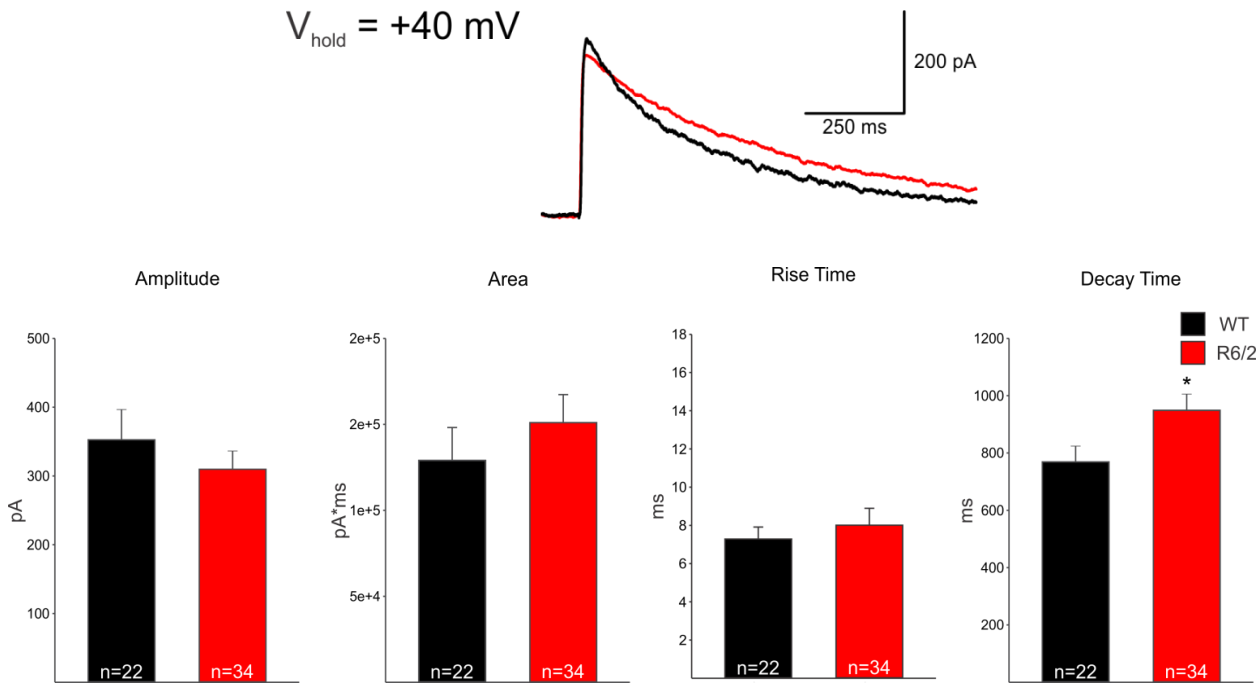

Figure 2.6. NMDA receptor-mediated currents evoked by thalamostriatal stimulation. **(Top)** Representative sample traces of NMDA receptor-mediated responses evoked by thalamostriatal stimulation, recorded in an MSN from a WT mouse (black) and R6/2 mouse (red). **(Bottom)** Average amplitudes, areas, rise times, and decay times (± SE) of NMDA receptor-mediated responses evoked by thalamostriatal stimulation. Ns are shown in each bar. * $p < 0.05$, ** $p < 0.01$, *** $p < 0.001$.

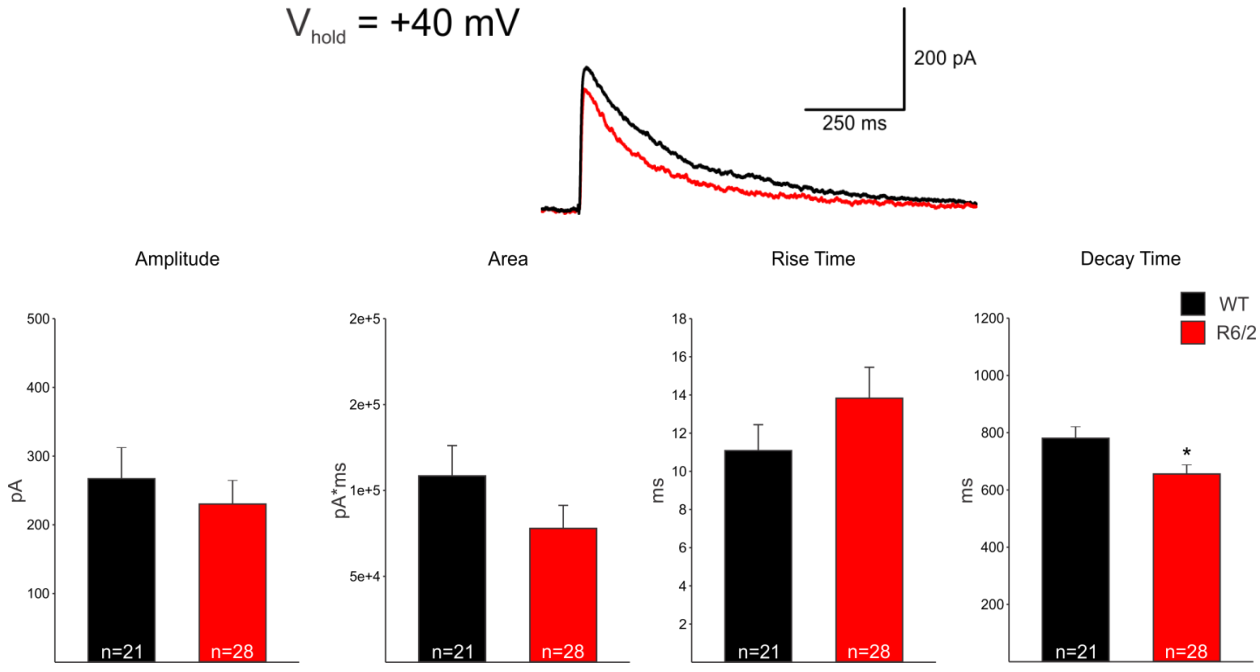

Figure 2.7. NMDA receptor-mediated currents evoked by corticostriatal stimulation. (Top) Representative sample traces of NMDA receptor-mediated responses evoked by corticostriatal stimulation, recorded in an MSN from a WT mouse (black) and R6/2 mouse (red). **(Bottom)** Average amplitudes, areas, rise times, and decay times (± SE) of NMDA receptor-mediated responses evoked by corticostriatal stimulation. Ns are shown in each bar. * $p < 0.05$, ** $p < 0.01$, *** $p < 0.001$.

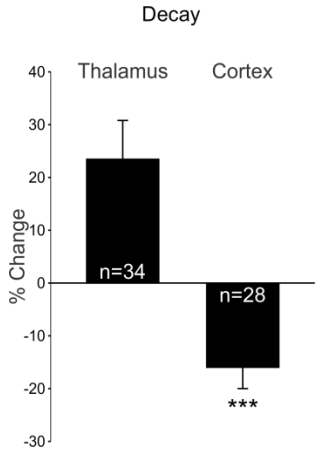

Figure 2.8. Percent change of decay times of NMDA receptor-mediated currents evoked by thalamostriatal and corticostriatal stimulation. Decay time of the NMDA receptor-mediated current from each R6/2 MSN was compared to average decay time of all NMDA receptor-mediated currents for WT MSNs, for responses evoked by thalamostriatal and corticostriatal stimulation. Ns are shown in each bar, error bars indicate ± SE. * $p < 0.05$, ** $p < 0.01$, *** $p < 0.001$.

As noted previously, thalamic and cortical projections utilize distinct vesicular glutamate transporters (Fremeau et al., 2001, 2004; Herzog et al., 2001; Fujiyama et al., 2004; Lei et al., 2013). Differential effects of mHTT on VGLUT2 and VGLUT1 may be in part responsible for the distinct changes of postsynaptic responses observed at thalamostriatal and corticostriatal projections respectively. However, because the most consistent and largest changes observed were in the decay times and not amplitudes, the most probable explanation is alteration of glutamate reuptake.

After glutamate is released, glutamate must be removed from the synaptic cleft by Na^+ dependent high affinity transporters, which becomes even more vital in the case of increased glutamate neurotransmission as seen in HD. Glutamate transporters are located primarily on astrocytes, although neuronal transporters have also been reported (Danbolt, 2001). To date, five glutamate transporters have been described (named as excitatory amino acid transporters [EAAT] in humans): 1) EAAT1/GLAST (glutamate aspartate transporter), 2) GLT1 (glutamate transporter 1)/EAAT2, 3) EAAC1 (excitatory amino acid carrier 1)/EAAT3, 4) EAAT4, 5) EAAT5 (Arriza et al., 1994). GLAST and GLT1 are mainly located on astrocytes, while EAAC1 is solely found on neurons. Extracellular glutamate taken up by astrocytes is metabolized to glutamine, which is released to the extracellular space and taken up by the presynaptic neurons, where it is recycled and again metabolized to glutamate to replenish the transmitter pool (Schousboe et al., 2011). If this process fails and glutamate is not properly removed, the high extracellular concentration of glutamate can result in excitotoxicity. Too much glutamate causes over-stimulation of glutamate receptors, which turns on Ca^{2+} dependent protease activity, oxidative damage, and eventually results in death of the postsynaptic neuron (Estrada-Sánchez

and Rebec, 2012). Failure in glutamate uptake and the resulting excitotoxicity has been shown to occur in HD models (Estrada-Sánchez et al., 2008).

The astrocytic glutamate transporter GLT1 has received a lot of attention in HD and undergoes numerous alterations throughout the progression of the disease. Postmortem tissue shows a reduction of GLT1 mRNA (Arzberger et al., 1997). The caudate nuclei of HD patients show a grade-dependent reduction of GLT1 itself, even when the number of astrocytes is controlled (Faideau et al., 2010). Decreased glutamate uptake is observed in postmortem prefrontal cortex in very early stages of HD (Hassel et al., 2008). Similar changes have been consistently described in HD animal models. R6/2s, as well as other mouse models, display reduced levels of GLT1 mRNA and of the GLT1 protein itself (Liévens et al., 2001; Behrens et al., 2002; Estrada-Sánchez et al., 2009; Faideau et al., 2010). Consistent with the reduction in GLT1, R6/2s, as well as young presymptomatic R6/1s, show a reduction in glutamate uptake (NicNiocaill et al., 2001; Miller et al., 2008). Palmitoylation (the post-translational addition of palmitate to specific cysteine residues), one of the regulatory mechanisms of GLT1 function, is reduced in YAC128 mice, which also show a parallel reduction in glutamate uptake (Huang et al., 2010). Mutant *HTT* expression restricted to astrocytes is sufficient to decrease GLT1 levels, and elicit the HD behavioral phenotype (Bradford et al., 2009). Several mechanisms by which mHTT causes decreased functioning of GLT1 have been proposed. These include altered transcription of GLT1 caused by mHTT fragments and cytoplasmic inclusions (DiFiglia et al., 1997; Liévens et al., 2005), inhibited function caused by accumulated and toxic reactive oxygen species (Trotti et al., 1996; Chen, 2011), and deficient ATP production (Browne and Beal, 2004).

Ceftriaxone, a beta-lactam antibiotic that crosses the blood–brain barrier, increases brain GLT1 expression in mice (Rothstein et al., 2005). R6/2 mice treated with ceftriaxone show

increased striatal GLT1 expression, increased glutamate uptake, and importantly, improvement in some HD behavioral deficits (Miller et al., 2008, 2012). Due to several adverse side effects, clinical use of ceftriaxone requires caution (Bellesi et al., 2009, 2012; Omrani et al., 2009), however the positive implications of increasing functional GLT1 expression in HD patients are noteworthy.

Although GLT1 alterations have received the most attention in HD, alterations in GLAST and EAAC1 are observed as well. GLAST protein levels are reduced in symptomatic R6/2 mice (Liu et al., 2007; Estrada-Sánchez et al., 2009). Expression of mHTT results in reduced astrocytic protein levels of GLAST (Faideau et al., 2010). Cultured cortical neurons expressing exon 1of mHTT display altered function of EAAC1, attributed to deficient glutathione synthesis and increased oxidative damage (Li et al., 2010). More studies examining GLAST and EAAC1 are necessary to associate alterations observed in HD with deficits in these specific transporters. However, in summary, consistent evidence shows a link between altered glutamate reuptake and HD-induced excitotoxicity. Distinct changes of GLT1 and GLAST glutamate transporters on presynaptic membranes of thalamic inputs can explain the observed findings. A reduction in the number or function in one or both of these transporters at thalamostriatal terminals could explain increased decay times of AMPA and NMDA receptor-mediated currents evoked by thalamostriatal stimulation.

The mechanism to explain alterations of AMPA and NMDA receptor-mediated currents evoked by corticostriatal projections must be more complicated as decay times of these currents are not affected in the same pattern. Decay times of AMPA currents are unchanged while decay times of NMDA currents are decreased. Therefore, a series of experiments were conducted to examine glutamate reuptake at both thalamostriatal and corticostriatal projections.

TBOA is a non-selective glutamate transporter blocker with a high affinity for all 5 glutamate transporters. Blocking glutamate transporters impairs glutamate reuptake which 1) impairs glutamate clearing from the synaptic cleft allowing it more time to keep postsynaptic receptors open/active and 2) hinders glutamate recycling by the astrocytes to the presynaptic terminal. NMDA receptor-mediated currents were compared before and 14 minutes after the application of 30 μM TBOA.

NMDA currents evoked by thalamostriatal stimulation showed differential effects in MSNs from R6/2s and WTs when exposed to TBOA bath application (Figure 2.9). TBOA had a very minimal effect on amplitude and decay time of NMDA currents evoked by thalamostriatal stimulation in MSNs from R6/2 and WTs. Average areas were increased in MSNs from R6/2s and WTs, although R6/2s trended to show a higher increase ($p = 0.16$). As expected, shutting off transporters increased decay times of NMDA currents in MSNs from both genotypes.

Time to peak of NMDA currents was significantly increased after TBOA application. As can be seen in the sample traces in Figure 2.9, the increase in time to peak is caused by the rightward shift in the peak. The initial rise time looks very similar in MSNs from both genotypes. However, after the initial immediate almost vertical slope, the slope significantly decreases and the time to reach maximum amplitude is significantly lengthened. The extended time to reach maximum peak drives the observed increase in area. We propose NMDA currents take longer to reach peak in TBOA because as TBOA blocks transporters, glutamate reuptake by astrocytes is impaired. Compromised reuptake decreases the amount of glutamate recycled, thereby decreasing the amount of glutamate available to the presynaptic terminals to be released next time a stimulating blue light pulse is delivered. Therefore the presynaptic terminal takes much longer to release the same amount of glutamate, resulting in the slower time to peak.

TBOA's effect on time to peak was observed in MSNs from both R6/2s and WTs however, it increased the time to peak of NMDA currents recorded in R6/2 MSNs almost 13 times more than those recorded in WT MSNs. Presumably, if the number and function of glutamate transporters is reduced in R6/2s, the few remaining active transporters are handling all the work. Therefore blocking a large portion of glutamate transporters is going to make a much bigger difference and have a much more deleterious effect on glutamate reuptake in the already strained R6/2 system. This finding is consistent with our hypothesis that decay times of AMPA and NMDA receptor-mediated currents are slower in MSNs from R6/2s than WTs because of deficits in glutamate transport, and with previously published data showing decreased receptor expression and function of glutamate transporters in HD mice.

Amplitude, area, time to peak, and decay time of NMDA currents evoked by corticostriatal stimulation were also altered post TBOA application (Figure 2.10). Unlike NMDA currents evoked by thalamostriatal stimulation which showed a very minimal increase in average amplitude, NMDA currents evoked by corticostriatal stimulation showed a slightly larger decrease in average amplitude. Areas, time to peaks, and decay times were increased, with the increase being more prominent in MSNs from R6/2 mice than WT mice.

The differences in the effect of TBOA between MSNs from R6/2 and WT mice were less pronounced in currents evoked by corticostriatal than thalamostriatal stimulation. This parallels the less consistent alterations in decay times of AMPA and NMDA receptor-mediated currents evoked by corticostriatal than thalamostriatal stimulation. Decay times of AMPA currents were unchanged while decay times of NMDA currents were increased at cortical inputs in R6/2s compared to WTs. This suggests that the alterations in kinetics observed at corticostriatal

projections can not be completely attributed to deficits in glutamate reuptake, but are also a result of additional synaptic alterations.

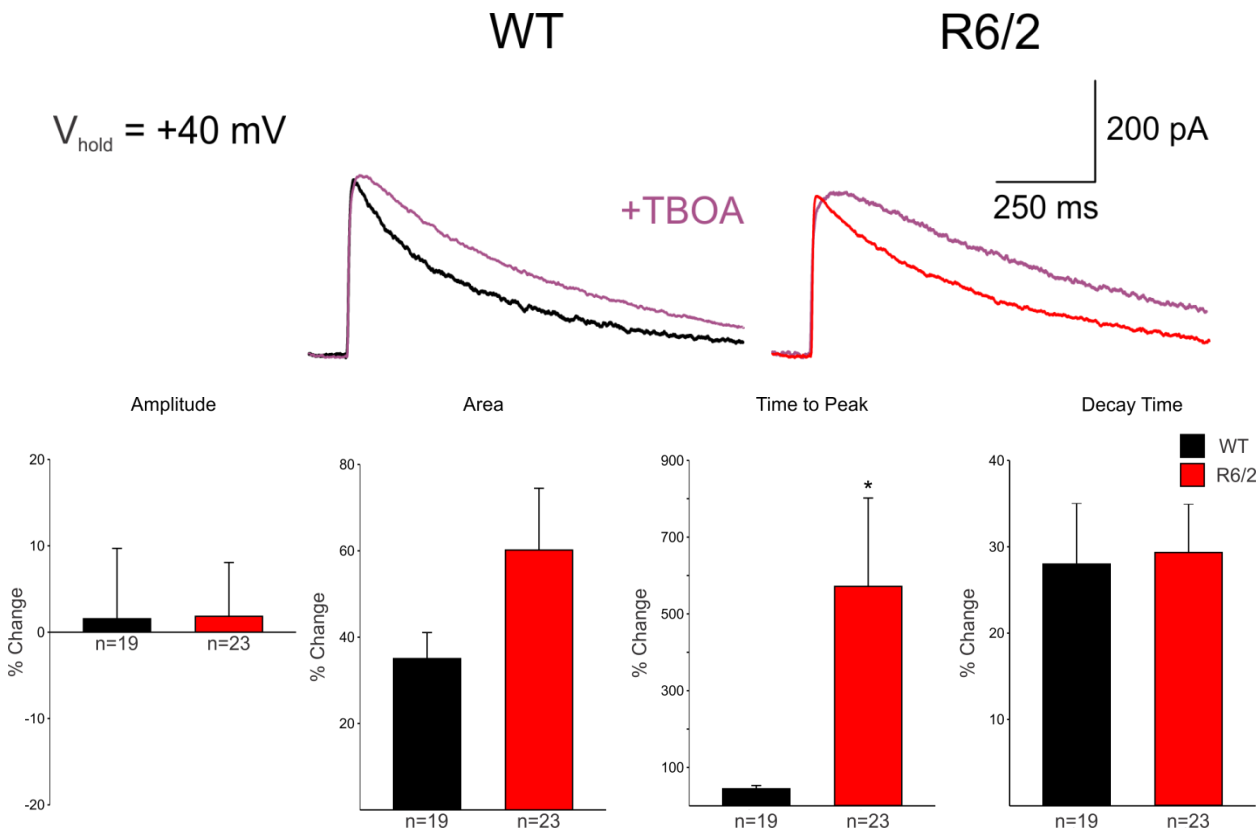

Figure 2.9. Percent change of NMDA receptor-mediated currents evoked by thalamostriatal stimulation in 30 µM TBOA. (Top) Representative sample traces of NMDA receptor-mediated responses evoked by thalamostriatal stimulation, recorded in an MSN from a WT mouse (black) and R6/2 mouse (red), before and after TBOA application (purple). **(Bottom)** Average percent change of amplitudes, areas, rise times, and decay times (± SE) of NMDA receptor-mediated currents evoked by thalamostriatal stimulation 14 minutes post bath application of TBOA. Ns are shown in each bar. * $p < 0.05$, ** $p < 0.01$, *** $p < 0.001$.

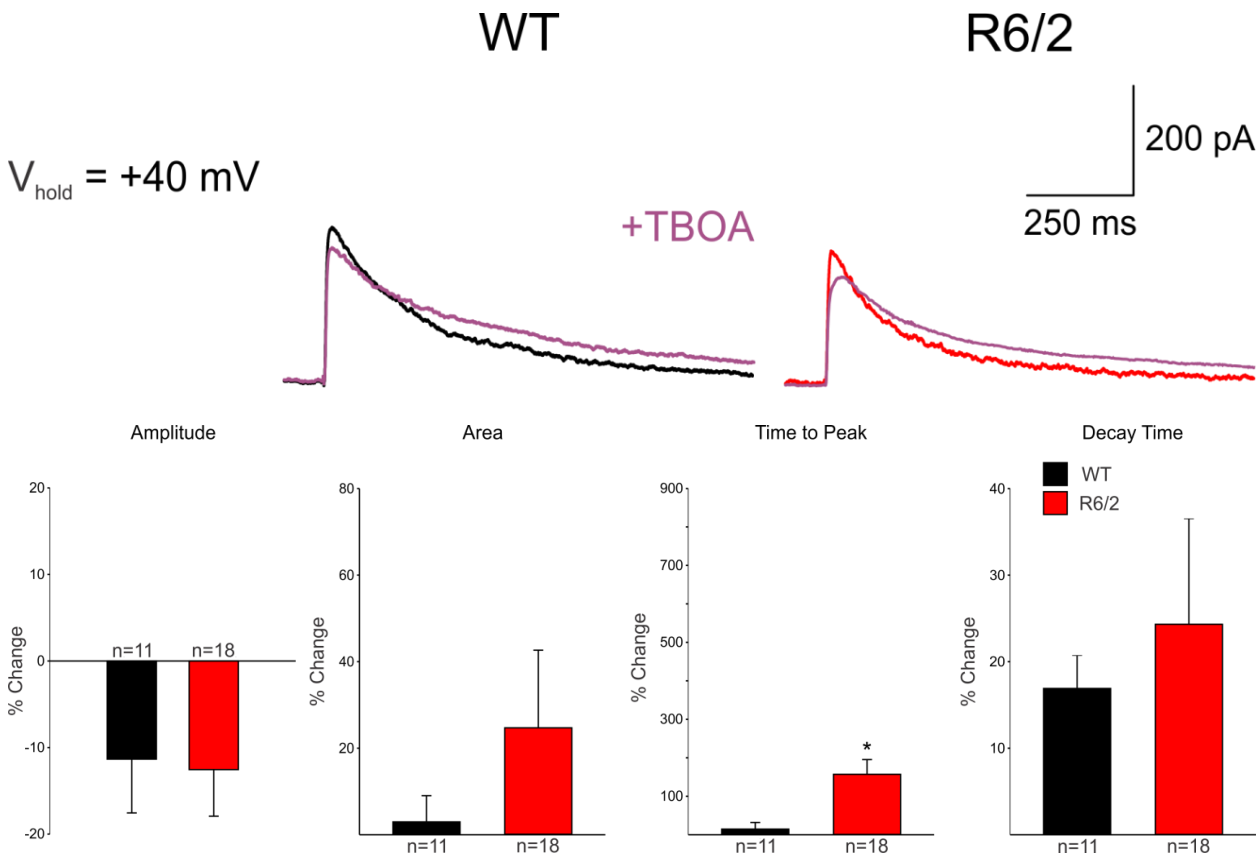

Figure 2.10. Percent change of NMDA receptor-mediated currents evoked by corticostriatal stimulation in 30 µM TBOA. (Top) Representative sample traces of NMDA receptor-mediated responses evoked by corticostriatal stimulation, recorded in an MSN from a WT mouse (black) and R6/2 mouse (red), before and after TBOA application (purple). **(Bottom)** Average percent change of amplitudes, areas, rise times, and decay times (± SE) of NMDA receptor-mediated currents evoked by corticostriatal stimulation 14 minutes post bath application of TBOA. Ns are shown in each bar. * $p < 0.05$, ** $p < 0.01$, *** $p < 0.001$.

One component of the excitotoxicity hypothesis proposes abnormalities in MSN NMDA receptor function. Postsynaptic effects of NMDA receptor activation depend on the location of the receptors. Generally, synaptic NMDA receptors activate cellular survival pathways including BDNF transcription while extrasynaptic receptors activate pathways that lead to apoptosis (Papadia and Hardingham, 2007). Therefore, the densities and locations of NMDA receptors at synaptic sites can influence whether cell survival or cell death pathways are activated. The striata of HD mice exhibit enhanced expression of extrasynaptic NMDA receptors, increased currents, and reduced activation of nuclear cAMP response element-binding protein (Milnerwood et al., 2010). Interestingly, memantine, a compound which preferentially blocks extrasynaptic NMDA receptor activity, reduces neuropathological and behavioral deficits in symptomatic YAC128 mice (Okamoto et al., 2009).

The subunit composition of NMDA receptors also plays a role in the postsynaptic effects of NMDA receptor signaling in HD. Potentiation of NMDA responses by D1 DA receptors is enhanced by blockade of GluN2A subunits and reduced by blockade of GluN2B subunits (Jocoy et al., 2011). Heteromers containing GluN1 plus GluN2B subunits mediate a current that decays three to four times more slowly than receptors composed of GluN1 plus GluN2A subunits (Vicini et al., 1998; Cull-Candy et al., 2001; Erreger et al., 2005). A cell with a higher percentage of GluN2B subunit-containing NMDA receptors with slower decaying currents would result in increased excitation compared to a similar cell with a lower percentage of GluN2B subunit-containing NMDA receptors. Interestingly, GluN2B-type NMDARs are enriched in adult striatal projection neurons relative to other brain regions (Landwehrmeyer et al., 1995; Christie et al., 2000; Li et al., 2003b) .

YAC72 mice demonstrate altered trafficking of NMDA receptor subunits consisting of a shift of GluN1 and GluN2B subunits from internal pools to the plasma membrane and a significantly faster rate of NMDA receptor insertion to the surface (Fan et al., 2007). GluN2B subunit-containing NMDA receptors display increased surface expression, current, and toxicity in MSNs from HD mice (Shehadeh et al., 2006; Fan et al., 2007). Overexpression of GluN2B subunits also increases striatal neuronal loss in HD mice (Heng et al., 2009). In addition, R6/1 mice exhibit alterations in synaptic plasticity and LTD. Blocking GluN2B subunit-containing NMDA receptors reduces the magnitude of LTD in brain slices from these mice, strongly suggesting that LTD deficits may be attributed to alterations of these receptors (Milnerwood et al., 2006). GluN2B-mediated currents are enhanced in cultured striatal neurons (Zeron et al., 2002, 2004) and at corticostriatal synapses in acute slices (Li et al., 2004) from YAC128 mice. Similarly, NMDAR currents are larger in cells coexpressing mHTT and GluN1/GluN2B subunits, but not mHTT and GluN1/GluN2A (Chen et al., 1999).

Aberrant activity of the GluN3A NMDA receptor subunit also has been recently demonstrated in HD (Marco et al., 2013). Through a yet unknown mechanism, mHTT redirects GluN3A subunit-containing NMDA receptors from the intracellular store to the membranes of MSNs by disrupting the activity of the endocytic adaptor protein PACSIN1. Overexpression of GluN3A in WT mice recapitulates synapse degeneration seen in mouse models of HD. Conversely, genetic deletion of GluN3A in YAC128 mice prevents synapse loss, improves motor and cognitive decline, reduces striatal atrophy and neuronal death, and restores enhanced NMDA receptor currents observed in HD (Marco et al., 2013).

Taken together, these data provide evidence that in HD MSNs may be more prone to excitotoxic insults due to increased expression of extrasynaptic NMDA receptors, which can

activate pathways leading to apoptosis and hyperexcitability in response to glutamate release. In addition, overexpression and aberrant activity of GluN2B subunit-containing NMDA receptors can potentiate such effects (Raymond et al., 2011).

To examine alterations of GLUN2B subunit-containing NMDA receptors at thalamostriatal and corticostriatal synapses in the R6/2 HD model, ifenprodil was used. Ifenprodil is a selective GLUN2B subunit-containing NMDA receptor antagonist. NMDA receptor-mediated currents evoked by thalamostriatal or corticostriatal stimulation were compared before and after bath application of 1 μM of ifenprodil (Figure 2.11). As expected, average amplitude of NMDA receptor-mediated currents was decreased as early as 5 minutes post ifenprodil application, and continued to decrease over time. This is true for NMDA receptor-mediated currents evoked by activation of both thalamostriatal and corticostriatal projections (Figure 2.11A). However, there was no difference in the drug's effect on average amplitude, area, or kinetics (not pictured) of NMDA receptor-mediated currents recorded in MSNs from R6/2 versus WT mice (Figure 2.11B). Comparison between responses evoked by thalamostriatal and corticostriatal stimulation after ifenprodil application also did not result in any significant differences.

Despite numerous studies providing evidence for alterations in GLUN2B subunit-containing NMDA receptors, one possible explanation for lack of significant changes observed in the present study may be due to the mouse model examined. Single cell RT-PCR failed to detect any significant decrease in the proportion of cells expressing GLUN2B in the R6/2s compared to WTs (Ali and Levine, 2006). Daily subcutaneous injections of ifenprodil failed to rescue survival, motor declines (measured by rotarod, balance beam task, and activity), or post-mortem striatal volumes, in R6/2 mice. Similar experiments should be conducted in the YAC128

model as this model has shown alterations of GLUN2B subunits electrophysiologically (Raymond et al., 2011).

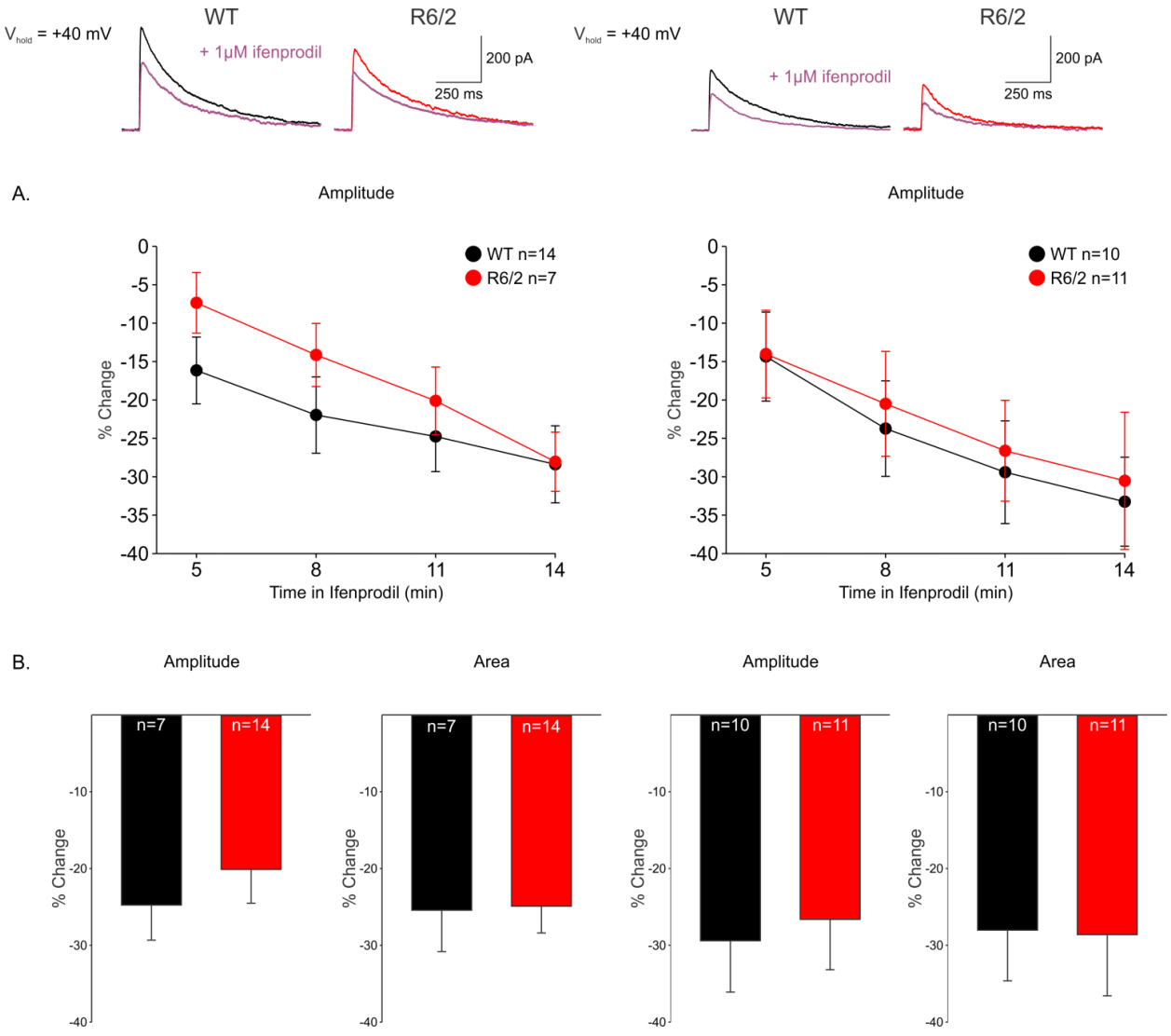

Figure 2.11. Percent change of NMDA receptor-mediated responses in 1 μM ifenprodil. **(Top)** Representative sample traces of NMDA receptor-mediated responses evoked by thalamostriatal (left) and corticostriatal (right) stimulation, recorded in MSNs from a WT mouse (black) and R6/2 mouse (red) before and after bath application of ifenprodil (purple). **(A)** Average percent change of amplitudes (± SE) of NMDA receptor-mediated currents over time evoked by thalamostriatal and corticostriatal stimulation. **(B)** Average percent change of amplitudes and areas (± SE) of NMDA receptor-mediated currents evoked by thalamostriatal and corticostriatal stimulation 11 minutes post bath application of ifenprodil. Ns are shown in each bar. * $p < 0.05$, ** $p < 0.01$, *** $p < 0.001$.

2.6 NMDA/AMPA ratios

Absolute amplitudes of AMPA and NMDA receptor-mediated currents are potentially confounded by the amount of ChR2 expressed. More ChR2 in presynaptic inputs would result in larger EPSCs, and vice versa. Although no differences in viral expression were qualitatively observed between WT and R6/2 mice, because no quantitative comparison was done, this potential confound should still be considered. In addition, possible differences in the amount of ChR2 expressed by thalamostriatal versus corticostriatal projections should be noted when comparing properties of AMPA or NMDA receptor-mediated currents between input types. To account for potential differences in viral expression, NMDA/AMPA ratios were calculated. For each neuron, the amplitude, area, rise, and decay time of the NMDA receptor-mediated current evoked was divided by the amplitude, area, rise time, and decay time measure of the AMPA receptor-mediated current. The NMDA/AMPA ratios of each neuron were than averaged within their appropriate group (WT versus R6/2, and thalamostriatal versus corticostriatal stimulation) and compared. This calculation helped to account for variability in ChR2 expression because when high ChR2 expression resulted in relatively large AMPA currents, it also resulted in proportionally large NMDA currents (or vice versa). Dividing one by the other normalized these parallel differences. The resultant values predicted the relative NMDA to AMPA receptor contribution at each set of inputs.

NMDA/AMPA ratios for amplitude, area, rise time, and decay time at thalamostriatal projections were unchanged in R6/2s compared to their WT littermates (Figure 2.12). Interestingly, ratios of decay times were comparable between R6/2s and WTs, although R6/2s showed increased decay times of both AMPA and NMDA receptor-mediated currents (Figures 2.4 and 2.6). This suggests the decay times of AMPA and NMDA currents are altered in a

similar manner and further support the hypothesis that they are affected due to deficits in glutamate reuptake, rather than alterations in subunit composition of the receptors.

NMDA/AMPA ratios of the amplitude, area, rise and decay times, of responses evoked by corticostriatal stimulation are shown in Figure 2.13. Amplitude and area ratios were similar between MSNs from R6/2 and WT mice. Ratios of rise time were significantly increased in R6/2s compared to WTs suggesting that at cortical synapses, rise times of AMPA and NMDA receptor-mediated currents were affected differently. Rise time changes may be due to postsynaptic mechanisms such as subunit composition variations of AMPA receptors in MSNs of R6/2s compared to WTs. However, due to lack of alterations in other measures of AMPA receptor-mediated currents, a conclusive prediction should not be made. Decay time ratios of NMDA and AMPA currents at corticostriatal projections were unaffected, again highlighting the difference between alterations at thalamostriatal versus corticostriatal projections.

To further assess differences in relative contributions of thalamostriatal and corticostriatal glutamatergic inputs to NMDA and AMPA receptors, NMDA/AMPA amplitude ratios at thalamostriatal versus corticostriatal projections were compared (Figure 2.14). Thalamostriatal projections had larger amplitude NMDA/AMPA ratios compared to corticostriatal projections, in MSNs from both WT (Figure 2.14A) and R6/2 (Figure 2.14B) mice. This difference was due to both larger NMDA currents, and smaller AMPA currents, at thalamostriatal inputs compared to corticostriatal projections (although these individual differences were not significant). This finding agrees with previously published data reporting larger NMDA/AMPA ratios at thalamostriatal projections than corticostriatal projections (Smeal et al., 2008).

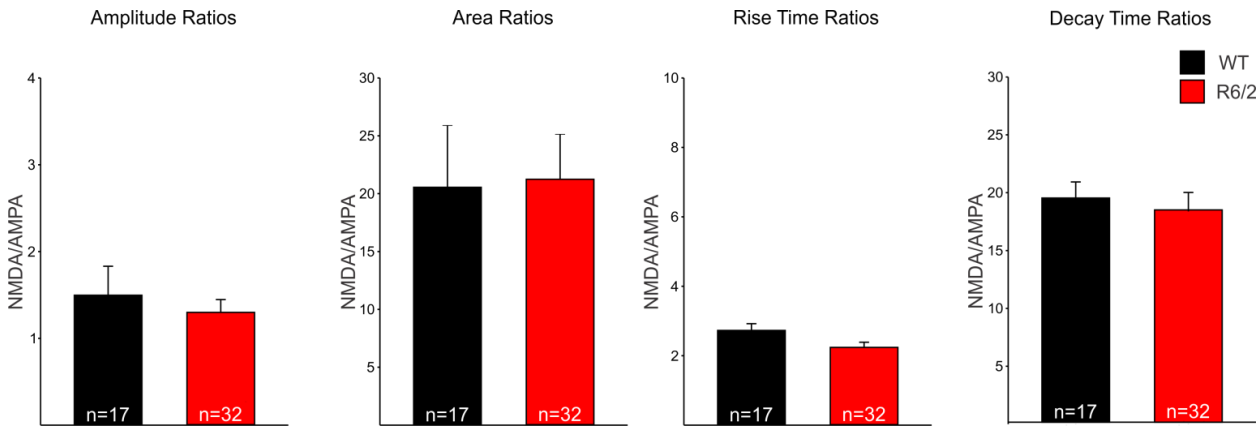

Figure 2.12. NMDA/AMPA ratios evoked by thalamostriatal stimulation. Amplitude, area, rise time, and decay time of the NMDA receptor-mediated current divided by the amplitude, area, rise time, and decay time measure of the AMPA receptor-mediated current evoked by thalamostriatal stimulation, for each neuron, and then averaged across neurons. Ns are shown in each bar, error bars indicate ± SE. * $p < 0.05$, ** $p < 0.01$, *** $p < 0.001$.

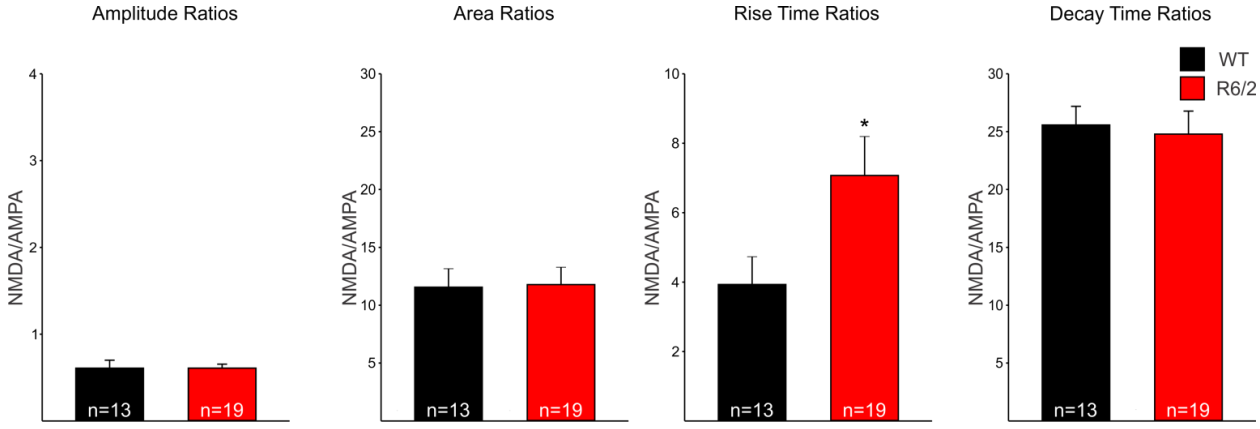

Figure 2.13. NMDA/AMPA ratios evoked by corticostriatal stimulation. Amplitude, area, rise time, and decay time of the NMDA receptor-mediated current divided by the amplitude, area, rise time, and decay time measure of the AMPA receptor-mediated current evoked by corticostriatal stimulation, for each neuron, and then averaged across neurons. Ns are shown in each bar, error bars indicate ± SE. * $p < 0.05$, ** $p < 0.01$, *** $p < 0.001$.

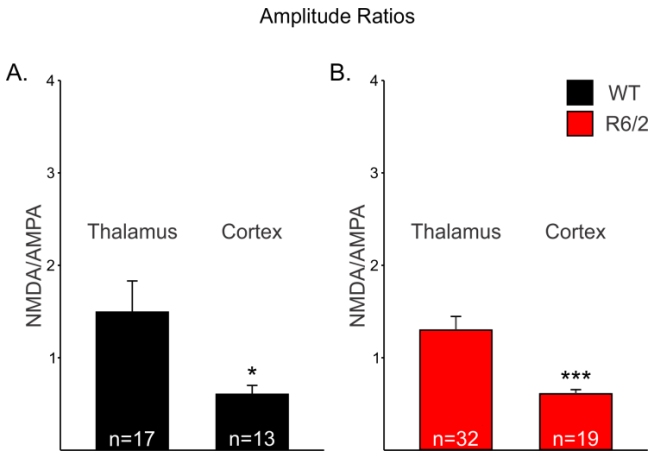

Figure 2.14. NMDA/AMPA ratios evoked by thalamostriatal versus corticostriatal stimulation. (A) Ratios of average amplitudes of NMDA and AMPA receptor-mediated currents evoked by thalamostriatal stimulation compared to ratios of NMDA and AMPA receptor-mediated currents evoked by corticostriatal stimulation in MSNs from WT mice. **(B)** Ratios of average amplitudes of NMDA and AMPA receptor-mediated currents evoked by thalamostriatal stimulation compared to ratios of NMDA and AMPA receptor-mediated currents evoked by corticostriatal stimulation in MSNs from R6/2 mice. Ns are shown in each bar, error bars indicate ± SE. * $p < 0.05$, ** $p < 0.01$, *** $p < 0.001$.

2.7 Paired-pulse ratios (PPRs)

The HD excitotoxicity hypothesis predicts striatal MSNs are degenerating due to increased excitation caused by glutamate. Besides the ideas that MSNs may be hypersensitive to glutamate or that the glutamate has a greater effect due to slower clearing from the synaptic cleft, the amount of glutamate released may also be increased. For example, increased firing of striatal MSNs in R6/2 mice may be explained by increased presynaptic glutamatergic release (Rebec et al., 2006). Direct pathway MSNs in 1-2 month old YAC128 mice and BACHD mice also display increased glutamate release (André et al., 2011). To examine and compare release at thalamostriatal and corticostriatal projections, the paired-pulse protocol (Zucker, 1989) was administered in a selected population of MSN which did not undergo TBOA or ifenprodil treatment. For this set of neurons, the paired-pulse protocol was administered after passive membrane properties were recorded, 10 μM BIC was bath applied, and basic AMPA receptor-mediated currents were recorded. Two 2ms 470 nm pulses were given at 75ms, 100ms, 200ms, and 400ms interpulse intervals. PPR was calculated by dividing the amplitude of the second response (measured from baseline of trace to peak) by the amplitude of the first response (also measured from baseline of trace to peak). In addition, due to the long decay of NMDA receptor-mediated currents, a second set of PPR calculations was performed. PPRs were still calculated by dividing the amplitude of the second response by the amplitude of the first response, but in this case amplitude for the second peak was calculated from beginning of peak to top of peak, instead of from baseline of trace to top of peak. After running the protocol at V_{hold} of -70 mV, NBQX was bath applied, basic NMDA receptor-mediated currents were recorded, and the protocol was once again repeated at V_{hold} of +40 mV.

Results of the paired-pulse stimulation of thalamostriatal projections (amplitudes of responses calculated from baseline to peak) are shown in Figure 2.16. MSNs from WT animals displayed paired-pulse depression at V_{hold} of -70 mV as the second response was smaller than the first. At V_{hold} of +40 mV, no paired-pulse depression or facilitation was observed. In MSNs from R6/2s however, paired-pulse depression was seen at both holding potentials. This result is consistent with previously published data which found that thalamostriatal synapses display a high probability of release to an initial stimulus which declines rapidly with successive stimulation (Ding et al., 2008), a very fitting property for the role of thalamostriatal projections in transmitting precisely timed sporadic signals. At both holding potentials, PPRs were significantly smaller in R6/2s compared to WTs at longer interpulse intervals (200 and 400ms). Smaller PPRs indicate stronger paired-pulse depression in R6/2s and suggest an increased probability of release at thalamostriatal projections in R6/2 mice compared to WT mice.

PPRs calculated by measuring responses from bottom to top of peak, instead of from baseline to peak, showed a similar trend at V_{hold} of +40 mV. PPRs were [0.26 ± 0.03 (WT, n=16) vs. 0.39 ± 0.13 (R6/2, n=5) at 75ms; 0.39 ± 0.04 (WT, n=16) vs. 0.40 ± 0.13 (R6/2, n=6) at 100ms; 0.62 ± 0.12 (WT, n=15) vs. 0.41 ± 0.09 (R6/2, n=6) at 200ms; and 0.63 ± 0.05 (WT, n=15) vs. 0.46 ± 0.11 (R6/2, n=6) at 400ms]. None of these differences were significant, however MSNs from R6/2s showed a trend towards decreased PPRs at all interpulse intervals, and almost reached significance at 400ms (p=0.07).

Probability of release at corticostriatal synapses was also tested at both holding potentials (Figure 2.16, amplitudes of responses calculated from baseline to peak). Paired-pulse stimulation of corticostriatal projections produced very different curves than paired-pulse stimulation of thalamostriatal projections. PPRs at thalamostriatal projections decreased consistently with

increased interpulse intervals. However, PPRs at corticostriatal projections formed a bell-shaped curve as interpulse intervals were increased. At V_{hold} of -70 mV, in MSNs from both WT and R6/2 mice, paired-pulse depression was seen at shorter interpulse intervals (75 and 100ms), as well as the long interpulse interval (400ms), while a 200ms interpulse interval produced potentiation. At V_{hold} of +40 mV, paired-pulse potentiation was observed at all tested interpulse intervals. However, similar to the PPR curve at V_{hold} of -70 mV, max PPRs were recorded at an interpulse interval of 200ms. There were no significant differences between PPRs of MSNs from WTs and R6/2s at either of the holding potentials.

PPRs calculated by measuring responses at V_{hold} of +40 mV from bottom to top of peak, instead of from baseline to peak, showed a similar trend. PPRs were [0.28 ± 0.04 (WT, n=8) vs. 0.24 ± 0.04 (R6/2, n=7) at 75ms; 0.35 ± 0.05 (WT, n=9) vs. 0.38 ± 0.07 (R6/2, n=8) at 100ms; 0.70 ± 0.09 (WT, n=9) vs. 0.68 ± 0.06 (R6/2, n=8) at 200ms; and 0.65 ± 0.06 (WT, n=9) vs. 0.68 ± 0.04 (R6/2, n=8) at 400ms]. There were no significant differences between PPRs of MSNs from WTs and R6/2s at none of the four interpulse intervals.

In summary, compared to WTs, R6/2s display an increased probability of release at thalamostriatal projections, and no change in probability of release at corticostriatal projections. According to a previous report, in very young presymptomatic Q140 mice, 40% of thalamostriatal axodendritic and 20% of thalamostriatal axospinous terminals are lost, while corticostriatal projections are spared (Deng et al., 2013). Perhaps the increased release observed at thalamic inputs is a compensatory mechanism to make up for the lost thalamic inputs.

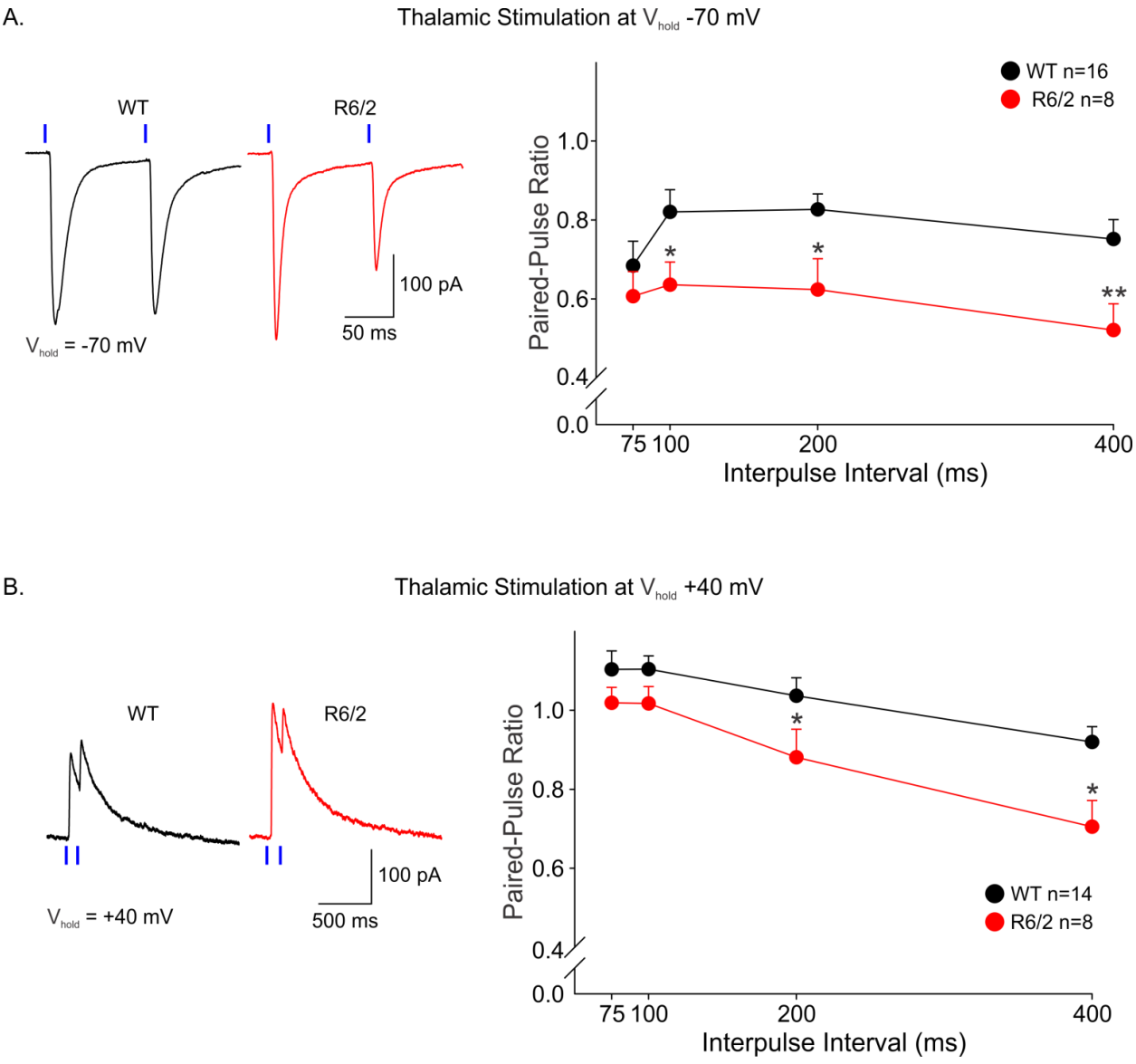

Figure 2.15. AMPA and NMDA receptor-mediated currents evoked by paired-pulse thalamostriatal stimulation. Representative sample traces **(left)** and average paired-pulse ratios ± SE **(right)** of EPSCs evoked by thalamostriatal stimulation at **(A)** V_{hold} = -70 mV and **(B)** V_{hold} = +40 mV. Ns are shown in the inset of each line graph. * $p < 0.05$, ** $p < 0.01$, *** $p < 0.001$.

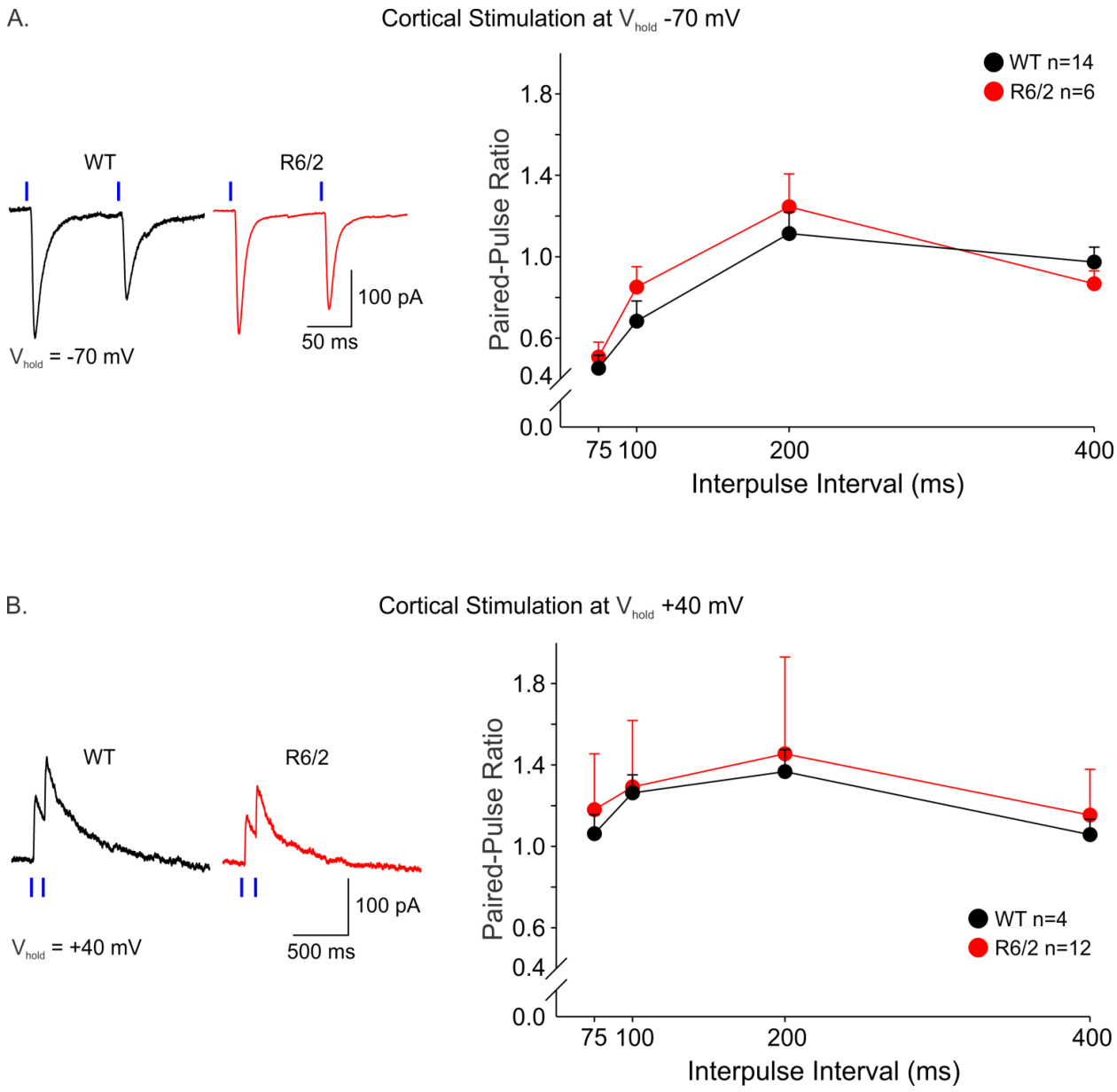

Figure 2.16. AMPA and NMDA receptor-mediated currents evoked by paired-pulse corticostriatal stimulation. Representative sample traces **(left)** and average paired-pulse ratios ± SE **(right)** of EPSCs evoked by corticostriatal stimulation at **(A)** V_{hold} = -70 mV and **(B)** V_{hold} = +40 mV. Ns are shown in the inset of each line graph. * $p < 0.05$, ** $p < 0.01$, *** $p < 0.001$.

2.8 LCIs

Although LCIs makeup only ~2% of the striatal neuronal population, they carry an important role in modulating the functional status of MSNs (Pisani et al., 2007; Ding et al., 2010). LCIs have been implicated in various striatal functions including motor control, associate learning, reward, and plasticity (Hanley and Bolam, 1997; Shen et al., 2005; Exley and Cragg, 2008; Shuen et al., 2008). Thalamostriatal projections play a large role in modulating and controlling the activity of LCIs. In fact, the majority of excitatory glutamatergic inputs to LCIs arise from the CMPf and less so from the cortex (Smith et al., 2004). Although LCIs are relatively spared from degeneration in HD, they show decreased acetylcholine release in HD mouse models (Vetter et al., 2003; Smith et al., 2006; Farrar et al., 2011). Sparse cortical inputs in conjunction with NMDA currents much smaller than those of MSNs (Cepeda et al., 2001b) may be the reasons LCIs are spared in HD. Therefore, AMPA and NMDA receptor-mediated currents evoked by thalamostriatal and corticostriatal stimulation were examined. The following data have been published (Holley et al., 2015)

An average MSN soma is 13.90 ± 0.23μm in diameter while an average LCI is 18.33 ± 0.34 μm in diameter (Guo et al., 2015). The significant size difference makes LCIs easy to identify in a striatal slice through IR imaging (Figure 2.17A). LCIs recorded in cell-attached mode exhibit tonic firing with an average frequency of approximately 1-3 Hz (Figure 2.17B) (Holley et al., 2015). This characteristic tonic firing is regulated by behavioral context, exhibiting pauses of several hundred milliseconds following presentation of salient sensory stimuli (Morris et al., 2004; Apicella, 2007). It also helps to identify LCIs and to distinguish them from MSNs which do not show spontaneous firing in the slice.

Table 2.2 lists the average membrane capacitance, input resistance, time constant, and holding current of LCIs from WT and R6/2 mice recorded at V_{hold} of -70 mV. R6/2s do not show a significant difference between any of the measured passive membrane properties, although they do show a trend for increased membrane input resistance ($p = 0.07$). This suggests LCIs from R6/2 mice are smaller in size and more electrotonically compact than LCIs from WT mice and is consistent with reduced somatic area of R6/2 LCIs determined by ChAT immunohistochemistry (Holley et al., 2015). LCIs have larger average input resistance and smaller average time constants compared to MSNs. Note the membrane properties of LCIs are much less affected than those of MSNs (Table 2.1), consistent with LCIs being spared in HD.

Average amplitudes, areas, rise times, and decay times of AMPA and NMDA receptor-mediated currents recorded from LCIs evoked by activation of thalamostriatal projections are shown in Figure 2.18A and Figure 2.18B respectively. Average amplitudes of both AMPA and NMDA currents were slightly increased in LCIs from R6/2s, however these differences were not statistically significant. Similarly, average area, rise time, and decay time of NMDA currents in LCIs of R6/2s were slightly increased but these changes were also not statistically significant.

LCIs patched in slices from both WT and R6/2 mice injected in the cortex failed to produce a response. After repeated attempts to evoke a response from 8 LCIs in 5 mice, examination of AMPA and NMDA receptor-mediated currents in LCIs evoked by corticostriatal stimulation was terminated. This result is not surprising as LCIs receive the majority of their inputs from thalamic projections (Smith et al., 2004).

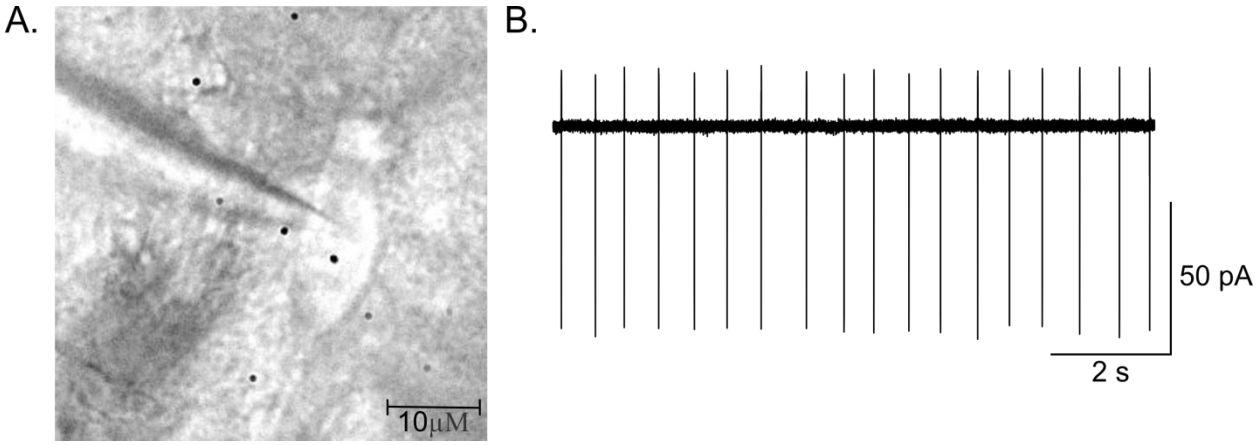

Figure 2.17. Identifying LCIs. (A) IR image of an LCI in a striatal slice. LCIs are large in size and easy to distinguish from striatal MSNs. **(B)** Representative trace of a WT LCIs characteristic tonic firing in cell-attached mode.

Table 2.2: Passive membrane properties of LCIs from WT and R6/2s.

	WT: CMPf	R6/2: CMPf
Cm (pF)	73.71 ± 3.10 (10)	79.86 ± 6.62 (7)
Rm (MΩ)	137.14 ± 14.79 (10)	187.20 ± 20.43 (7) p = 0.07
Tau (ms)	0.96 ± 0.12 (10)	1.20 ± 0.13 (7)
Hold (pA)	-102.49 ± 10.15 (10)	-83.41 ± 24.26 (7)

Values are mean ± SE (number of cells). * $p < 0.05$, ** $p < 0.01$, *** $p < 0.001$.

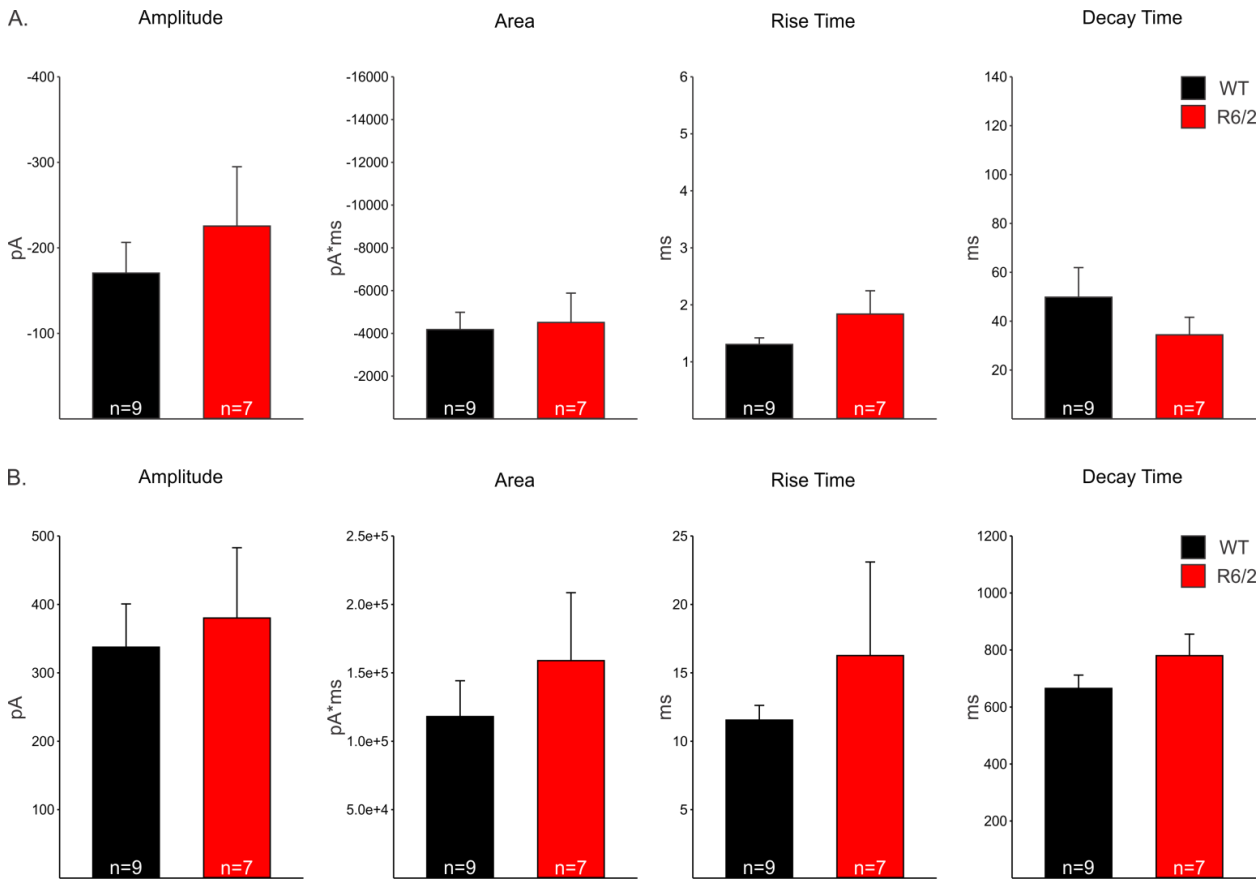

Figure 2.18. AMPA and NMDA receptor-mediated currents of LCIs evoked by thalamostriatal stimulation. Average amplitudes, areas, rise times, and decay times (± SE) of **(A)** AMPA receptor-mediated responses and **(B)** NMDA receptor-mediated responses evoked by thalamostriatal stimulation. Ns are shown in each bar. * $p < 0.05$, ** $p < 0.01$, *** $p < 0.001$.

2.9 Conclusions

Optogenetics allowed us to specifically activate thalamostriatal and corticostriatal projections in MSNs of R6/2 and WT mice. Alterations of AMPA and NMDA receptor-mediated currents occurring at the two sets of projections could then be separated. AMPA and NMDA currents evoked by thalamostriatal stimulation showed longer decay times in MSNs from R6/2 mice when compared to MSNs from WT mice. Examination of NMDA currents before and after TBOA, the glutamate transporter blocker, suggested the lengthened decay times may be caused by deficits in glutamate reuptake at thalamostriatal projections in R6/2s. PPR data also suggested increased probability of glutamate release from thalamic inputs to MSNs from R6/2s compared to MSNs from WTs. Increased glutamate release would lead to increased glutamate in the synaptic cleft and therefore may also contribute to longer decay times. Data from ifenprodil studies did not support alterations in subunit composition of NMDA receptors, specifically in the proportion of NMDA receptors containing GLUN2B subunits. In addition, LCI recordings did not show any alterations in AMPA or NMDA receptor-mediated currents, consistent with sparing of these non-GABAergic interneurons in HD.

Recordings of AMPA and NMDA currents evoked by corticostriatal stimulation showed that corticostriatal and thalamostriatal projections undergo differential alterations in R6/2 mice. AMPA currents exhibited faster rise times and NMDA currents exhibited faster decay times in MSNs from R6/2 mice when compared to MSNs from WT mice. Blocking glutamate transporters lead to disparate responses in MSNs from R6/2 and WT mice suggesting there are alterations in glutamate reuptake at cortical inputs. However, the discrepancy between TBOA's effect on responses of MSNs from R6/2s and WTs was much smaller at corticostriatal than thalamostriatal projections, suggesting aberrant glutamate reuptake may be more prominent at

thalamostriatal projections. In conjunction, probability of release was found to be unaffected. Proportion of GLUN2B containing NMDA receptors was not altered at cortical inputs.

Comparison of NMDA/AMPA ratios suggested a higher contribution of NMDA receptors at thalamic inputs compared to cortical inputs. This is true for both R6/2 and WT mice. A higher relative proportion of NMDA receptors at thalamostriatal-MSN synapses, longer decay times of AMPA and NMDA receptor-mediated currents, and increased glutamate release, support the role of thalamostriatal projections in excitotoxicity. In addition, this evidence begins to provide a mechanistic explanation for early degeneration of thalamostriatal projections observed in the Q140 mouse (Deng et al., 2013).

Chapter 3

Alterations of Thalamostriatal Projections in Direct and Indirect Pathway Projecting MSNs in the R6/2 Mouse Model of Huntington's Disease

3.1 Introduction

Striatal MSNs are segregated into two subpopulations based on the DA receptors and neuropeptides they express (Gerfen, 1992; Bolam et al., 2000), as well as the target sites of their projections (Shuen et al., 2008). Direct pathway MSNs express D1 DA receptors and increase excitatory firing of the thalamus onto the cortex, which results in increased cortical activity. Indirect pathway MSNs express D2 DA receptors and activity of these neurons decreases excitatory firing of the thalamus onto the cortex and decreases cortical activity (Albin et al., 1989; Alexander and Crutcher, 1990; Gerfen et al., 1990; Mink, 1996). Activation of the direct pathway facilitates movement while activation of the indirect pathway suppresses movement (Albin et al., 1989; Alexander and Crutcher, 1990; DeLong, 1990). Optogenetic activation of direct pathway MSNs increases locomotion while activation of the indirect pathway MSNs induces increased freezing, bradykinesia, decreased locomotion, and results in a Parkinsonian-like state (Kravitz et al., 2010). Balance in the activity of these opposing pathways is critical for precise motor control.

When this balance is disturbed by HD pathogenesis, undesired movement (chorea) or inability to move (akinesia) results (Galvan et al., 2012). Differential alteration of the two pathways has been shown in HD mouse models. The increased sEPSC frequency seen in MSNs from presymptomatic 1-1.5 month old YAC128 mice is more pronounced in direct versus indirect pathway projecting MSNs (Joshi et al., 2009; André et al., 2011) and is most likely due to increased glutamate release onto direct pathway-projecting MSNs (André et al., 2011). Similarly, the decrease in sEPSC frequency in MSNs from symptomatic 12 month old YAC128 mice is more evident in direct versus indirect pathway projecting MSNs, and shown to be due to decreased glutamate release onto these neurons at the late symptomatic stage (André et al.,

2011). Conversely, the increase in sIPSC frequency is more evident in indirect pathway MSNs and less so in direct pathway MSNs (André et al., 2011; Cepeda et al., 2013). DA modulation has also been shown to be affected differently in the direct versus indirect pathway projecting striatal neurons (André et al., 2011).

Alterations of thalamostriatal projections onto direct versus indirect pathway projecting MSNs were compared in R6/2 mice. Treating direct and indirect pathway-projecting MSNs as one population risks masking or overlooking an effect that is specific to one of the two subtypes of MSNs. Conversely, pathway specific differences may be driving the statistically significant alterations observed in the grouped data. Therefore, R6/2 mice expressing tDTomato under the D1 DA promoter were used to identify direct pathway MSNs during electrophysiology experiments described in this chapter. Fluorescent cells were treated as D1 receptor-expressing (direct pathway projecting MSNs) and non-fluorescent cells were treated as D2 receptor-expressing (indirect pathway projecting MSNs).

3.2 Membrane properties

Membrane properties of MSNs recorded from each subgroup of mice are shown in Table 3.1. D1 MSNs from R6/2s had a smaller average membrane capacitance than D1 MSNs from WTs. This difference was not observed when D2 MSNs from R6/2s were compared to D2 MSNs from WTs. The two-way ANOVA test indicated a statistically significant difference in input resistance across genotype; MSNs from R6/2 mice had a higher membrane input resistance than MSNs from WT mice, consistent with grouped data in Table 2.1 and previously published data (Klapstein et al., 2001). D2 MSNs from R6/2s had higher input resistance than D1 MSNs from R6/2s. D2 MSNs from R6/2s had significantly longer time constants than D2 MSNs from WTs. D1 MSNs showed a similar trend, however this difference was not significant. From the

membrane properties alone, it is apparent that some distinct differences exist in the way HD affects the two subpopulations of neurons.

Table 3.1: Passive membrane properties of D1 and D2 MSNs from WT and R6/2s.

	D1 WT	D1 R6/2	D2 WT	D2 R6/2
Cm (pF)	97.97 ± 8.81 (9)	75.96 ± 2.71 (13) *	80.11 ± 5.40 (9)	74.25 ± 2.26 (18)
Rm (MΩ)	59.15 ± 3.30 (8)	120.85 ± 4.71 (12) ***	57.30 ± 4.68 (9)	173.27 ± 16.72 (17) *** ##
Tau (ms)	1.46 ± 0.16 (9)	1.63 ± 0.13 (13)	1.24 ± 0.09 (9)	1.52 ± 0.09 (18) *
Hold (pA)	-78.93 ± 11.82 (9)	-47.48 ± 13.56 (13)	-72.69 ± 35.19 (9)	-32.69 ± 8.22 (18)

* WT versus R6/2, within MSN subtype
# D1 versus D2, within genotype

Values are mean ± SE (number of cells). * $p < 0.05$, ** $p < 0.01$, *** $p < 0.001$.

3.3 AMPA and NMDA receptor-mediated currents

Optogenetically evoked AMPA and NMDA receptor-mediated currents were recorded according to the same protocol outlined in Chapter 2.4. AMPA currents were measured at V_{hold} = -70 mV in 10 µM BIC and NMDA currents were measured at V_{hold} = +40 mV, in 10 µM BIC, and in 10 µM NBQX. Average decay times of AMPA and NMDA receptor-mediated currents were increased. When D1 and D2 decay times were grouped together and compared across genotype, the decay times of AMPA currents showed a trend to be increased (Figure 3.1A). The two-way ANOVA showed a significant increase for decay times of NMDA receptor-mediated currents across genotype (Figure 3.1B). This replicates the finding presented in Chapter 2 (Figure 2.4 and Figure 2.6). Comparing the MSN subtypes individually uncovers that this group effect was driven more strongly by alterations in direct versus indirect pathway neurons.

AMPA and NMDA receptor-mediated currents evoked by thalamostriatal stimulation were affected differently in D1 compared to D2 MSNs from R6/2 mice (Figure 3.2 and Figure 3.3). Across all 4 groups (D1 WT, D1 R6/2, D2 WT, D2 R6/2), a two-way ANOVA showed no differences in average amplitude or rise time of AMPA or NMDA currents. This is consistent

with the grouped data reported in Chapter 2. However, although not statistically significant, AMPA receptor-mediated currents recorded in D1 R6/2 MSNs tended to have larger areas ($p = 0.26$) compared to D1 WT MSNs. Similarly, the difference in area of NMDA receptor-mediated currents was not significant, however, R6/2 D1 MSNs showed a trend for increased area compared to WT D1 MSNs ($p = 0.09$). The average areas of AMPA-receptor mediated currents between R6/2 D2 and WT D2 MSNs were similar.

D1 R6/2 MSNs had longer decay times of AMPA ($p = 0.12$) and NMDA receptor-mediated currents evoked by thalamostriatal stimulation. Consistent with the hypothesis presented in Chapter 2 that longer decay times of AMPA and NMDA currents are caused by deficits in glutamate reuptake from the synaptic cleft by astrocytes, this finding further suggests that glutamate uptake is more affected at inputs terminating on D1 MSNs than those terminating on D2 MSNs.

Longer decay times of direct pathway projecting MSNs suggest these neurons could be undergoing prolonged periods of excitation. Increased excitation of D1 MSNs is consistent with the increased sEPSC frequency found in these neurons in presymptomatic and symptomatic YAC128 mice (André et al., 2011). Prolonged excitation of D1 MSNs would result in increased activity of the direct pathway and therefore increased motor activity consistent with chorea symptoms observed in HD patients.

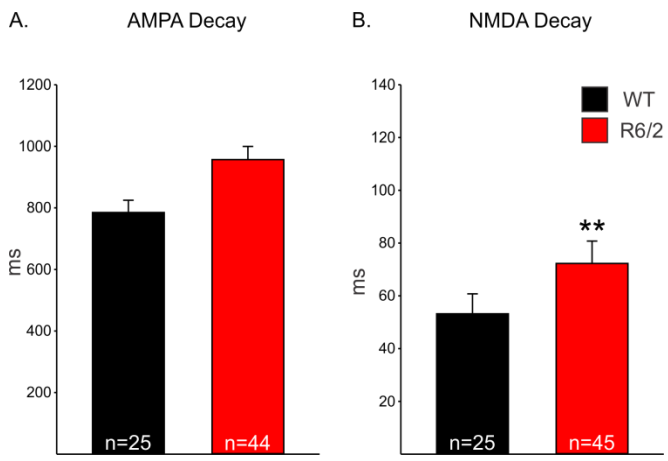

Figure 3.1. Average decay times of AMPA and NMDA receptor-mediated currents evoked by thalamostriatal stimulation. Decay times (± SE) of AMPA and NMDA receptor-mediated currents of grouped D1 and D2 WT MSNs compared to decay times of grouped D1 and D2 R6/2 MSNs. Ns are shown in each bar. * $p < 0.05$, ** $p < 0.01$, *** $p < 0.001$.

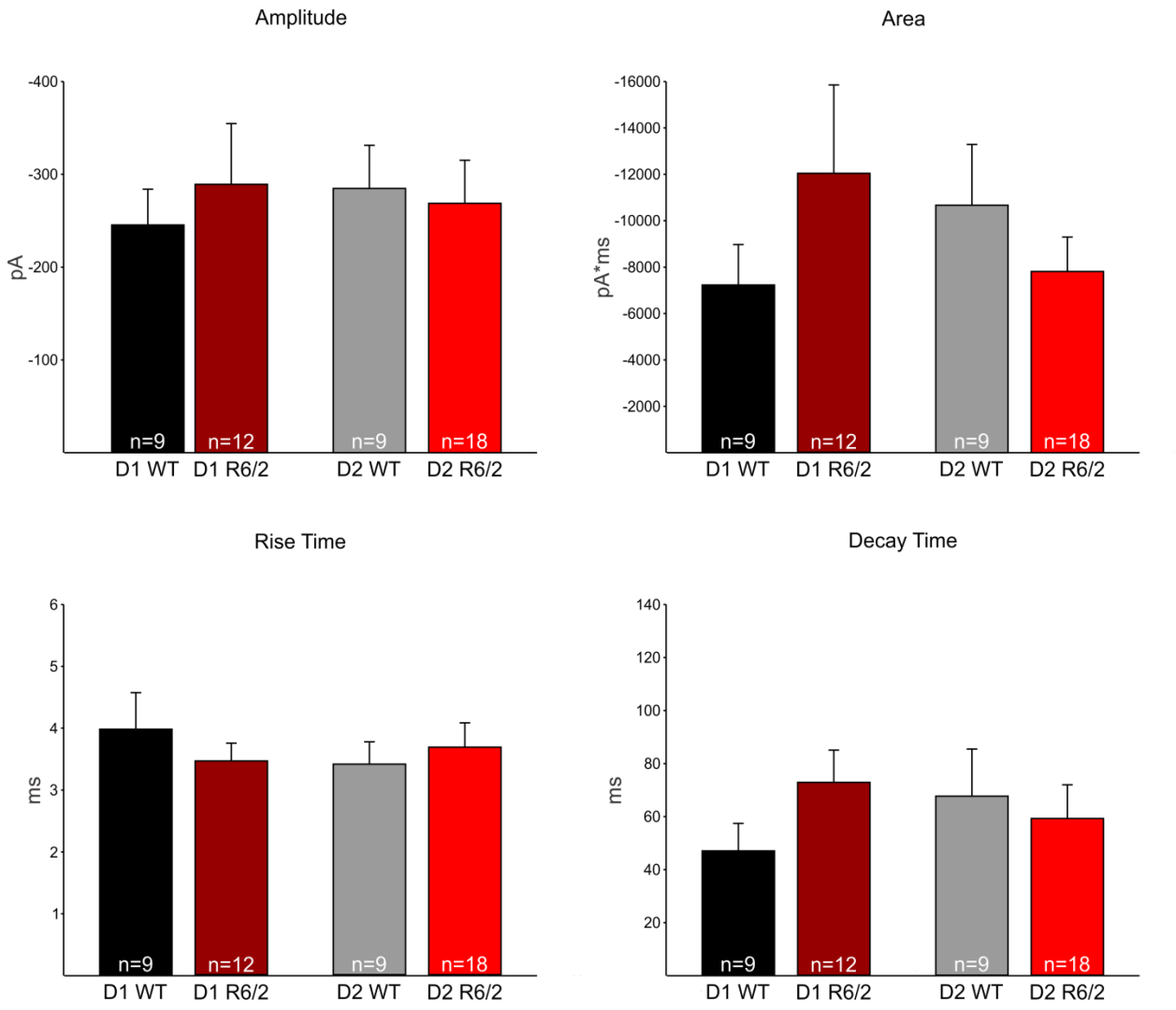

Figure 3.2. AMPA receptor-mediated currents evoked by thalamostriatal stimulation in D1 versus D2 MSNs. Average amplitudes, areas, rise times, and decay times (± SE) of AMPA receptor-mediated responses evoked by thalamostriatal stimulation compared in D1 and D2 WT versus D1 and D2 R6/2 MSNs. Ns are shown in each bar. * $p < 0.05$, ** $p < 0.01$, *** $p < 0.001$.

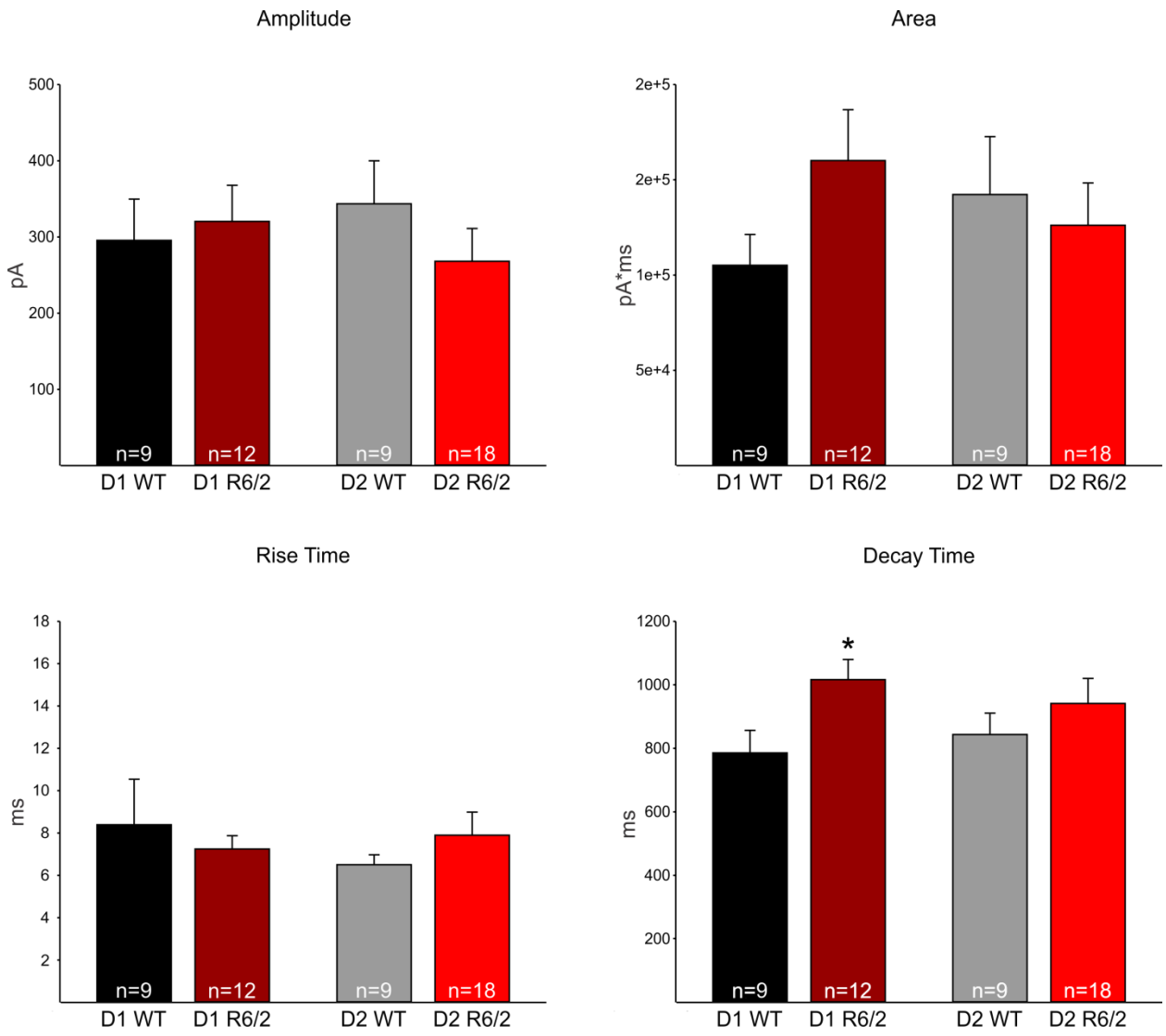

Figure 3.3. NMDA receptor-mediated currents evoked by thalamostriatal stimulation in D1 versus D2 MSNs. Average amplitudes, areas, rise times, and decay times (± SE) of NMDA receptor-mediated responses evoked by thalamostriatal stimulation compared in D1 and D2 WT versus D1 and D2 R6/2 MSNs. Ns are shown in each bar. * $p < 0.05$, ** $p < 0.01$, *** $p < 0.001$.

3.4 NMDA/AMPA ratios

NMDA/AMPA ratios were calculated to compare the relative contribution of AMPA and NMDA receptor-mediated currents across genotype in direct versus indirect pathway MSNs (Figure 3.4). Ratios of amplitudes and rise times were similar for all 4 groups. However, differences were seen in area and decay time ratios.

Ratios of areas of AMPA and NMDA receptor-mediated currents were affected differently in the R6/2s at direct and indirect pathway MSNs. R6/2 D1 MSNs showed a trend for smaller area ratios when compared to WT D1 MSNs ($p = 0.13$). However, R6/2 D2 MSNs showed a trend for larger area ratios when compared to WT D2 MSNs ($p = 0.06$). In addition, WT D2 MSNs had smaller area ratios than WT D1 MSNs ($p = 0.11$), while R6/2 D2 MSNs had larger area ratios than R6/2 D1 MSNs ($p = 0.08$).

Decay time ratios of AMPA and NMDA receptor-mediated currents showed a very similar pattern as the area ratios. R6/2 D1 MSNs showed a trend for smaller decay ratios when compared to WT D1 MSNs ($p = 0.26$). However, R6/2 D2 MSNs showed a trend for larger decay ratios when compared to WT D2 MSNs ($p = 0.26$). There was a trend for R6/2 D2 MSNs to have larger area ratios than R6/2 D1 MSNs ($p = 0.09$).

The opposing changes occurring in the R6/2s at the direct versus indirect pathway MSNs are important to note. Firstly, splitting up the data by MSN subtype uncovers an effect that was concealed in the grouped data in Chapter 2 (Figure 2.12). The grouped data showed no differences in area or decay NMDA/AMPA ratios between WTs and R6/2s. However, the data presented here suggest the grouped data did not differ because the area and decay time ratios of the two MSN subpopulations are altered in opposite directions; the changes canceled themselves out. Secondly, these competing alterations may be the brain's way of compensating for the HD

alterations occurring and its way to maintain the inherent and desired balance that is required of this circuit. The brain may be aiming to stabilize and compensate for the increased excitation to one subpopulation of MSNs by decreasing excitation to another.

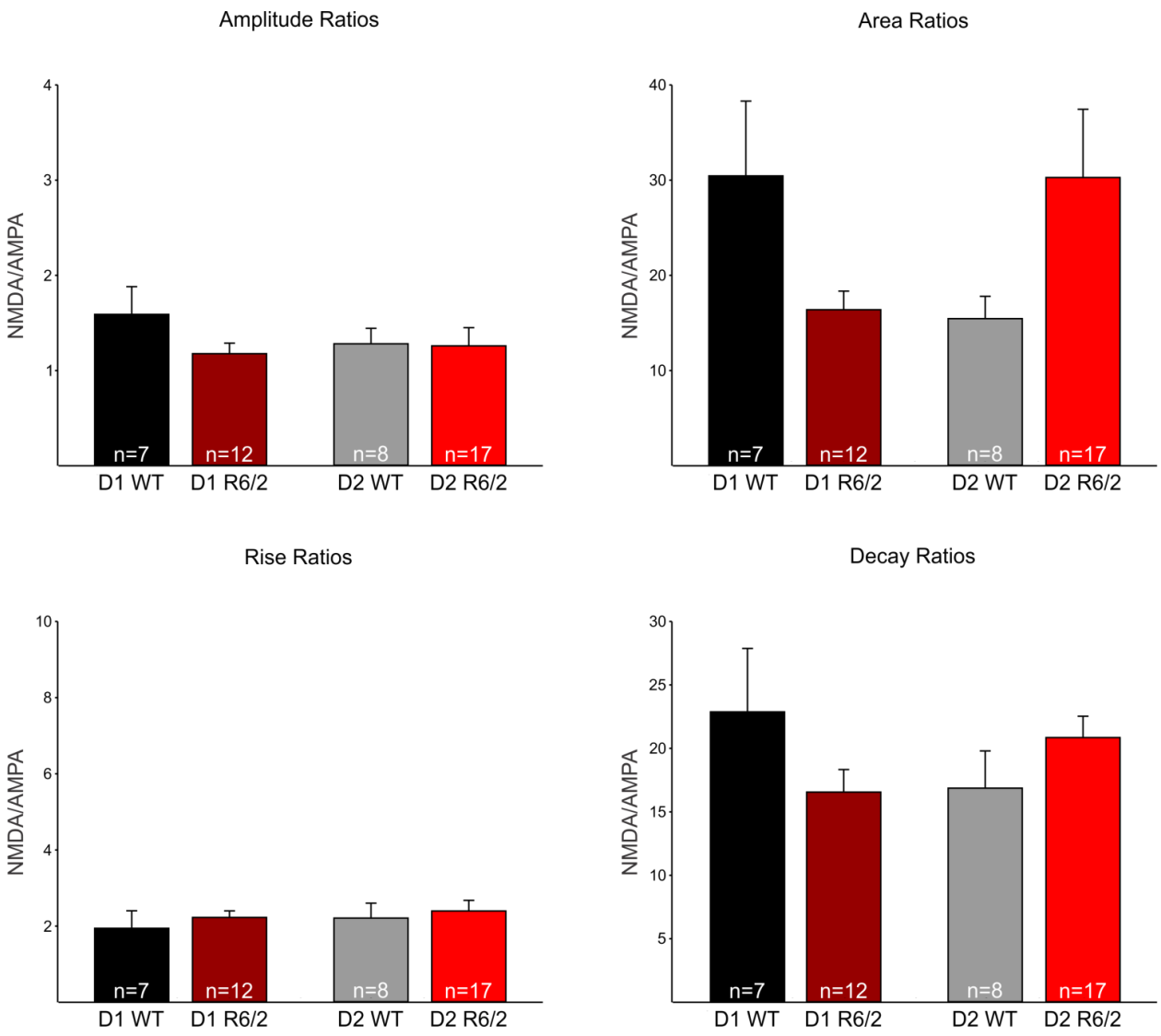

Figure 3.4. NMDA/AMPA ratios evoked by thalamostriatal stimulation in D1 versus D2 MSNs. Amplitude, area, rise time, and decay time of the NMDA receptor-mediated current divided by the amplitude, area, rise time, and decay time of the AMPA receptor-mediated current evoked by thalamostriatal stimulation, for each neuron, and then averaged across neurons and compared in D1 and D2 WT versus D1 and D2 R6/2 MSNs. Ns are shown in each bar, error bars indicate ± SE. * $p < 0.05$, ** $p < 0.01$, *** $p < 0.001$.

3.5 Conclusions

Genetically engineered mice expressing tDTomato in D1 DA expressing MSNs provided a method to separately examine alterations of thalamic inputs to direct pathway D1 MSNs versus thalamic inputs to indirect pathway D2 MSNs. The data confirmed longer decay times of AMPA and NMDA receptor-mediated currents at thalamostriatal projections. But more specifically, the current data showed that this effect is mostly driven by alterations occurring at thalamic inputs synapsing onto direct pathway MSNs. Therefore direct pathway projecting MSNs may be more susceptible than indirect pathway projecting MSNs to increased excitation originating at thalamic inputs. NMDA/AMPA ratios are altered in opposing directions at the two subsets of MSNs, suggesting alterations at one type of MSNs may be compensating for alterations at the other type. This discrepancy is important to note and consider in development of HD treatments. The divergent pattern of alterations implies that a treatment designed to solely inhibit NMDA receptors or conversely to stimulate NMDA receptors will not be effective.

Chapter 4

Alterations of Thalamostriatal and Corticostriatal Projections in the YAC128 Mouse Model of Huntington's Disease

4.1 Introduction

HD motor symptoms are biphasic; adult onset HD patients present increased motor activity (chorea) earlier in the disease and impairment of voluntary movements (akinesia) later in the disease (Bird, 1980; Harper, 1996; Bonelli and Hofmann, 2007). Cognitive and psychiatric symptoms are progressive and worsen throughout the course of the disease. Mouse models of HD also show biphasic alterations of excitatory glutamatergic transmission and progressive alterations of inhibitory GABAergic transmission. The frequency of large amplitude sEPCSs is increased in 5-7 week old R6/2s and decreased in older R6/2s (Cepeda et al., 2003). Frequency of sEPCSs is increased in presymptomatic YAC128 mice but decreased in symptomatic YAC128 mice (Joshi et al., 2009; André et al., 2011). Frequency of sIPSCs is progressively decreased over time in Q175 mice when 2-, 7-, and 12-month-old mice are compared (Indersmitten et al., 2015). DA modulation also fluctuates throughout disease progression. In MSNs from WT mice, activation of D1 receptors increases the frequency of sEPSCs. However, in MSNs from early symptomatic YAC128 mice, activation of D1 receptors does not affect sEPSC frequencies in D1 MSNs, but causes the expected increases at the late symptomatic stage (André et al., 2011). In summary, like HD symptoms, synaptic changes induced by mHTT are complex and non-linear and therefore should be examined at various stages of disease progression.

The R6/2 fragment model is often compared to juvenile onset HD due to the occurrence of seizures (Mangiarini et al., 1996; Cummings et al., 2009) and extremely rapid disease progression in these mice (Gambardella et al., 2001; Seneca et al., 2004; Wojaczyńska-Stanek et al., 2006). The fast disease onset and early death of R6/2 mice do not make the R6/2 model suitable for examining how alterations develop at various time points throughout disease progression. The YAC128 full length model is more representative of slower disease progression

associated with adult onset HD and allows the examination of disease progression at multiple time points. Therefore, alterations of thalamostriatal and corticostriatal projections were examined in presymptomatic (~3-month-old) and symptomatic (~13-month-old) YAC128 mice.

4.2 MSN membrane properties

Membrane capacitance (C_m), membrane input resistance (R_m), time constant (Tau), and holding current (Hold) are unchanged in MSNs from presymptomatic YAC128 mice when compared to MSNs from their age-matched WT littermates (Table 4.1). YAC128 MSNs show a trend for increased tau but this effect was not statistically significant ($p = 0.10$). This is consistent with a previous publication which showed no significant differences in mean cell capacitance, input resistance, and membrane time constants in YAC128 and WT mice at 1 month (Joshi et al., 2009; André et al., 2011).

MSNs from symptomatic YAC128 mice show a similar pattern as MSNs from presymptomatic YAC128 mice when compared to MSNs from their age-matched WT littermates (Table 4.2). Membrane capacitance and resistance are unchanged in MSNs from symptomatic YAC128 mice. The unaffected membrane capacitance and membrane input resistance observed in YAC128 mice are very noticeably different than the drastic alterations reported in R6/2 mice (Table 2.1 and Table 3.1) (Klapstein et al., 2001). YAC128 mice exhibit a much milder and slower progressing phenotype than R6/2 mice. Tau in MSNs from YAC128 mice is significantly increased, consistent with the trend observed in 3-month-old mice. A decrease in membrane time constants and increase in mean input resistance in MSNs from 7-month-old YAC128 mice compared with MSNs from WT mice has been previously reported (Joshi et al., 2009). Unlike the robust alterations of MSN membrane properties in R6/2s which have been examined and replicated in an extensive number of experiments, membrane properties of YAC128 mice have

not been consistently reported. One can not determine the source of the discrepancy between the current data and published data, however it may be due to inconsistences in disease progression between the mouse colonies used in the two studies. For future studies, an older 18 month group of YAC128 mice should be examined to confirm whether membrane properties are affected in MSNs of YAC128 mice.

An aging effect is observed. MSNs from 13-month-old WT mice show a trend for increased capacitance ($p = 0.13$) and significantly increased membrane input resistance ($p = 0.008$**) when compared to MSNs from 3-month-old WT mice. Thirteen-month-old YAC128 mice have significantly higher average membrane capacitance ($p = 0.02$), input resistance ($p = 0.046$), and longer time constant ($p = 0.004$) than 3-month-old YAC128 mice. Therefore, MSNs from YAC128 month show a similar aging effect as MSNs from WT mice.

Table 4.1. Passive membrane properties of MSNs from presymptomatic YAC128 mice and their WT littermates.

	WT	YAC128 (3 months)
Cm (pF)	81.60 ± 4.27 (18)	82.11 ± 3.39 (18)
Rm (MΩ)	65.38 ± 3.84 (18)	68.64 ± 7.20 (17)
Tau (ms)	1.38 ± 0.11 (18)	1.50 ± 0.10 (18)
Hold (pA)	-74.98 ± 9.92 (18)	-91.03 ± 10.53 (18)

Values are mean ± SE (number of cells). * $p < 0.05$, ** $p < 0.01$, *** $p < 0.001$.

Table 4.2. Passive membrane properties of MSNs from symptomatic YAC128 mice and their WT littermates.

	WT	YAC128 (13 months)
Cm (pF)	90.63 ± 4.19 (40)	97.39 ± 5.07 (36)
Rm (MΩ)	97.01 ± 10.71 (39)	97.98 ± 12.43 (35)
Tau (ms)	1.59 ± 0.12 (40)	2.02 ± 0.14 (36) *
Hold (pA)	-99.94 ± 12.13 (40)	-105.11 ± 11.93 (36)

Values are mean ± SE (number of cells). * $p < 0.05$, ** $p < 0.01$, *** $p < 0.001$.

4.3 AMPA receptor-mediated currents

AMPA receptor-mediated currents were recorded at V_{hold} = -70 mV in bath applied 10 μM BIC to block inhibitory currents. AMPA currents evoked by thalamostriatal projection were measured in MSNs from 3-month-old and 13-month-old YAC128 mice, and their age-matched WT littermates (Figure 4.1 and Figure 4.2). There were no significant differences in average amplitudes, areas, rise times, or decay times, between YAC128 and WT mice at either age group. AMPA currents evoked by corticostriatal stimulation were recorded in the older 13-month-old group only (Figure 4.3). Similarly, AMPA receptor-mediated currents were of similar amplitude, area, rise time, and decay time in YAC128 and WT mice.

Average areas and decay times of AMPA receptor-mediated currents evoked by thalamostriatal stimulation were significantly higher than those evoked by corticostriatal stimulation in both 13-month-old YAC128 mice and their age-matched WT controls (Figure 4.4). Higher area and decay times of AMPA currents at thalamic inputs into the striatum may suggest higher predisposition to excitotoxicity at thalamic inputs.

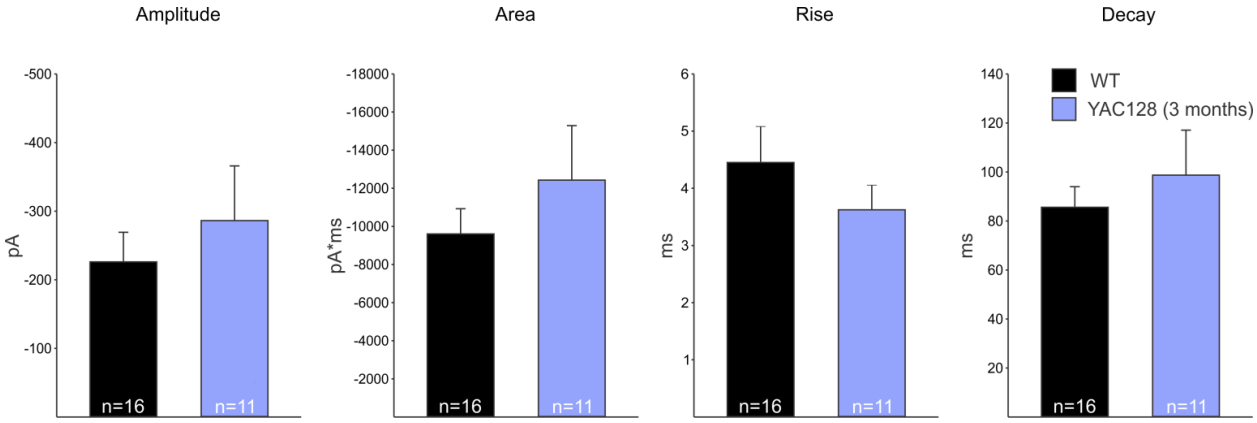

Figure 4.1. AMPA receptor-mediated currents evoked by thalamostriatal stimulation in presymptomatic YAC128 mice. Average amplitudes, areas, rise times, and decay times (± SE) of AMPA receptor-mediated responses evoked by thalamostriatal stimulation in 3-month-old YAC128s and their WT littermates. Ns are shown in each bar. * $p < 0.05$, ** $p < 0.01$, *** $p < 0.001$.

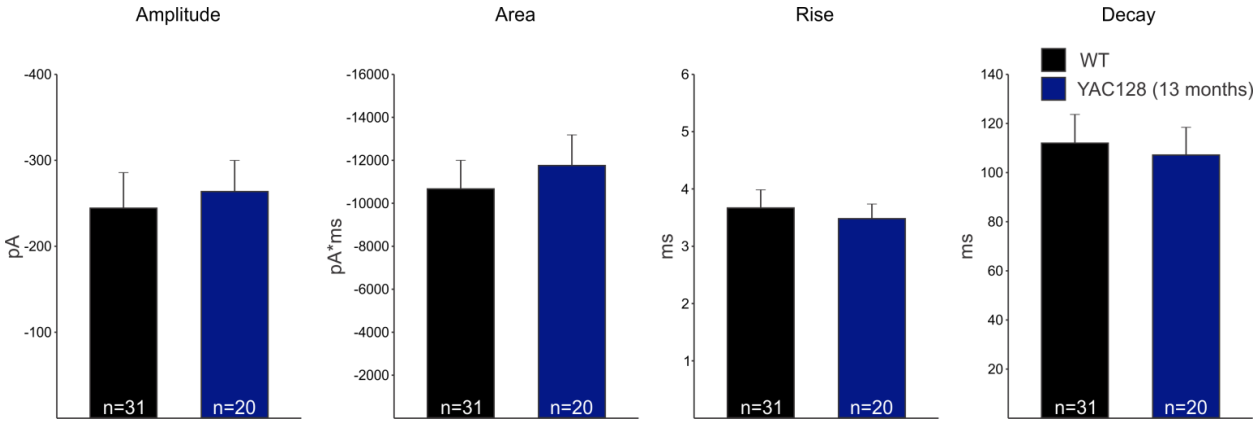

Figure 4.2. AMPA receptor-mediated currents evoked by thalamostriatal stimulation in symptomatic YAC128 mice. Average amplitudes, areas, rise times, and decay times (± SE) of AMPA receptor-mediated responses evoked by thalamostriatal stimulation in 13-month-old YAC128s and their WT littermates. Ns are shown in each bar. * $p < 0.05$, ** $p < 0.01$, *** $p < 0.001$.

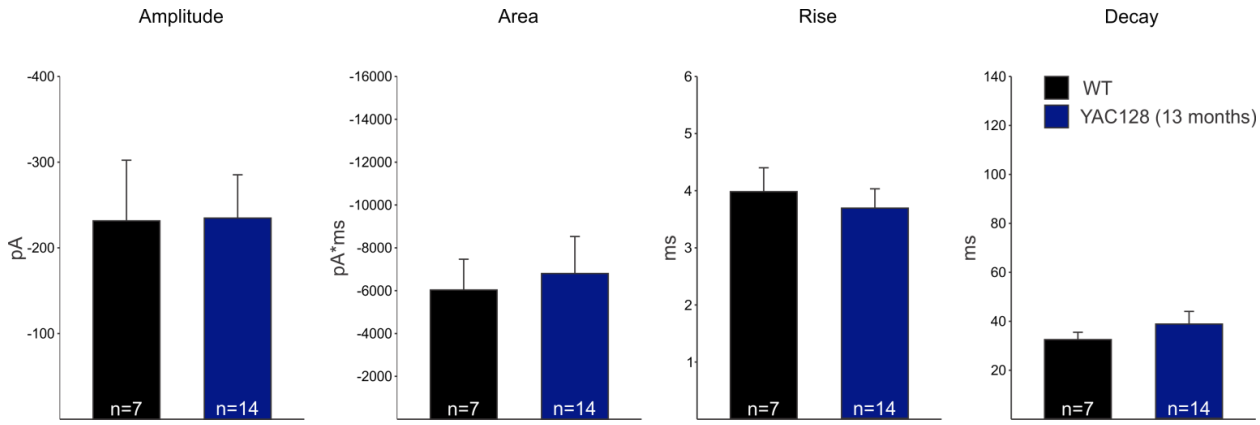

Figure 4.3. AMPA receptor-mediated currents evoked by corticostriatal stimulation in symptomatic YAC128 mice. Average amplitudes, areas, rise times, and decay times (± SE) of AMPA receptor-mediated responses evoked by corticostriatal stimulation in 13-month-old YAC128s and their WT littermates. Ns are shown in each bar. * $p < 0.05$, ** $p < 0.01$, *** $p < 0.001$.

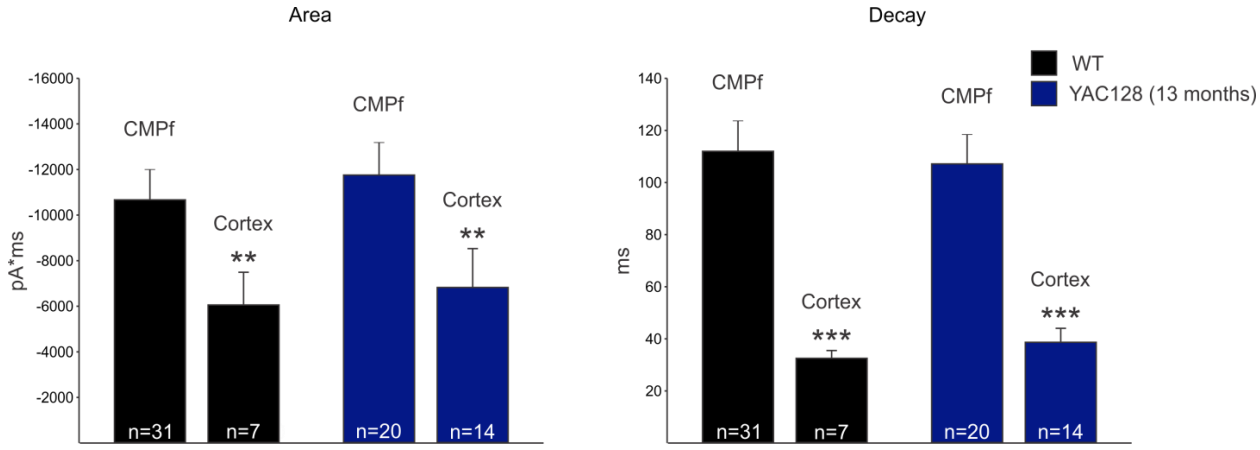

Figure 4.4. Areas and decay times of AMPA receptor-mediated currents evoked by thalamostriatal and corticostriatal stimulation. Comparing average areas and decay times (±SE) of AMPA receptor-mediated responses evoked by thalamostriatal versus corticostriatal stimulation in 13-month-old YAC128s and their WT littermates. Ns are shown in each bar. * $p < 0.05$, ** $p < 0.01$, *** $p < 0.001$.

4.4 NMDA receptor-mediated currents

NMDA receptor-mediated currents were recorded at V_{hold} = +40 mV in bath applied 10 μM BIC, and in 10 μM NBQX to block AMPA receptor-mediated currents. Like AMPA currents, NMDA currents evoked by thalamostriatal stimulation did not show significant differences in average amplitude, area, rise time, or decay time, between YAC128 and WT mice in the 3-month-old presymptomatic group or the 13-month-old symptomatic group (Figure 4.5 and Figure 4.6). NMDA currents evoked by corticostriatal stimulation were also unchanged in 13-month-old YAC128 compared to 13-month-old WT mice (Figure 4.7).

Amplitudes, areas, rise times, and decay times of NMDA receptor-mediated currents evoked by thalamostriatal and corticostriatal projections were compared in 13-month-old YAC128 and their WT littermates (Figure 4.8). NMDA currents evoked by thalamostriatal stimulation had significantly higher amplitudes, areas, and decay times, and significantly lower rise times, in both YAC128 and WT mice. This is consistent with the AMPA data (Figure 4.4). Presumably, these differences may be due to differences in synapse location of the two inputs. While corticostriatal projections preferentially synapse onto dendritic spines (Smith and Bolam, 1990), thalamostriatal projections predominantly synapse onto dendritic shafts (Smith and Bolam, 1990; Sadikot et al., 1992; Smith et al., 1994; Sidibé and Smith, 1996). High amplitudes and longer decays of excitatory inputs from the CMPf may carry a high risk of toxic excitation to the MSNs. This finding provides supporting evidence for a 40% loss of thalamostriatal terminals, but no loss of corticostriatal terminals, in 1-month-old Q140 mice (Deng et al., 2013).

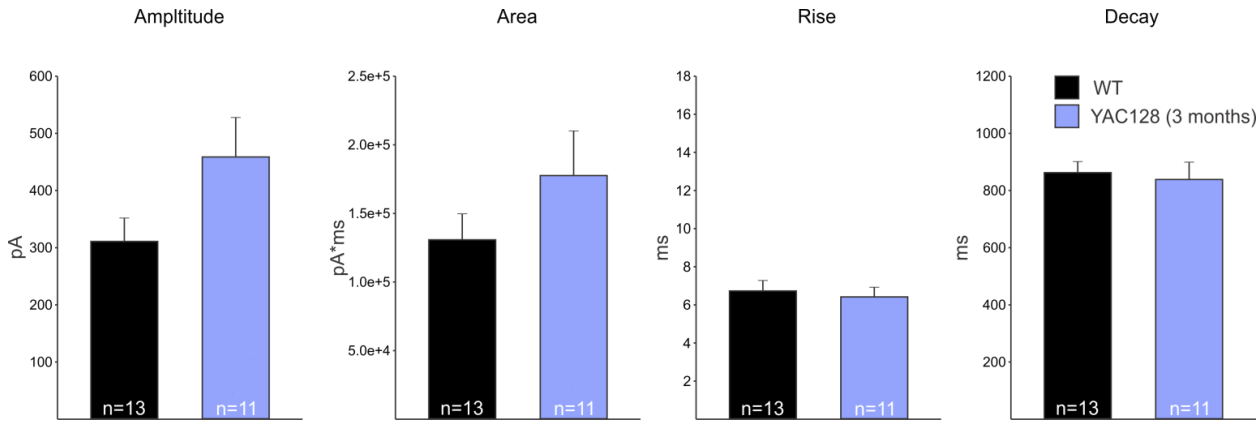

Figure 4.5. NMDA receptor-mediated currents evoked by thalamostriatal stimulation in presymptomatic YAC128 mice. Average amplitudes, areas, rise times, and decay times (± SE) of NMDA receptor-mediated responses evoked by thalamostriatal stimulation in 3-month-old YAC128s and their WT littermates. Ns are shown in each bar. * $p < 0.05$, ** $p < 0.01$, *** $p < 0.001$.

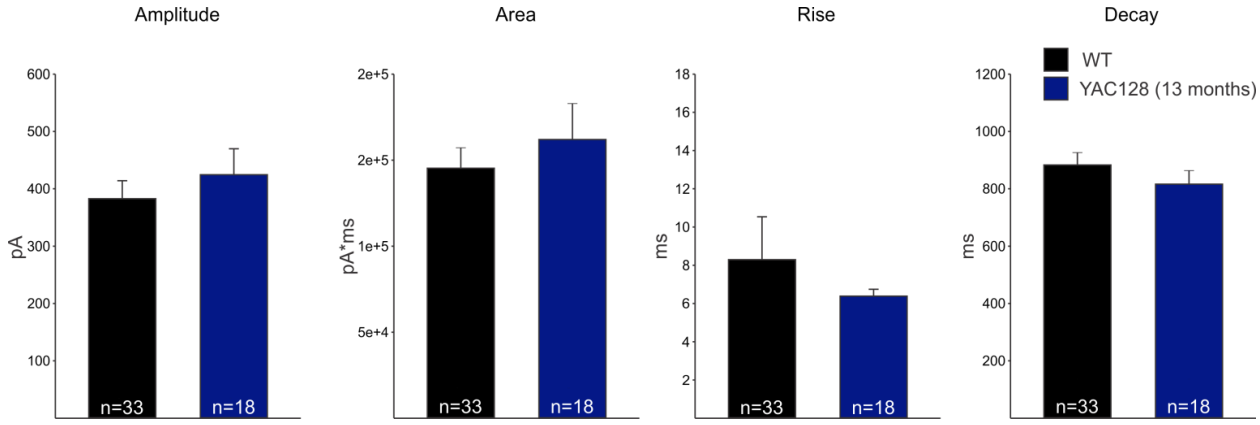

Figure 4.6. NMDA receptor-mediated currents evoked by thalamostriatal stimulation in symptomatic YAC128 mice. Average amplitudes, areas, rise times, and decay times (± SE) of NMDA receptor-mediated responses evoked by thalamostriatal stimulation in 13-month-old YAC128s and their WT littermates. Ns are shown in each bar. * $p < 0.05$, ** $p < 0.01$, *** $p < 0.001$.

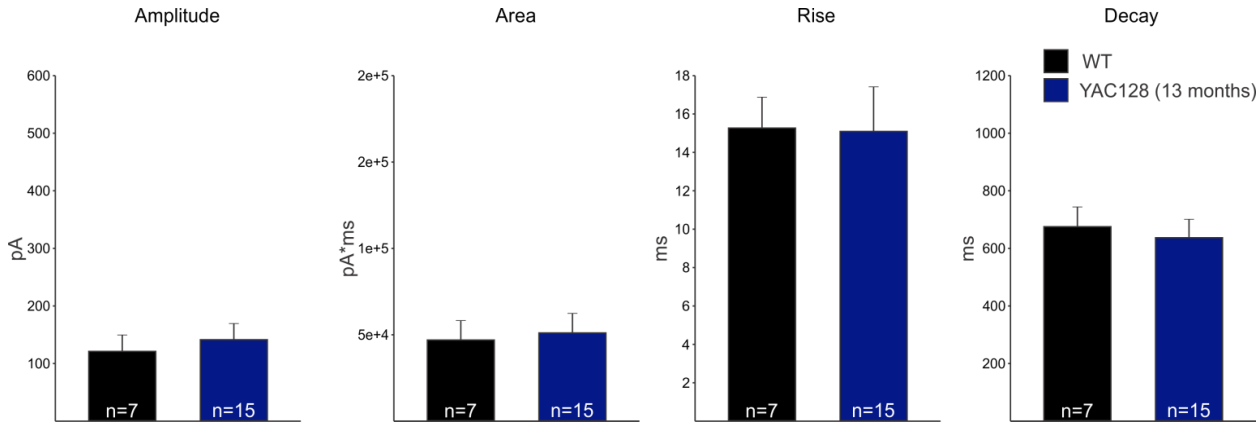

Figure 4.7. NMDA receptor-mediated currents evoked by corticostriatal stimulation in symptomatic YAC128 mice. Average amplitudes, areas, rise times, and decay times (± SE) of NMDA receptor-mediated responses evoked by corticostriatal stimulation in 13-month-old YAC128s and their WT littermates. Ns are shown in each bar. * $p < 0.05$, ** $p < 0.01$, *** $p < 0.001$.

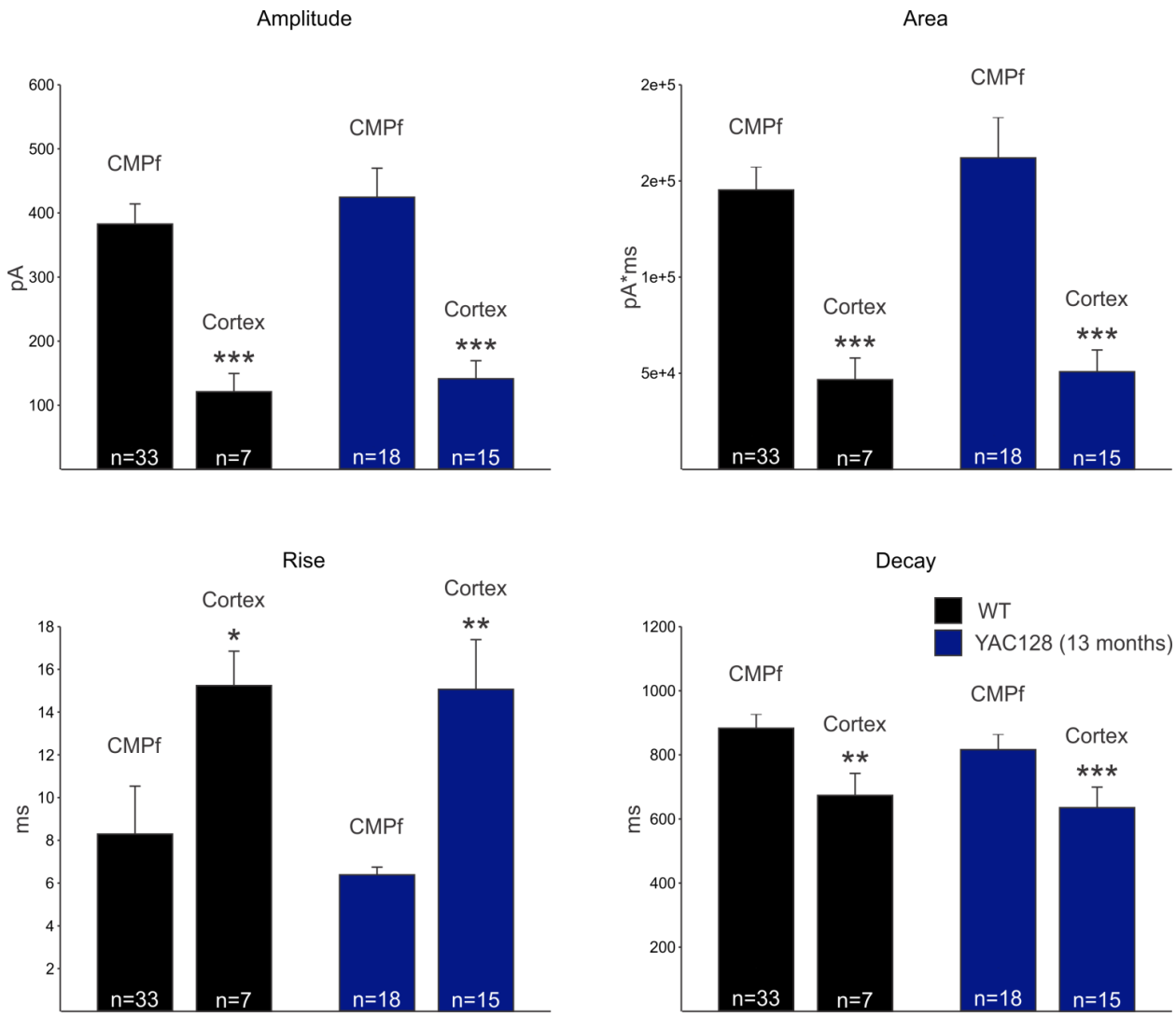

Figure 4.8. NMDA receptor-mediated currents evoked by thalamostriatal versus corticostriatal stimulation. Comparing average amplitudes, areas, rise times, and decay times (±SE) of NMDA receptor-mediated responses evoked by thalamostriatal versus corticostriatal stimulation in 13-month-old YAC128s and their WT littermates. Ns are shown in each bar. * $p < 0.05$, ** $p < 0.01$, *** $p < 0.001$.

4.5 NMDA/AMPA ratios

NMDA/AMPA ratios were calculated for the amplitude, area, rise time, and decay time measurements of NMDA and AMPA receptor-mediated currents for each neuron. As in Chapter 2.6, this was done to account for any potential differences in viral expression across genotype (YAC128 versus WT) and across type of projection stimulated (thalamostriatal versus corticostriatal). No differences were seen for ratios measured at thalamostriatal projections for currents recorded in MSNs from 3- or 13-month-old YAC128 mice when compared to their aged-matched controls (Figure 4.9 and 4.10).

No statistically significant differences between NMDA/AMPA ratios were observed at corticostriatal synapses as well, however some trends did emerge (Figure 4.11). NMDA/AMPA amplitude ratios of currents evoked by corticostriatal stimulation showed a trend towards being increased in MSNs from 13-month-old YAC128 mice ($p = 0.18$). This trend was not observed for ratios of NMDA and AMPA currents evoked by thalamostriatal stimulation. Area ratios were also slightly increased, although this trend was weaker ($p = 0.23$). It may be possible that these changes are the beginning of a progressive relative shift in the proportion of NMDA and AMPA receptors at corticostriatal synapses. A later, more advanced and symptomatic time point, may need to be examined to detect significant, more pronounced, alterations in synaptic neurotransmission in YAC128 mice.

NMDA/AMPA amplitude ratios were different at the two sets of projections in 13-month-old WT mice (Figure 4.12A). Thalamostriatal projections had higher NMDA/AMPA ratios than corticostriatal projections, consistent with data collected in MSNs from R6/2 mice and their WT littermates (Figure 2.14), as well as previously published data collected in rats (Smeal et al., 2008). However, NMDA/AMPA ratios are not different between the two input

types in 13-month-old YAC128 mice (Figure 4.12B). The difference seen in WT mice is absent in the YAC128 mice because the NMDA/AMPA amplitude ratios show a trend to be increased at thalamostriatal projections ($p = 0.18$). This might be an attempt by the cortex to compensate for decreased excitation, as observed in symptomatic YAC128 mice in previous publications (Joshi et al., 2009; André et al., 2011).

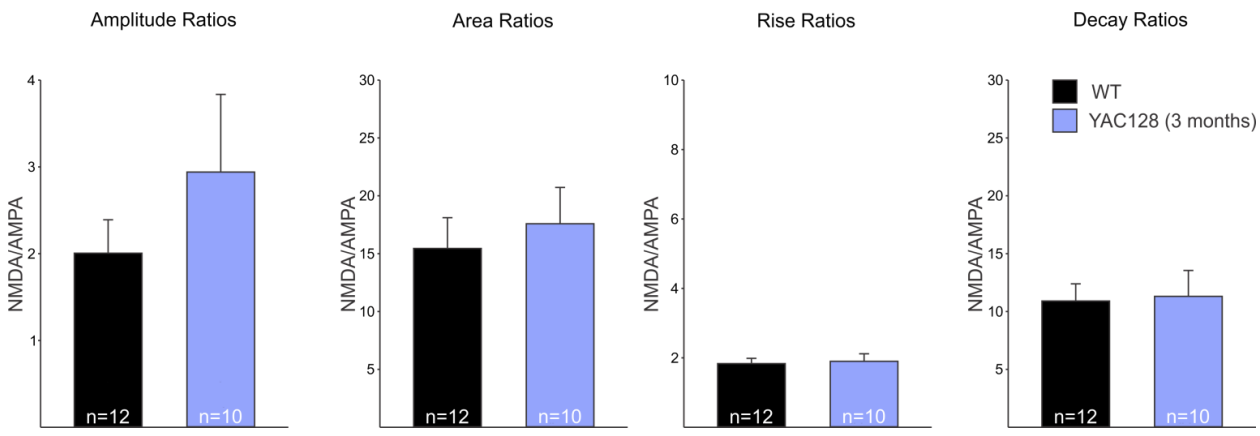

Figure 4.9. NMDA/AMPA ratios evoked by thalamostriatal stimulation in presymptomatic mice. Amplitude, area, rise time, and decay time of the NMDA receptor-mediated current divided by the amplitude, area, rise time, and decay time measure of the AMPA receptor-mediated current evoked by thalamostriatal stimulation, for each neuron, and then averaged across neurons in 3-month-old YAC128s and their WT littermates. Ns are shown in each bar, error bars indicate ± SE. * $p < 0.05$, ** $p < 0.01$, *** $p < 0.001$.

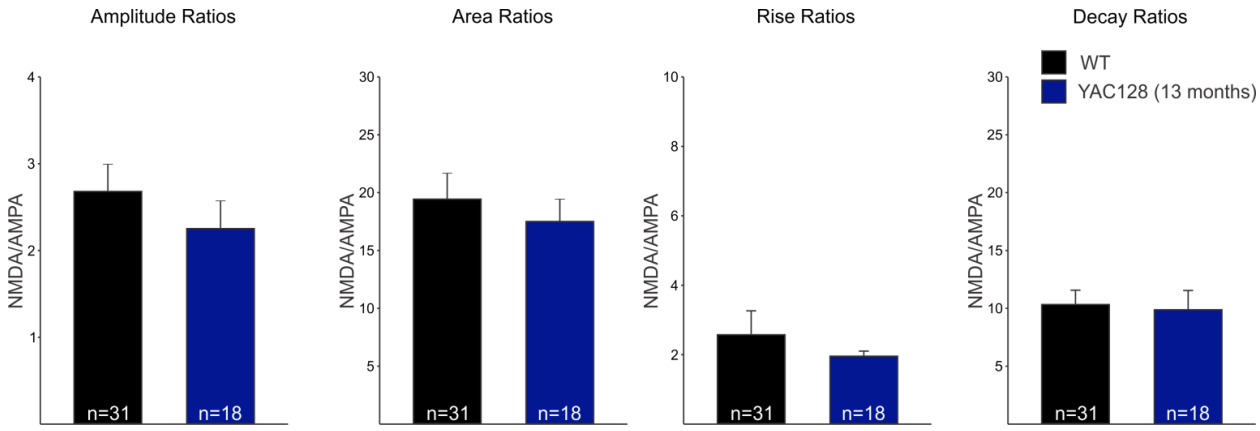

Figure 4.10. NMDA/AMPA ratios evoked by thalamostriatal stimulation in symptomatic mice. Amplitude, area, rise time, and decay time of the NMDA receptor-mediated current divided by the amplitude, area, rise time, and decay time measure of the AMPA receptor-mediated current evoked by thalamostriatal stimulation, for each neuron, and then averaged across neurons in 13-month-old YAC128s and their WT littermates. Ns are shown in each bar, error bars indicate ± SE. * $p < 0.05$, ** $p < 0.01$, *** $p < 0.001$.

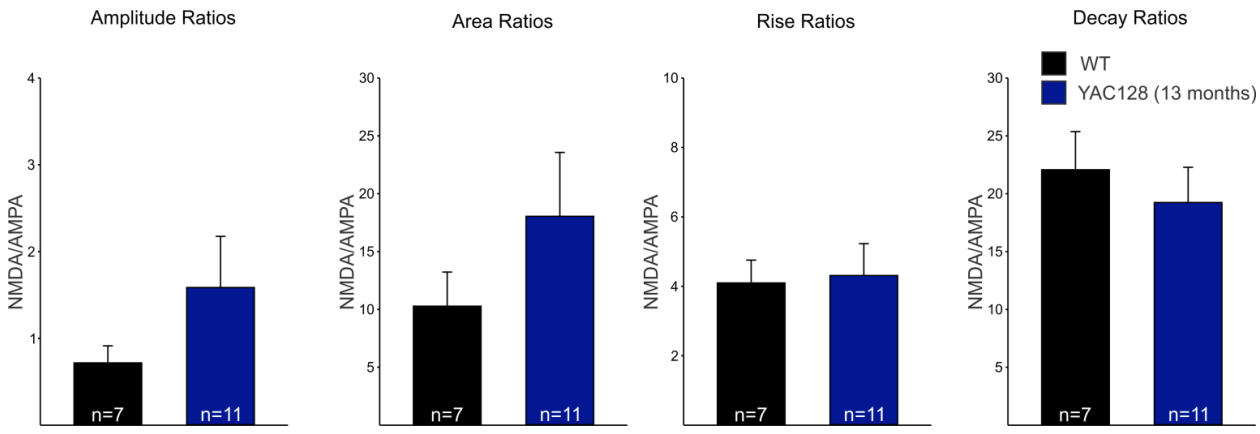

Figure 4.11. NMDA/AMPA ratios evoked by corticostriatal stimulation in symptomatic mice. Amplitude, area, rise time, and decay time of the NMDA receptor-mediated current divided by the amplitude, area, rise time, and decay time measure of the AMPA receptor-mediated current evoked by corticostriatal stimulation, for each neuron, and then averaged across neurons in 13-month-old YAC128s and their WT littermates. Ns are shown in each bar, error bars indicate ± SE. * $p < 0.05$, ** $p < 0.01$, *** $p < 0.001$.

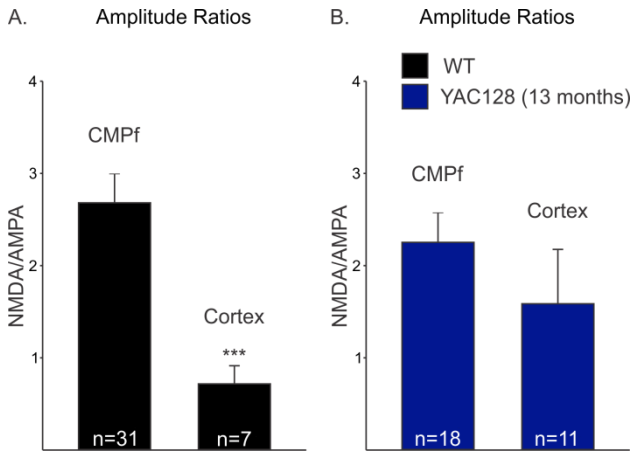

Figure 4.12. NMDA/AMPA ratios evoked by thalamostriatal versus corticostriatal stimulation. (A) Ratios of average amplitudes of NMDA and AMPA receptor-mediated currents evoked by thalamostriatal stimulation compared to ratios of NMDA and AMPA receptor-mediated currents evoked by corticostriatal stimulation in MSNs from 13-month-old WT mice. **(B)** Ratios of average amplitudes of NMDA and AMPA receptor-mediated currents evoked by thalamostriatal stimulation compared to ratios of NMDA and AMPA receptor-mediated currents evoked by corticostriatal stimulation in MSNs from 13-month-old YAC128 mice. Ns are shown in each bar, error bars indicate ± SE. * $p < 0.05$, ** $p < 0.01$, *** $p < 0.001$.

4.6 Conclusions

Examination of AMPA and NMDA receptor-mediated currents in MSNs from YAC128 mice did not display significant alterations when compared to currents in MSNs from age-matched WT mice. This was true for currents evoked by both thalamostriatal and corticostriatal stimulation, at both presymptomatic and symptomatic stages. Perhaps, the alterations in synaptic transmission are not yet severe enough at the disease stages examined to be detected by the optogenetics technique. However, interesting differences were observed at thalamostriatal versus corticostriatal projections. AMPA and NMDA currents were of larger average areas and longer average decay times when evoked by thalamic versus cortical inputs. In addition, NMDA/AMPA ratios suggested that MSN synapses with thalamic inputs have a proportionally higher composition of NMDA receptors than MSN synapses with cortical inputs. Both of these features may predispose thalamostriatal synapses to increased excitation, a hallmark of HD.

Chapter 5

Conclusions and Future Directions

5.1 Summary of key findings

Neurodegeneration of the striatum in HD involves a complicated interplay of presynaptic and postsynaptic mechanisms. With the use of BACHD and Cre mice, mHTT expression has been reduced in distinct brain regions to study how regional specificity of mHTT affects the HD phenotype. Reduction of mHTT expression in the cortex partially improved the behavioral and psychiatric phenotype but not cell death, reduction of mHTT in the striatum partially rescued the psychiatric phenotype and cell death in the forebrain, while reduction of mHTT in the cortex and striatum simultaneously ameliorated all behavioral deficits and brain atrophy (Wang et al., 2014). Therefore, understanding and managing the alterations occurring at striatal inputs is vital for efficient HD therapeutics. The striatum receives two sets of excitatory projections, cortical and thalamic; however the functional alterations occurring at cortical projections have received the majority of the field's attention due to prior technical limitations. Selective activation of distinct axonal projections with optogenetics allowed extensive examination of cortical and thalamic projections into the striatum and demonstrated that these excitatory convergent inputs undergo differential alterations.

In the R6/2 mouse model, thalamostriatal projections displayed increased decay times of both AMPA and NMDA receptor-mediated currents, alterations in glutamate reuptake, and increased probability of glutamate release. These effects were more prominent at thalamic connections with direct pathway MSNs. Corticostriatal projections showed much more discrete changes. The differences in kinetics of AMPA and NMDA receptor-mediated currents were contrasting, changes in glutamate reuptake were smaller than those at thalamostriatal projections, and no change in the probability of glutamate release was detected.

Beginning with the very early HD mouse models which used quinolinic acid to activate NMDA receptors (Coyle and Schwarcz, 1976; McGeer and McGeer, 1976; Beal et al., 1986, 1991; Ferrante et al., 1993), aberrant function of NMDA receptors has been implicated in excitotoxicity, which was the hypothesized cause of neurodegeneration observed in HD (DiFiglia, 1990; Freese et al., 1990; Beal et al., 1993; Ferrante et al., 2000). Both the YAC128 and R6/2 mouse models showed that NMDA/AMPA ratios at thalamostriatal projections are >1, indicating NMDA currents are relatively larger than AMPA currents. However, NMDA/AMPA ratios at corticostriatal projections are <1, signifying AMPA receptors drive relatively larger currents than NMDA receptors. This finding suggests that thalamostriatal synapses are at a higher risk for increased excitation and the associated toxicity.

5.2 Optogenetics as a tool to study synaptic alterations in HD

Due to the complex and heterogenous organization of the striatum, optogenetics served as vital tool to examine alterations at thalamostriatal and corticostriatal projections separately. Intra-striatal electrical stimulation or electrical stimulation of the corpus callosum is unable to target individual pathways while viral expression of ChR2 can be very specific. However, the two techniques should be employed concurrently to study synaptic transmission in HD as they both bring their own set of advantages and disadvantages.

Based on previous data reported in the R6/2 and YAC128 model, we expected to see changes in amplitude of AMPA receptor-mediated currents. Prior studies have found that R6/2 MSNs display increased frequencies of large amplitude sEPSCs and decreased frequencies of small amplitude sEPSCs as early as 5-7 weeks (Cepeda et al., 2003). Firing of striatal neurons is increased in R6/2 mice at 6-9 weeks (Rebec et al., 2006) which is predicted to be caused by increased excitation from the cortex (Cummings et al., 2009). Therefore, decreased paired pulse

ratios were predicted at corticostriatal synapses. Presymptomatic YAC128 mice have been shown to display increased amplitudes of evoked EPSCs and increased glutamate release at 1-1.5 month via stimulation of the corpus callosum (André et al., 2011). Symptomatic mice display reduced evoked glutamate currents (Joshi et al., 2009). Similarly, changes in amplitude of NMDA receptor-mediated currents were expected as YAC128 HD mice were shown to exhibit enhanced expression of extrasynaptic NMDA receptors, increased currents, and reduced activation of nuclear cAMP response element-binding protein (Milnerwood et al., 2010). However, optogenetically evoked responses did not show alterations in amplitude of AMPA or NMDA currents.

We suspect discrepancies between previous findings and the present outcomes are due to the following reasons. First, optogenetics uses an artificial channel to elicit an action potential instead of the native voltage gated Na^+ channels that are utilized during natural neurotransmission or *via* electrical stimulation. For a number of neurons, a light intensity versus response amplitude input-output curve was measured. Interestingly, optogenetic stimulation of thalamostriatal and corticostriatal projections resulted in all-or-none responses. Each neuron had a threshold below which a light pulse did not produce a response and above which all responses were of similar amplitude. This suggests that there exists some threshold below which ChR2 is not activated, and above which activation of ChR2 on the presynaptic terminal releases the maximum available amount of glutamate. Hence, in R6/2 and YAC128 mice, the ready to be released pool of vesicles may be unaffected compared to their WT littermates and therefore we did not detect changes in amplitudes of AMPA or NMDA receptor-mediated currents. However, this does not imply that the amount of glutamate released naturally or the naturally occurring

AMPA and NMDA currents in MSNs of these animals are unaltered; this change may not be able to be detected by the optogenetic methods used in present experiments.

Second, the area activated by optogenetic stimulation is markedly different than the area stimulated by electrical stimulation. For electrical stimulation, the stimulating electrode is usually placed 200-300 μm from the recorded cell. Therefore, stimulation is restricted to this small radius. However, with optogenetic stimulation, ChR2 is expressed in the majority of either cortical or thalamic inputs within the dorsal striatum, so when the blue light is turned on, the entire field or slice is illuminated, and all ChR2 fibers within this relatively large region are stimulated to release glutamate. The widespread recruitment of fibers results in large currents which may be indicative of maximum AMPA and NMDA receptor-mediated postsynaptic currents in the recorded MSNs. A ceiling effect may be occurring so no change in amplitude of these responses is able to be measured. In the future, using a fiber optics to deliver a light pulse may be beneficial because it allows one to adjust the size of the aperture and the distance of the fiber tip from the slice to regulate the extent of the area illuminated, and therefore the number of fibers recruited and activated. In short, the ability to selectively activate brain regions, sets of projections, or neuronal types, with the use of optogenetics is an extremely useful tool that currently has no replacement. However, one must be aware of the limitations of optogenetics and take into account its constraints when designing experiments, asking questions and interpreting results.

5.3 Future experiments and applications for therapeutics

Despite the extensive neuronal and glial loss observed in the thalamus of HD patients (Heinsen et al., 1996; Kassubek et al., 2004a, 2004b), examination of altered synaptic neurotransmission at thalamostriatal projections has been previously overlooked. This

dissertation provides one of the first attempts into understanding functional alterations at these projections and delivers evidence that these alterations may lead to excitotoxicity, neuronal dysfunction, and in turn neurodegeneration.

One of the key recurrent findings throughout the previous chapters is altered decay times of AMPA and NMDA receptors hypothesized to be caused by deficits in glutamate reuptake. Ceftriaxone is an antibiotic which increases GLT1 expression (Rothstein et al., 2005), GLT1 function, and improves the HD behavioral phenotype in mice (Miller et al., 2008, 2012). An interesting future experiment would be to test AMPA and NMDA receptor mediated currents evoked by optogenetic thalamostriatal stimulation in R6/2 mice, before and after ceftriaxone treatment. Clinical trials of ceftriaxone have not been initiated due to side effects such as its impairment of synaptic plasticity (Omrani et al., 2009) and cognitive processing (Bellesi et al., 2009). Yet, the benefits of ceftriaxone treatment provide support for treatments targeting glutamate reuptake. Perhaps these adverse side effects may be prevented if glutamate reuptake function is increased at specific sets of synapses, i.e. thalamostriatal projections synapsing onto direct pathway projecting MSNs, instead of globally as with administration of ceftriaxone. The effects of gene targeting and overexpression of GLT1 in CMPf neurons also would be interesting to examine.

The differential alterations observed at thalamostriatal compared to corticostriatal projections suggest that the effects of mHTT occurring in the basal ganglia circuit are complex, diverse, and not universal. Therefore, HD treatments aimed at globally decreasing NMDA currents, increasing GLT1 function, or decreasing glutamate release, will continuously result in unfavorable side effects. Treatments designed to target these and other mechanisms altered in HD should be directed to affect specific brain regions, projections, and neuronal types.

Chapter 6

Materials and Methods

6.1 Animals

All experimental procedures were performed in accordance with the United States Public Health Service Guide for Care and Use of Laboratory Animals and were approved by the Institutional Animal Care and Use Committee at the University of California, Los Angeles (UCLA). Every effort was made to minimize pain and discomfort. Experiments were conducted in two mouse models of HD: R6/2 and YAC128. All mice were obtained from breeding colonies at UCLA. Genotyping was performed using polymerase chain reaction (PCR) of DNA obtained from tail samples, once at weaning and again following electrophysilogical recordings. Data from both males and females were combined.

A. R6/2

Colony was maintained by crossing WT C57BL/6xCBA males (Jackson Laboratories: Bar Harbor, Maine 04609, USA) with R6/2 ovary-transplanted WT C57BL/6xCBA females (Jackson Laboratories). CAG repeat lengths were determined by Laragen Inc. (Culver City, CA). CAG repeats ranged 145-163 and averaged 154.9 ± 1.1 (n = 19 animals). Mice were used for recordings at 64 - 87 days of age.

WT C57BL/6xCBA males or WT FVB/N males (Jackson Laboratories) expressing DsRed fluorescent protein tDTomato were bred to the R6/2 ovary-transplanted WT C57BL/6xCBA females to produce R6/2D1tom mice which expressed tDTomato in D1 receptor expressing MSNs. CAG repeats ranged 148-164 and averaged 157.2 ± 1.7 (n = 9). Mice were used for recordings at 60 - 72 days of age.

B. YAC128

Colony was originally derived from the breeding colony at the University of British Columbia and maintained by continuous crossings. Mice were used at two ages to examine

presymptomatic and symptomatic stages of HD. Mice were recorded at 94 - 108 days old for the presymptomatic stage and at 347 - 469 days old for the sympotamtic stage. YAC128D1GFP (YAC128 x D1GFP FVB), YAC128D2GFP (YAC128 x D2GFP FVB), and YAC128Thcre (YAC128 x ThCre FVB) mice were used in addition to the original YAC128 colony to supplement data when needed. Additional YAC128 colonies expressing tDTomato in D1 receptor expressing MSNs were bred. These included YAC128D1Tom (YAC128 FVB x D1Tom FVB), YAC128ThCreD1Tom (YAC128D1Tom x ThCre FVB), and YAC128ThCreD1TomD2GFP (YAC128ThCre FVB crossed to offspring of D1Tom FVB x D2GFP FVB).

6.2 Optogenetics

Mice were anesthetized with isoflurane and placed in a stereotaxic frame. An AAV expressing ChR2 (H134R) and eYFP under the CaMKIIa promoter was injected. Plasmids were obtained from Dr. K. Deisseroth, virus made by the University of Iowa Gene Vector Core. Injections were made with a 33 gauge blunt needle, 10 µl World Precision Instruments syringe, using a Chemyx NanoJet pump. Each injection site received 0.5 µl of virus, infused at 0.2 µl/min. Thalamic injections were performed bilaterally into the CMPf nuclear complex of the thalamus (AP: -2.18, ML +/- 0.7, DV -3.8; and AP: -1.58, ML +/- 0.7, DV -3.8). Sensorimotor cortical injections were either bilateral (AP: +2.22, ML +/- 1.7, DV-1.8) or unilateral (AP: +2.22, ML - 1.7, DV-1.8). In animals which received unilateral injections, only the injected hemisphere was used for recordings. Animals were monitored for ~4 weeks until euthanized for recordings.

6.3 Electrophysiology

A. Slice preparation and cell visualization

Mice were anesthetized with isoflurane and decapitated. The brain was rapidly removed and placed into ice-cold slicing artificial cerebrospinal fluid (ACSF) containing (in mM): 26 $NaHCO_3$, 1.25 $NaHPO_4$, 208 sucrose, 10 glucose, 2.5 KCl, 1.3 $MgCl_2$, 8 $MgSO_4$ (pH 7.2; aerated with 95% O2/5% CO2; 290–300 mOsm/l). The cerebellum was removed using a razor blade and brain was glued to the stage of a vibrating microtome (Model VT1000 S, Leica Microsystems, Buffalo Grove, IL). The brain was sliced into 300 μm coronal slices. Slices which included dorsolateral striatum were cut in half to separate left and right hemispheres. To ensure only axons, and not somata, are stimulated in animals injected in the cortex, and to reduce the possibility of stimulating thalamocortical collaterals in animals injected in the thalamus, the striatum was isolated from cortical and thalamic inputs in all animals before recording. Following preparation, slices were stored in room temperature ACSF containing (in mM): 26 $NaHCO_3$, 1.25 $NaHPO_4$, 10 glucose, 130 NaCl, 3 KCl, 2 $MgCl_2$, 2 $CaCl_2$ (pH 7.2; aerated with 95% O2/5% CO2; 290–300 mOsm/l). They were allowed to recover for at least 1 hour prior to recording.

Cells were visualized with infrared illumination and differential interference contrast optics (i.e., IR-DIC microscopy). MSNs and LCIs were identified by somatic size and basic membrane properties (input resistance, capacitance and time constant). LCIs were also identified by spontaneous action potential firing in cell attached mode.

B. Recording and stimulation

Patch pipettes were filled with cesium methanesulfonate solution containing (in mM): 8 HEPES, 9 EGTA, 125 cesium methanesulfonate, 4 NaCl, 3 KCl, 1 $MgCl_2$, 10 disodium phosphocreatine, 0.1 leupeptin(HCl), 5 MgATP, 1 TrisGTP, (pH 7.2; 270–280 mOsm/l). Also

4.4 µM QX-314 Chloride (Na^+ channel blocker, Tocris 2313) to prevent action potentials and biocytin (0.2%) to later identify recorded neurons, were added. Access resistances were 4-6 MΩ.

After whole-cell configuration was obtained, basic membrane properties were recorded in voltage-clamp mode at a membrane holding potential (V_{hold}) of -70 mV. Only data from cells with access resistance values smaller than 30 MΩ (which did not vary more than 20% during the course of the experiment) were included. Membrane capacitances and input resistances were measured by applying a 10 mV depolarizing step voltage command and using the membrane test function integrated in pClamp 8.2 or 10.3 (Axon Instruments, Molecular Devices, Sunnyvale, CA).

Excitatory responses were evoked by a brief light-emitting diode (LED, CoolLED) light pulse (2ms duration, 470nm, 15.2 – 18.1mW) at 30 second intervals in the presence of 10 µM bicuculline (Tocris 0109) to block $GABA_A$ receptor activity. AMPA currents were recorded at a holding potential of -70 mV. NMDA currents were recorded at a holding potential of +40 mV, in bath applied 10 µM bicuculline and 10 µM 2,3-dihydroxy-6-nitro-7-sulfamoyl-benzo[f]quinoxaline-2,3-dione (NBQX, Tocris 1044) to block AMPA receptor-mediated currents.

After completion of AMPA and NMDA current recordings, a population of cells underwent the paired-pulse protocol to examine probability of release at presynaptic terminals (Zucker, 1989) and were applied at 75ms, 100ms, 200ms, and 400ms intervals. This protocol was run at both -70 mV and +40 mV to examine paired-pulse ratios (PPRs) mediated by both AMPA and NMDA receptors. This helped assure consistency and provide support that the ratios observed are a function of presynaptic mechanisms and not a function of the postsynaptic receptors. In a separate population of cells, after completion of AMPA and NMDA current

recordings, NMDA currents were further examined. NMDA currents before and 14 minutes after bath application of 30 µM TBOA (glutamate transporter blocker, Tocris 1223) were compared to study alterations of glutamate transporters in HD. Similarly, NMDA currents before and 5, 8, 11, and 14 minutes after bath application of 1 µM Ifenprodil (NR2B subunit-containing NMDA receptor selective antagonist, Sigma I2892) were compared to study alterations specific to NMDA receptors containing the NR2B subunit.

Recordings of LCIs followed the same protocol as recordings of MSNs. Cell attached recordings were initially performed to track the spontaneous firing characteristic of LCIs to help identify these neurons. AMPA receptor-mediated currents were recorded at V_{hold} of -70 mV in 10 µM bicuculline and followed by recordings of NMDA receptor-mediated currents at V_{hold} of +40 mV after the addition of 10 µM NBQX.

Notably, off target staining occurred on the rare occasion that virus targeted to the cortex may have leaked or spread into the striatum. Therefore, to assure responses were evoked by presynaptic stimulation, data from slices which contained fluorescent MSN cells bodies instead of the desired axonal staining were not used. Also, all AMPA receptor-mediated responses were blocked by NBQX. If the responses could not be blocked by the AMPA receptor antagonist, data from the corresponding cell were omitted. In addition, all cells with responses whose amplitude was larger than 1000 pA were excluded as these large responses were multi-peaked and most likely not mediated by direct presynaptic stimulation.

6.4 Histology

Some animals injected with virus were retained for histology and did not undergo electrophysiology experiments. These animals were perfused with 20 ml of phosphate buffered saline (PBS) and then 60 ml of paraformaldehyde (PFA). Whole brains were extracted and fixed

in PFA, then moved to 15% sucrose PBS solution, and finally to 30% sucrose PBS solution, overnight each. Brains were frozen on dry ice and a cryostat was used to prepare 30 μm thick coronal slices of the entire striatum and site of injection. One of every six sections was mounted with mowiol mounting medium and imaged with a Leica MZ FLIII fluorescence stereomicroscope equipped with a Leica DFC3000 G grayscale USB 3.0 microscope camera to visualize viral YFP expression at site of injection and in striatum.

Slices used for recordings were fixed in paraformaldehyde (PFA) and processed for biocytin by standard techniques (Horikawa and Armstrong, 1988) to allow post-hoc identification of the recorded MSNs, as well as visualization of virus expression.

6.5 Data analysis and statistics

Evoked currents were analyzed offline using Clampfit 10.0 (Axon Instruments, Molecular Devices, Sunnyvale, CA). Peak amplitudes were calculated by measuring the difference in amplitude between the highest absolute value of the response and average baseline. Area was calculated by summing the entire area under the response, from baseline to baseline. Rise and decay times were calculated by measuring the time the response took to rise from 10% to 90% of the peak amplitude and decay from 90% to 10% of the peak amplitude respectively. For each cell, five sweeps measuring AMPA receptor-mediated currents were recorded 30 seconds apart. Each sweep was analyzed separately and then averaged to find the means for each cell. Three sweeps measuring NMDA receptor-mediated currents were recorded 30 seconds apart and averaged in a similar manner. Percent change of NMDA receptor-mediated response decay times was calculated by dividing the decay time of each NMDA receptor-mediated response recorded from an R6/2 mouse by the average NMDA receptor-mediated response from WT mice.

For cells that underwent TBOA or Ifenprodil treatment, the percent change of peak amplitudes, areas, half widths, rise, and decay times, of the NMDA receptor-mediated response times were calculated. NMDA/AMPA ratios were calculated for each measure of the evoked responses (amplitude, area, rise, and decay times). The ratios were calculated for each analyzed neuron and then combined and averages reported. This method of analysis accounts for any possible differences in virus expression. Paired-pulse ratios were calculated by dividing the amplitude of the second response by the amplitude of the first. Amplitudes were calculated in two manners: 1) from baseline of entire trace to each peak (for AMPA and NMDA receptor-mediated currents) and 2) from where peak begins to top of peak (only for NMDA receptor-mediated currents). Both analyses are presented in chapter 2. Paired-pulse facilitation (PPF) was defined as ratios greater than 1, and paired-pulse depression (PPD) was defined as ratios less than 1.

In the text, data values are presented as mean ± stand error (number of cells). Group means were compared using Student's t-tests or two way ANOVAs followed by Bonferonni t-tests using SigmaStat software (Version 3.5; SPSS, Chicago, IL). Differences were considered statistically significant when $p<0.05$. In tables and figures, $p<0.5$ is labeled as *, $p<0.1$ is labeled as **, and $p<0.001$ is labeled as ***.

Bibliography

striatal medium spiny neurons. J. Neurosci. 28:1185–1197.

Albin RL, Reiner A, Anderson KD, Dure LS, Handelin B, Balfour R, Whetsell WO, Penney JB, Young AB (1992) Preferential loss of striato-external pallidal projection neurons in presymptomatic Huntington's disease. Ann Neurol. 31:425-430.

Albin RL, Young AB, Penney JB (1989) The functional anatomy of basal ganglia disorders. Trends Neurosci. 12:366–375.

Albin RL, Young AB, Penney JB, Handelin B, Balfour R, Anderson KD, Markel DS, Tourtellotte WW, Reiner A (1990) Abnormalities of striatal projection neurons and N-methyl-D-aspartate receptors in presymptomatic Huntington's disease. N. Engl. J. Med. 322:1483–1487.

Alexander GE, Crutcher MD (1990) Functional architecture of basal ganglia circuits: neural substrates of parallel processing. Trends Neurosci. 13:266–271.

Alexander GE, DeLong MR, Strick PL (1986) Parallel organization of functionally segregated circuits linking basal ganglia and cortex. Annu. Rev. Neurosci. 9:357–381.

Ali NJ, Levine MS (2006) Changes in expression of N-methyl-D-aspartate receptor subunits occur early in the R6/2 mouse model of Huntington's disease. Dev. Neurosci. 28:230–238.

Altar CA, Cai N, Bliven T, Juhasz M, Conner JM, Acheson AL, Lindsay RM, Wiegand SJ (1997) Anterograde transport of brain-derived neurotrophic factor and its role in the brain. Nature 389:856–860.

André VM, Cepeda C, Cummings DM, Jocoy EL, Fisher YE, William Yang X, Levine MS (2010) Dopamine modulation of excitatory currents in the striatum is dictated by the expression of D1 or D2 receptors and modified by endocannabinoids. Eur. J. Neurosci. 31:14–28.

André VM, Cepeda C, Fisher YE, Huynh M, Bardakjian N, Singh S, Yang XW, Levine MS (2011) Differential Electrophysiological Changes in Striatal Output Neurons in Huntington's Disease. J. Neurosci. 31:1170–1182.

Andrew SE, Goldberg YP, Kremer B, Telenius H, Theilmann J, Adam S, Starr E, Squitieri F, Lin B, Kalchman MA (1993) The relationship between trinucleotide (CAG) repeat length and clinical features of Huntington's disease. Nat. Genet. 4:398–403.

Antonini A, Leenders KL, Spiegel R, Meier D, Vontobel P, Weigell-Weber M, Sanchez-Pernaute R, Yébenez JG de, Boesiger P, Weindl A, Maguire RP (1996) Striatal glucose metabolism and dopamine D2 receptor binding in asymptomatic gene carriers and patients with Huntington's disease. Brain 119:2085–2095.

Apicella P (2007) Leading tonically active neurons of the striatum from reward detection to context recognition. Trends Neurosci. 30:299–306.

Ariano MA, Aronin N, Difiglia M, Tagle DA, Sibley DR, Leavitt BR, Hayden MR, Levine MS (2002) Striatal Neurochemical Changes in Transgenic Models of Huntington's Disease. J. Neurosci. Res. 68:716–729.

Arriza JL, Fairman WA, Wadiche JI, Murdoch GH, Kavanaugh MP, Amara SG (1994) Functional comparisons of three glutamate transporter subtypes cloned from human motor cortex. J. Neurosci. 14:5559–5569.

Arzberger T, Krampfl K, Leimgruber S, Weindl A (1997) Changes of NMDA receptor subunit (NR1, NR2B) and glutamate transporter (GLT1) mRNA expression in Huntington's disease-an in situ hybridization study. J. Neuropathol. Exp. Neurol. 56:440–454.

Augood SJ, Faull RLM, Emson PC (1997) Dopamine D1 and D2 receptor gene expression in the striatum in Huntington's disease. Ann. Neurol. 42:215–221.

Ballion B, Mallet N, Bézard E, Lanciego JL, Gonon F (2008) Intratelencephalic corticostriatal neurons equally excite striatonigral and striatopallidal neurons and their discharge activity is selectively reduced in experimental parkinsonism. Eur. J. Neurosci. 27:2313–2321.

Bamford NS, Zhang H, Schmitz Y, Wu N-P, Cepeda C, Levine MS, Schmauss C, Zakharenko SS, Zablow L, Sulzer D (2004) Heterosynaptic dopamine neurotransmission selects sets of corticostriatal terminals. Neuron 42:653–663.

Bates GP, Dorsey R, Gusella JF, Hayden MR, Kay C, Leavitt BR, Nance M, Ross C a., Scahill RI, Wetzel R, Wild EJ, Tabrizi SJ (2015) Huntington disease. Nat. Rev. Dis. Prim. 1:1–21.

Beal MF, Ferrante RJ, Swartz KJ, Kowall NW (1991) Chronic quinolinic acid lesions in rats closely resemble Huntington's disease. J. Neurosci. 11:1649–1659.

Beal MF, Hyman BT, Koroshetz W (1993) Do defects in mitochondrial energy metabolism underlie the pathology of neurodegenerative diseases? Trends Neurosci. 16:125–131.

Beal MF, Kowall NW, Ellison DW, Mazurek MF, Swartz KJ, Martin JB (1986) Replication of the neurochemical characteristics of Huntington's disease by quinolinic acid. Nature 321:168–171.

Becher MW, Kotzuk JA, Sharp AH, Davies SW, Bates GP, Price DL, Ross CA (1998) Intranuclear neuronal inclusions in Huntington's disease and dentatorubral and pallidoluysian atrophy: correlation between the density of inclusions and IT15 CAG triplet repeat length. Neurobiol. Dis. 4:387–397.

Behrens PF, Franz P, Woodman B, Lindenberg KS, Landwehrmeyer GB (2002) Impaired glutamate transport and glutamate-glutamine cycling: downstream effects of the Huntington mutation. Brain 125:1908–1922.

Bellesi M, Melone M, Gubbini A, Battistacci S, Conti F (2009) GLT-1 upregulation impairs prepulse inhibition of the startle reflex in adult rats. Glia 57:703–713.

Bellesi M, Vyazovskiy V V., Tononi G, Cirelli C, Conti F (2012) Reduction of EEG theta power and changes in motor activity in rats treated with ceftriaxone. PLoS One 7:1–7.

Berendse HW, Groenewegen HJ (1990) Organization of the thalamostriatal projections in the rat, with special emphasis on the ventral striatum. J. Comp. Neurol. 299:187–228.

Bernard V, Somogyi P, Bolam JP (1997) Cellular, subcellular, and subsynaptic distribution of AMPA-type glutamate receptor subunits in the neostriatum of the rat. J. Neurosci. 17:819–833.

Bernheimer H, Birkmayer W, Hornykiewicz O, Jellinger K, Seitelberger F (1973) Brain dopamine and the syndromes of Parkinson and Huntington. Clinical, morphological and neurochemical correlations. J. Neurol. Sci. 20:415–455.

Berretta S, Parthasarathy HB, Graybiel AM (1997) Local release of GABAergic inhibition in the motor cortex induces immediate-early gene expression in indirect pathway neurons of the striatum. J. Neurosci. 17:4752–4763.

Bezzi P, Gundersen V, Galbete JL, Seifert G, Steinhäuser C, Pilati E, Volterra A (2004) Astrocytes contain a vesicular compartment that is competent for regulated exocytosis of glutamate. Nat. Neurosci. 7:613–620.

Bibb JA, Yan Z, Svenningsson P, Snyder GL, Pieribone VA, Horiuchi A, Nairn AC, Messer A, Greengard P (2000) Severe deficiencies in dopamine signaling in presymptomatic Huntington's disease mice. PNAS 97:6809–6814.

Bird ED (1980) Chemical Pathology of Huntington's Disease. Annu. Rev. Pharmacol. 20:533–551.

Bird ED, Iversen L (1974) Huntington's chorea. Post-mortem measurement of glutamic acid decarboxylase, choline acetyltransferase and dopamine in basal ganglia. Brain 97:457–472.

Bolam JP, Hanley JJ, Booth PA, Bevan MD (2000) Synaptic organisation of the basal ganglia. J. Anat. 196:527–542.

Bonelli RM, Hofmann P (2007) A systematic review of the treatment studies in Huntington's disease since 1990. Expert Opin. Pharmacother. 8:141–153.

Bordelon YM, Chesselet MF (1999) Early effects of intrastriatal injections of quinolinic acid on microtubule-associated protein-2 and neuropeptides in rat basal ganglia. Neuroscience 93:843–853.

Borrell-Pagès M, Zala D, Humbert S, Saudou F (2006) Huntington's disease: from huntingtin function and dysfunction to therapeutic strategies. Cell. Mol. Life Sci. 63:2642–2660.

Bradford J, Shin J-Y, Roberts M, Wang C-E, Li X-J, Li S-H (2009) Expression of mutant huntingtin in mouse brain astrocytes causes age-dependent neurological symptoms. PNAS 106:22480–22485.

Brickley SG, Mody I (2012) Extrasynaptic GABAa Receptors: Their Function in the CNS and Implications for Disease. Neuron 73:23–34.

Brinkman RR, Mezei MM, Theilmann J, Almqvist E, Hayden MR (1997) The likelihood of being affected with Huntington disease by a particular age, for a specific CAG size. Am. J. Hum. Genet. 60:1202–1210.

Brito V, Puigdellívol M, Giralt A, Toro D del, Alberch J, Ginés S (2013) Imbalance of p75(NTR)/TrkB protein expression in Huntington's disease: implication for neuroprotective therapies. Cell Death Dis. 4:e595.

Browne SE, Beal MF (2004) The Energetics of Huntington's Disease. Neurochem. Res. 29:531–546.

Byers RK, Dodge JA (1967) Huntington's chorea in children. Report of four cases. Neurology 17:587–596.

Callahan JW, Abercrombie ED (2011) In vivo Dopamine Efflux is Decreased in Striatum of both Fragment (R6/2) and Full-Length (YAC128) Transgenic Mouse Models of Huntington's Disease. Front. Syst. Neurosci. 5:1–10.

Caviston JP, Holzbaur ELF (2009) Huntingtin as an Essential Integrator of Intracellular Vesicular Trafficking. Trends Cell Biol. 19:147–155.

Centonze D, Rossi S, Prosperetti C, Tscherter A, Bernardi G, Maccarrone M, Calabresi P (2005) Abnormal sensitivity to cannabinoid receptor stimulation might contribute to altered gamma-aminobutyric acid transmission in the striatum of R6/2 huntington's disease mice. Biol. Psychiatry 57:1583–1589.

Cepeda C, Buchwald NA, Levine MS (1993) Neuromodulatory actions of dopamine in the neostriatum are dependent upon the excitatory amino acid receptor subtypes activated. PNAS 90:9576–9580.

Cepeda C, Cummings DM, André VM, Holley SM, Levine MS (2010) Genetic Mouse Models of Huntington's Disease: Focus on Electrophysiological Mechanisms. ASN Neuro 2:103–114.

Cepeda C, Galvan L, Holley SM, Rao SP, André VM, Botelho EP, Chen JY, Watson JB, Deisseroth K, Levine MS (2013) Multiple sources of striatal inhibition are differentially affected in Huntington's disease mouse models. J. Neurosci. 33:7393–7406.

Cepeda C, Hurst RS, Altemus KL, Flores-Hernández J, Calvert CR, Jokel ES, Grandy DK, Low MJ, Rubinstein M, Ariano MA, A., Levine MS (2001) Facilitated glutamatergic transmission in the striatum of D2 dopamine receptor-deficient mice. J. Neurophysiol. 85:659–670.

Cepeda C, Hurst RS, Calvert CR, Hernandez-Echeagaray E, Nguyen OK, Jocoy EL, Christian LJ, Ariano MA, Levine MS (2003) Transient and Progressive Electrophysiological Alterations in the Corticostriatal Pathway in a Mouse Model of Huntington's Disease. J. Neurosci. 23:961–969.

Cepeda C, Itri JN, Flores-Hernández J, Hurst RS, Calvert CR, Levine MS (2001)(b) Differential sensitivity of medium- and large-sized striatal neurons to NMDA but not kainate receptor activation in the rat. Eur. J. Neurosci. 14:1577–1589.

Cepeda C, Levine MS (1998) Dopamine and N-methyl-D-aspartate receptor interactions in the Neostriatum. Dev. Neurosci. 20:1–18.

Cepeda C, Starling AJ, Wu N-P, Nguyen OK, Uzgil B, Soda T, André VM, Ariano MA, Levine MS (2004) Increased GABAergic function in mouse models of Huntington's disease: Reversal by BDNF. J. Neurosci. Res. 78:855–867.

Cha JHJ, Frey AS, Alsdorf SA, Kerner JA, Kosinski CM, Mangiarini L, Penney JB, Davies SW, Bates GP, Young AB (1999) Altered neurotransmitter receptor expression in transgenic mouse models of Huntington's disease. Philos Trans R Soc Lond B Biol Sci. 354:981–990.

Cha JHJ, Kosinski CM, Kerner JA, Alsdorf SA, Mangiarini L, Davies SW, Penney JB, Bates GP, Young AB (1998) Altered Brain Neurotransmitter Receptors in Transgenic Mice Expressing a Portion of an Abnormal Human Huntington disease Gene. PNAS 95:6480–6485.

Chen C-M (2011) Oxidative Stress in Huntington's Disease. Chang Gung Med. J. 34:135–152.

Chen JY, Wang EA, Cepeda C, Levine MS (2013) Dopamine imbalance in Huntington's disease: A mechanism for the lack of behavioral flexibility. Front. Neurosci. 7:1–14.

Chen N, Luo T, Wellington C, Metzler M, McCutcheon K, Hayden MR, Raymond LA (1999) Subtype-specific enhancement of NMDA receptor currents by mutant huntingtin. J. Neurochem. 72:1890–1898.

Choi DW (1988) Glutamate neurotoxicity and diseases of the nervous system. Neuron 1:623–634.

Christie JM, Jane D avi. E, Monaghan DT (2000) Native N-methyl-D-aspartate receptors containing NR2A and NR2B subunits have pharmacologically distinct competitive antagonist binding sites. J. Pharmacol. Exp. Ther. 292:1169–1174.

Coyle JT (1979) An animal model for Huntington's disease. Biol. Psychiatry 14:251–276.

Coyle JT, Schwarcz R (1976) Lesion of striatal neurones with kainic acid provides a model for Huntington's chorea. Nature 263:244–246.

Cudkowicz ME, Kowall NW (1990) Degeneration of pyramidal projection neurons in Huntington's disease cortex. Ann. Neurol. 27:200–204.

Cull-Candy S, Brickley S, Farrant M (2001) NMDA receptor subunits: Diversity, development and disease. Curr. Opin. Neurobiol. 11:327–335.

Cummings DM, Alaghband Y, Hickey MA, Joshi PR, Hong SC, Zhu C, Ando TK, André VM, Cepeda C, Watson JB, Levine MS (2012) A critical window of CAG repeat-length correlates with phenotype severity in the R6/2 mouse model of Huntington's disease. J. Neurophysiol. 107:677–691.

Cummings DM, André VM, Uzgil BO, Gee SM, Fisher YE, Cepeda C, Levine MS (2009) Alterations in Cortical Excitation and Inhibition in Genetic Mouse Models of Huntington's Disease. J. Neurosci. 29:10371–10386.

Danbolt NC (2001) Glutamate uptake. Prog. Neurobiol. 65:1–105.

Davies SW, Turmaine M, Cozens BA, DiFiglia M, Sharp AH, Ross CA, Scherzinger E, Wanker EE, Mangiarini L, Bates GP (1997) Formation of neuronal intranuclear inclusions underlies the neurological dysfunction in mice transgenic for the HD mutation. Cell 90:537–548.

DeLong MR (1990) Primate models of movement disorders of basal ganglia origin. Trends Neurosci. 13:281–285.

Deng Y, Lanciego J, Goff LK-L, Coulon P, Salin P, Kachidian P, Lei W, Mar N Del, Reiner A (2015) Differential organization of cortical inputs to striatal projection neurons of the matrix compartment in rats. Front. Syst. Neurosci. 9:1–14.

Deng YP, Albin RL, Penney JB, Young AB, Anderson KD, Reiner A (2004) Differential loss of striatal projection systems in Huntington's disease: A quantitative immunohistochemical study. J. Chem. Neuroanat. 27:143–164.

Deng YP, Wong T, Bricker-Anthony C, Deng B, Reiner A (2013) Loss of corticostriatal and thalamostriatal synaptic terminals precedes striatal projection neuron pathology in heterozygous Q140 Huntington's disease mice. Neurobiol. Dis. 60:89–107.

Deng YP, Wong T, Wan JY, Reiner A (2014) Differential loss of thalamostriatal and corticostriatal input to striatal projection neuron types prior to overt motor symptoms in the Q140 Huntington's disease knock-in mice. Front. Syst. Neurosci. 8:198.

DiFiglia M (1990) Excitotoxic Injury of the Neostriatum: a Model for Huntington's Disease. Trends Neurosci. 13:286–289.

DiFiglia M, Sapp E, Chase KO, Davies SW, Bates GP, Vonsattel J-P, Aronin N (1997) Aggregation of huntingtin in neuronal intranuclear inclusions and dystrophic neurites in brain. Science 277:1990–1993.

DiFiglia M, Sapp E, Chase KO, Schwarz C, Meloni A, Young C, Martin E, Vonsattel J-P, Carraway R, Reeves SA, Boyce FM, Aronin N (1995) Huntingtin is a Cytoplasmic Protein Associated With Vesicles in Human and Rat Brain Neurons. Neuron 14:1075–1081.

Ding JB, Guzman JN, Peterson JD, Goldberg JA, Surmeier DJ (2010) Thalamic Gating of Corticostriatal Signaling by Cholinergic Interneurons. Neuron 67:294–307.

Ding JB, Peterson JD, Surmeier DJ (2008) Corticostriatal and Thalamostriatal Synapses Have Distinctive Properties. J. Neurosci. 28:6483–6492.

Dragatsis I, Goldowitz D, Mar N Del, Deng YP, Meade CA, Liu L, Sun Z, Yue J, Reiner A (2009) CAG repeat lengths > or =335 attenuate the phenotype in the R6/2 Huntington's disease transgenic mouse. Neurobiol. Dis. 33:315–330.

Dumartin B, Jaber M, Gonon F, Caron MG, Giros B, Bloch B (2000) Dopamine tone regulates D1 receptor trafficking and delivery in striatal neurons in dopamine transporter-deficient mice. PNAS 97:1879–1884.

Dvorzhak A, Semtner M, Faber DS, Grantyn R (2013) Tonic mGluR5/CB1-dependent suppression of inhibition as a pathophysiological hallmark in the striatum of mice carrying a mutant form of huntingtin. J. Physiol. 591:1145–1166.

Erreger K, Geballe MT, Dravid SM, Snyder JP, Wyllie DJA, Traynelis SF (2005) Mechanism of partial agonism at NMDA receptors for a conformationally restricted glutamate analog. J. Neurosci. 25:7858–7866.

Estrada-Sánchez AM, Mejía-Toiber J, Massieu L (2008) Excitotoxic Neuronal Death and the Pathogenesis of Huntington's Disease. Arch. Med. Res. 39:265–276.

Estrada-Sánchez AM, Montiel T, Segovia J, Massieu L (2009) Glutamate toxicity in the striatum of the R6/2 Huntington's disease transgenic mice is age-dependent and correlates with decreased levels of glutamate transporters. Neurobiol. Dis. 34:78–86.

Estrada-Sánchez AM, Rebec G V. (2012) Corticostriatal dysfunction and glutamate transporter 1 (GLT1) in Huntington's disease: Interactions between neurons and astrocytes. Basal Ganglia 2:57–66.

Exley R, Cragg SJ (2008) Presynaptic nicotinic receptors: a dynamic and diverse cholinergic filter of striatal dopamine neurotransmission. Br. J. Pharmacol. 153:S283–S297.

Faber PW, Voisine C, King DC, Bates EA, Hart AC (2002) Glutamine/proline-rich PQE-1 proteins protect Caenorhabditis elegans neurons from huntingtin polyglutamine neurotoxicity. PNAS 99:17131–17136.

Faideau M, Kim J, Cormier K, Gilmore R, Welch M, Auregan G, Dufour N, Guillermier M, Brouillet E, Hantraye P, DéGlon N, Ferrante RJ, Bonvento G (2010) In vivo expression of polyglutamine-expanded huntingtin by mouse striatal astrocytes impairs glutamate transport: A correlation with Huntington's disease subjects. Hum. Mol. Genet. 19:3053–3067.

Fan MMY, Fernandes HB, Zhang LYJ, Hayden MR, Raymond LA (2007) Altered NMDA receptor trafficking in a yeast artificial chromosome transgenic mouse model of Huntington's disease. J. Neurosci. 27:3768–3779.

Farrar AM, Callahan JW, Abercrombie ED (2011) Reduced striatal acetylcholine efflux in the R6/2 mouse model of Huntington's disease: An examination of the role of altered inhibitory and excitatory mechanisms. Exp. Neurol. 232:119–125.

Fernandez S, Almeida A, Bolaños JP (2012) Antioxidant and bioenergetic coupling between neurons and astrocytes. Biochem. J. 443:3–11.

Ferrante RJ, Andreassen OA, Jenkins BG, Dedeoglu A, Kuemmerle S, Kubilus JK, Kaddurah-Daouk R, Hersch SM, Beal MF (2000) Neuroprotective effects of creatine in a transgenic mouse model of Huntington's disease. J. Neurosci. 20:4389–4397.

Ferrante RJ, Kowall NW, Cipolloni PB, Storey E, Beal MF (1993) Excitotoxin lesions in primates as a model for Huntington's disease: histopathologic and neurochemical characterization. Exp. Neurol. 119:46–71.

Flaherty AW, Graybiel AM (1994) Input-Output Organization of the Sensorimotor Striatum in the Squirrel Monkey. J. Neurosci. 14:599–610.

Flores-Hernández J, Galarraga E, Bargas J (1997) Dopamine selects glutamatergic inputs to neostriatal neurons. Synapse 25:185–195.

Freese A, DiFiglia M, Koroshetz WJ, Beal MF, Martin JB (1990) Characterization and mechanism of glutamate neurotoxicity in primary striatal cultures. Brain Res. 521:254–264.

Fremeau RT, Kam K, Qureshi T, Johnson J, Copenhagen DR, Storm-Mathisen J, Chaudhry FA, Nicoll RA, Edwards RH (2004) Vesicular glutamate transporters 1 and 2 target to functionally distinct synaptic release sites. Science. 304:1815–1819.

Fremeau RT, Troyer MD, Pahner I, Nygaard GO, Tran CH, Reimer RJ, Bellocchio EE, Fortin D, Storm-Mathisen J, Edwards RH (2001) The expression of vesicular glutamate transporters defines two classes of excitatory synapse. Neuron 31:247–260.

Fujiyama F, Kuramoto E, Okamoto K, Hioki H, Furuta T, Zhou L, Nomura S, Kaneko T (2004) Presynaptic localization of an AMPA-type glutamate receptor in corticostriatal and thalamostriatal axon terminals. Eur. J. Neurosci. 20:3322–3330.

Galvan L, Wang EA, Cepeda C, Levine MS (2012) Functional Differences Between Direct and Indirect Striatal Output Pathways in Huntington's Disease. J. Huntingtons. Dis. 1:17–25.

Gambardella A, Muglia M, Labate A, Magariello A, Gabriele AL, Mazzei R, Pirritano D, Conforti FL, Patitucci A, Valentino P, Zappia M, Quattrone A (2001) Juvenile Huntington's disease presenting as progressive myoclonic epilepsy. Neurology 57:708-711.

Garrett MC, Soares-da-Silva P (1992) Increased cerebrospinal fluid dopamine and 3,4-dihydroxyphenylacetic acid levels in Huntington's disease: evidence for an overactive dopaminergic brain transmission. J. Neurochem. 58:101–106.

Gerfen CR (1992) The neostriatal mosaic: multiple levels of compartmental organization. Trends Neurosci. 15:133–139.

Gerfen CR, Engber TM, Mahan LC, Susel Z, Chase TN, Monsma FJ, Sibley DR (1990) D1 and D2 dopamine receptor-regulated gene expression of striatonigral and striatopallidal neurons. Science 250:1429–1432.

Gil JM, Rego AC (2008) Mechanisms of neurodegeneration in Huntington's disease. Eur. J. Neurosci. 27:2803–2820.

Ginovart N, Lundin A, Farde L, Halldin C, Bäckman L, Swahn CG, Pauli S, Sedvall G (1997) PET study of the pre- and post-synaptic dopaminergic markers for the neurodegenerative process in Huntington's disease. Brain 120:503–514.

Giros B, Jaber M, Jones SR, Wightman RM, Caron MG (1996) Hyperlocomotion and indifference to cocaine and amphetamine in mice lacking the dopamine transporter. Nature 379:606–612.

Gomide V, Bibancos T, Chadi G (2005) Dopamine cell morphology and glial cell hypertrophy and process branching in the nigrostriatal system after striatal 6-OHDA analyzed by specific sterological tools. Int. J. Neurosci. 115:557–582.

Goodman AOG, Murgatroyd PR, Medina-Gomez G, Wood NI, Finer N, Vidal-Puig AJ, Morton AJ, Barker RA (2008) The metabolic profile of early Huntington's disease- a combined human and transgenic mouse study. Exp. Neurol. 210:691–698.

Gray M, Shirasaki DI, Cepeda C, André VM, Wilburn B, Lu X-H, Tao J, Yamazaki I, Li S-H, Sun YE, Li X-J, Levine MS, Yang XW (2008) Full-Length Human Mutant Huntingtin with a Stable Polyglutamine Repeat Can Elicit Progressive and Selective Neuropathogenesis in BACHD Mice. J. Neurosci. 28:6182–6195.

Gu X, André VM, Cepeda C, Li S-H, Li X-J, Levine MS, Yang XW (2007) Pathological cell-cell interactions are necessary for striatal pathogenesis in a conditional mouse model of Huntington's disease. Mol. Neurodegener. 2:1–11.

Gu X, Li C, Wei W, Lo V, Gong S, Li S-H, Iwasato T, Itohara S, Li X-J, Mody I, Heintz N, Yang XW (2005) Pathological cell-cell interactions elicited by a neuropathogenic form of mutant Huntingtin contribute to cortical pathogenesis in HD mice. Neuron 46:433–444.

Guo Q, Wang D, He X, Feng Q, Lin R, Xu F, Fu L, Luo M (2015) Whole-Brain Mapping of Inputs to Projection Neurons and Cholinergic Interneurons in the Dorsal Striatum. PLoS One 10:1–15.

Haber SN, Nauta WJH (1983) Ramifications of the globus pallidus in the rat as indicated by patterns of immunohistochemistry. Neuroscience 9:245–260.

Halliday GM, McRitchie DA, Macdonald V, Double KL, Trent RJ, McCusker E (1998) Regional specificity of brain atrophy in Huntington's disease. Exp. Neurol. 154:663–672.

Hamilton NB, Attwell D (2010) Do astrocytes really exocytose neurotransmitters? Nat. Rev. Neurosci. 11:227–238.

Hanley JJ, Bolam JP (1997) Synaptology of the nigrostriatal projection in relation to the compartmental organization of the neostriatum in the rat. Neuroscience 81:353–370.

Harper PS (1996) New Genes for Old Diseases: the Molecular Basis of Myotonic Dystrophy and Huntington's Disease. Lumleian Lect. 30:221–231.

Harper PS, Jones L (2002) Huntington's Disease: Genetic and Molecular Studies. Huntington's Dis. Third Ed.:113–158.

Hassel B, Tessler S, Faull RLM, Emson PC (2008) Glutamate uptake is reduced in prefrontal cortex in Huntington's disease. Neurochem. Res. 33:232–237.

Hedreen JC, Folstein SE (1995) Early loss of neostriatal striosome neurons in Huntington's disease. J. Neuropathol. Exp. Neurol. 54:105–120.

Hedreen JC, Peyser CE, Folstein SE, Ross CA (1991) Neuronal loss in layers V and VI of cerebral cortex in Huntington's disease. Neurosci. Lett. 133:257–261.

Heinsen H, Rüb U, Gangnus D, Jungkunz G, Bauer M, Ulmar G, Bethke B, Schüler M, Böcker F, Eisenmenger W, Götz M, Strik M (1996) Nerve Cell Loss in the Thalamic Centromedian-Parafascicular Complex in Patients with Huntington's Disease. Acta Neuropathol. 91:161–168.

Heinsen H, Strik M, Bauer M, Luther K, Ulmar G, Gangnus D, Jungkunz G, Eisenmenger W, Götz M (1994) Cortical and striatal neurone number in Huntington's disease. Acta Neuropathol. 88:320–333.

Heng MY, Detloff PJ, Wang PL, Tsien JZ, Albin RL (2009) In vivo evidence for NMDA receptor-mediated excitotoxicity in a murine genetic model of Huntington disease. J. Neurosci. 29:3200–3205.

Hertz L (1979) Functional interactions between neurons and astrocytes I. Turnover and metabolism of putative amino acid transmitters. Prog. Neurobiol. 13:277–323.

Herzog E, Bellenchi GC, Gras C, Bernard V, Ravassard P, Bedet C, Gasnier B, Giros B, Mestikawy S El (2001) The existence of a second vesicular glutamate transporter specifies subpopulations of glutamatergic neurons. J. Neurosci. 21:1–6.

Hickey MA, Chesselet M-F (2003) The use of transgenic and knock-in mice to study Huntington's disease. Cytogenet. Genome Res. 100:276–286.

Hickey MA, Reynolds GP, Morton AJ (2002) The Role of Dopamine in Motor Symptoms in the R6/2 Transgenic Mouse Model of Huntington's Disease. J. Neurochem. 81:46–59.

Hodgson JG, Agopyan N, Gutekunst CA, Leavitt BR, Lepiane F, Singaraja R, Smith DJ, Bissada N, McCutcheon K, Nasir J, Jamot L, Xiao-Jiang L, Stevens ME, Rosemond E, Roder JC, Phillips AG, Rubin EM, Hersch SM, Hayden MR (1999) A YAC mouse model for Huntington's disease with full-length mutant huntingtin, cytoplasmic toxicity, and selective striatal neurodegeneration. Neuron 23:181–192.

Hofer S, Frahm J (2006) Topography of the human corpus callosum revisited-Comprehensive fiber tractography using diffusion tensor magnetic resonance imaging. Neuroimage 32:989–994.

Hoffner G, Kahlem P, Djian P (2002) Perinuclear localization of huntingtin as a consequence of its binding to microtubules through an interaction with beta-tubulin: relevance to Huntington's disease. J. Cell Sci. 115:941–948.

Holley SM, Joshi PR, Parievsky A, Huynh MN, Cepeda C, Levine MS, Galvan L, Chen JY, Fisher YE (2015)(b) Enhanced GABAergic Inputs Contribute to Functional Alterations of Cholinergic Interneurons in the R6/2 Mouse Model of Huntington's. eNeuro 0008-14.2015

Horsten S Von et al. (2003) Transgenic rat model of Huntington's disease. Hum. Mol. Genet. 12:617–624.

Huang K, Kang MH, Askew C, Kang R, Sanders SS, Wan J, Davis NG, Hayden MR (2010) Palmitoylation and function of glial glutamate transporter-1 is reduced in the YAC128 mouse model of Huntington disease. Neurobiol. Dis. 40:207–215.

Huntington Study Group (2006) Tetrabenazine as antichorea therapy in Huntington disease: A randomized controlled trial. Neurology 66:366–372.

Indersmitten T, Tran CH, Cepeda C, Levine MS (2015) Altered Excitatory and Inhibitory Inputs to Striatal Medium-Sized Spiny Neurons and Cortical Pyramidal Neurons in the Q175 Mouse Model of Huntington's Disease. J. Neurophysiol. 310:1–43.

Jackson GR, Salecker I, Dong X, Yao X, Arnheim N, Faber PW, MacDonald ME, Zipursky SL (1998) Polyglutamine-expanded human huntingtin transgenes induce degeneration of Drosophila photoreceptor neurons. Neuron 21:633–642.

Jacobsen JC, Bawden CS, Rudiger SR, McLaughlan CJ, Reid SJ, Waldvogel HJ, MacDonald ME, Gusella JF, Walker SK, Kelly JM, Webb GC, Faull RLM, Rees MI, Snell RG (2010) An ovine transgenic Huntington's disease model. Hum. Mol. Genet. 19:1873–1882.

Jahanshahi A, Vlamings R, Kaya AH, Lim LW, Janssen MLF, Tan S, Visser-Vandewalle V, Steinbusch HWM, Temel Y (2010) Hyperdopaminergic status in experimental Huntington disease. J. Neuropathol. Exp. Neurol. 69:910–917.

Jahanshahi A, Vlamings R, Roon-Mom WMC van, Faull RLM, Waldvogel HJ, Janssen MLF, Yakkioui Y, Zeef DH, Kocabicak E, Steinbusch HWM, Temel Y (2013) Changes in brainstem serotonergic and dopaminergic cell populations in experimental and clinical Huntington's disease. Neuroscience 238:71–81.

Jia Y, Gall CM, Lynch G (2010) Presynaptic BDNF promotes postsynaptic long-term potentiation in the dorsal striatum. J. Neurosci. 30:14440–14445.

Jocoy EL, André VM, Cummings DM, Rao SP, Wu N-P, Ramsey AJ, Caron MG, Cepeda C, Levine MS (2011) Dissecting the contribution of individual receptor subunits to the enhancement of N-methyl-D-aspartate currents by dopamine D1 receptor activation in striatum. Front. Syst. Neurosci. 5:1–16.

Johnson MA, Rajan V, Miller CE, Wightman RM (2006) Dopamine release is severely compromised in the R6/2 mouse model of Huntington's disease. J. Neurochem. 97:737–746.

Joshi PR, Wu N-P, André VM, Cummings DM, Cepeda C, Joyce JA, Carroll JB, Leavitt BR, Hayden MR, Levine MS, Bamford NS (2009) Age-dependent alterations of corticostriatal activity in the YAC128 mouse model of Huntington disease. J. Neurosci. 29:2414–2427.

Kassubek J, Bernhard Landwehrmeyer G, Ecker D, Juengling FD, Muche R, Schuller S, Weindl A, Peinemann A (2004)(a) Global cerebral atrophy in early stages of Huntington's disease: quantitative MRI study. Neuroreport 15:363–365.

Kassubek J, Juengling FD, Kioschies T, Henkel K, Karitzky J, Kramer B, Ecker D, Andrich J, Saft C, Kraus P, Aschoff AJ, Ludolph AC, Landwehrmeyer GB (2004)(b) Topography of cerebral atrophy in early Huntington's disease: a voxel based morphometric MRI study. J. Neurol. Neurosurg. Psychiatry 75:213–220.

Kawaguchi Y, Wilson CJ, Emson PC (1990) Projection subtypes of rat neostriatal matrix cells revealed by intracellular injection of biocytin. J. Neurosci. 10:3421–3438.

Kieval JZ, Hubert GW, Charara A, Paré JF, Smith Y (2001) Subcellular and subsynaptic localization of presynaptic and postsynaptic kainate receptor subunits in the monkey striatum. J. Neurosci. 21:8746–8757.

Kim EH, Thu DC V., Tippett LJ, Oorschot DE, Hogg VM, Roxburgh R, Synek BJ, Waldvogel HJ, Faull RLM (2014) Cortical interneuron loss and symptom heterogeneity in Huntington disease. Ann. Neurol. 75:717–727.

Kimura M, Minamimoto T, Matsumoto N, Hori Y (2004) Monitoring and switching of cortico-basal ganglia loop functions by the thalamo-striatal system. Neurosci. Res. 48:335–360.

Kinomura S, Larsson J, Gulyás B, Roland PE (1996) Activation by attention of the human reticular formation and thalamic intralaminar nuclei. Science. 271:512–515.

Kirkwood SC, Su JL, Conneally P, Foroud T (2001) Progression of symptoms in the early and middle stages of Huntington disease. Arch. Neurol. 58:273–278.

Kish SJ, Shannak K, Hornykiewicz O (1987) Elevated serotonin and reduced dopamine in subregionally divided Huntington's disease striatum. Ann. Neurol. 22:386–389.

Kita H, Kitai ST (1988) Glutamate decarboxylase immunoreactive neurons in rat neostriatum: their morphological types and populations. Brain Res. 447:346–352.

Klapstein GJ, Fisher RS, Zanjani H, Cepeda C, Jokel ES, Chesselet M-F, Levine MS (2001) Electrophysiological and Morphological Changes in Striatal Spiny Neurons in R6/2 Huntington's Disease Transgenic Mice. J. Neurophysiol. 86:2667–2677.

Kravitz A V., Freeze BS, Parker PRL, Kay K, Thwin MT, Deisseroth K, Kreitzer AC (2010) Regulation of Parkinsonian Motor Behaviours by Optogenetic Control of Basal Ganglia Circuitry. Nature 466:622–629.

Kreitzer AC (2009) Physiology and pharmacology of striatal neurons. Annu. Rev. Neurosci. 32:127–147.

Kreitzer AC, Malenka RC (2005) Dopamine modulation of state-dependent endocannabinoid release and long-term depression in the striatum. J. Neurosci. 25:10537–10545.

Kress GJ, Yamawaki N, Wokosin DL, Wickersham IR, Shepherd GMG, Surmeier DJ (2013) Convergent cortical innervation of striatal projection neurons. Nat. Neurosci. 16:665–667.

Kunig G, Leenders KL, Sanchez-Pernaute R, Antonini A, Vontobel P, Verhagen A, Gunther I (2000) Benzodiazepine Receptor Binding in Huntington's Disease: [11C]Flumazenil Uptake Measured Using Positron Emission Tomography. Ann. Neurol. 47:156.

La Monte SM De, Vonsattel J-P, Richardson EP (1988) Morphometric demonstration of atrophic changes in the cerebral cortex, white matter, and neostriatum in Huntington's disease. J. Neuropathol. Exp. Neurol. 47:516–525.

Lacey CJ, Bolam JP, Magill PJ (2007) Novel and Distinct Operational Principles of Intralaminar Thalamic Neurons and Their Striatal Projections. J. Neurosci. 27:4374–4384.

Landwehrmeyer GB, Standaert DG, Testa CM, Penney JB, Young AB (1995) NMDA Receptor and Interneurons Subunit mRNA Expression by Projection Neurons and Interneurons in Rat Striatum. J. Neurosci. 15:5297–5307.

Lapper SR, Bolam JP (1992) Input from the frontal cortex and the parafascicular nucleus to cholinergic interneurons in the dorsal striatum of the rat. Neuroscience 51:533–545.

Leeflang EP, Zhang L, Tavaré S, Hubert R, Srinidhi J, MacDonald ME, Myers RH, Young M de, Wexler NS, Gusella JF (1995) Single sperm analysis of the trinucleotide repeats in the Huntington's disease gene: quantification of the mutation frequency spectrum. Hum. Mol. Genet. 4:1519–1526.

Lei W, Deng Y, Liu B, Mu S, Guley NM, Wong T, Reiner A (2013) Confocal laser scanning microscopy and ultrastructural study of VGLUT2 thalamic input to striatal projection neurons in rats. J. Comp. Neurol. 521:1354–1377.

Lei W, Jiao Y, Mar N Del, Reiner A (2004) Evidence for differential cortical input to direct pathway versus indirect pathway striatal projection neurons in rats. J. Neurosci. 24:8289–8299.

Levine MS, Altemus KL, Cepeda C, Cromwell HC, Crawford C, Ariano MA, Drago J, Sibley DR, Westphal H (1996) Modulatory actions of dopamine on NMDA receptor-mediated responses are reduced in D1A-deficient mutant mice. J. Neurosci. 16:5870–5882.

Levine MS, Cepeda C, Hickey MA, Fleming SM, Chesselet M-F (2004) Genetic Mouse Models of Huntington's and Parkinson's Diseases: Illuminating But Imperfect. Trends Neurosci. 27:691–697.

Levine MS, Klapstein GJ, Koppel A, Gruen E, Cepeda C, Vargas ME, Jokel ES, Carpenter EM, Zanjani H, Hurst RS, Efstratiadis A, Zeitlin S (1999) Enhanced Sensitivity to N-methyl-D-aspartate Receptor Activation in Transgenic and Knockin Mouse Models of Huntington's Disease. J. Neurosci. Res. 58:515–532.

Li J-Y, Plomann M, Brundin P (2003)(a) Huntington's disease: a synaptopathy? Trends Mol. Med. 9:414–420.

Li L, Fan MMY, Icton CD, Chen N, Leavitt BR, Hayden MR, Murphy TH, Raymond LA (2003)(b) Role of NR2B-type NMDA receptors in selective neurodegeneration in Huntington disease. Neurobiol. Aging 24:1113–1121.

Li L, Murphy TH, Hayden MR, Raymond LA (2004) Enhanced striatal NR2B-containing N-methyl-D-aspartate receptor-mediated synaptic currents in a mouse model of Huntington disease. J. Neurophysiol. 92:2738–2746.

Li X, Valencia A, Sapp E, Masso N, Alexander J, Reeves P, Kegel KB, Aronin N, Difiglia M (2010) Aberrant Rab11-dependent trafficking of the neuronal glutamate transporter EAAC1 causes oxidative stress and cell death in Huntington's disease. J. Neurosci. 30:4552–4561.

Liévens JC, Rival T, Iché M, Chneiweiss H, Birman S (2005) Expanded polyglutamine peptides disrupt EGF receptor signaling and glutamate transporter expression in Drosophila. Hum. Mol. Genet. 14:713–724.

Liévens JC, Woodman B, Mahal A, Spasic-Boscovic O, Samuel D, Kerkerian-Le Goff L, Bates GP (2001) Impaired glutamate uptake in the R6 Huntington's disease transgenic mice. Neurobiol. Dis. 8:807–821.

Lin CH, Tallaksen-Greene S, Chien WM, Cearley JA, Jackson WS, Crouse AB, Ren S, Li XJ, Albin RL, Detloff PJ (2001) Neurological abnormalities in a knock-in mouse model of Huntington's disease. Hum. Mol. Genet. 10:137–144.

Liu X, Miller BR, Rebec G V., Clemmera DE (2007) NIH Public Access. J. Proteome Res. 6:3134–3142.

Lloyd KG, Davidson L (1979) [3H]GABA binding in brains from Huntington's chorea patients: altered regulation by phospholipids? Science 205:1147–1149.

Lloyd KG, Dreksler S, Bird ED (1977) Alterations in 3H-GABA binding in Huntington's chorea. Life Sci. 21:747–753.

Luthi-Carter R, Strand A, Peters NL, Solano SM, Hollingsworth ZR, Menon AS, Frey AS, Spektor BS, Penney EB, Schilling G, Ross CA, Borchelt DR, Tapscott SJ, Young AB, Cha JHJ, Olson JM (2000) Decreased expression of striatal signaling genes in a mouse model of Huntington's disease. Hum. Mol. Genet. 9:1259–1271.

Macchi G, Bentivoglio M, Molinari M, Minciacchi D (1984) The thalamo-caudate versus thalamo-cortical projections as studied in the cat with fluorescent retrograde double labeling. Exp. Brain Res. 54:225–239.

MacDonald ME, Barnes G, Srinidhi J, Duyao MP, Ambrose CM, Myers RH, Gray J, Conneally PM, Young A, Penney J (1993) Gametic but not somatic instability of CAG repeat length in Huntington's disease. J. Med. Genet. 30:982–986.

Macdonald V, Halliday GM (2002) Pyramidal cell loss in motor cortices in Huntington's disease. Neurobiol. Dis. 10:378–386.

Maejima T, Ohno-Shosaku T, Kano M (2001) Endogenous cannabinoid as a retrograde messenger from depolarized postsynaptic neurons to presynaptic terminals. Neurosci. Res. 40:205–210.

Mangiarini L, Sathasivam K, Seller M, Cozens B, Harper A, Hetherington C, Lawton M, Trottier Y, Lehrach H, Davies SW, Bates GP (1996) Exon 1 of the HD gene with an expanded CAG repeat is sufficient to cause a progressive neurological phenotype in transgenic mice. Cell 87:493–506.

Mann DM, South PW (1993) The topographic distribution of brain atrophy in frontal lobe dementia. Acta Neuropathol. 85:334–340.

Manyam NVB, Hare. TA, Katz L, Glaeser BS (1978) Huntington's Disease. Arch. Neurol. 35:728–730.

Marco S, Giralt A, Petrovic MM, Pouladi MA, Martínez-Turrillas R, Martínez-Hernández J, Kaltenbach LS, Torres-Peraza J, Graham RK, Watanabe M, Luján R, Nakanishi N, Lipton SA, Lo DC, Hayden MR, Alberch J, Wesseling JF, Pérez-Otaño I (2013) Suppressing aberrant GluN3A expression rescues synaptic and behavioral impairments in Huntington's disease models. Nat. Med. 19:1030–1038.

McGeer EG, McGeer PL (1976) Duplication of biochemical changes of Huntington's chorea by intrastriatal injections of glutamic and kainic acids. Nature 263:517–519.

Menalled LB et al. (2012) Comprehensive Behavioral and Molecular Characterization of a New Knock-In Mouse Model of Huntington's Disease: zQ175. PLoS One 7:1–14.

Menalled LB, Chesselet M-F (2002) Mouse models of Huntington's disease. Trends Pharmacol. Sci. 23:32–39.

Menalled LB, Sison JD, Dragatsis I, Zeitlin S, Chesselet MF (2003) Time course of early motor and neuropathological anomalies in a knock-in mouse model of Huntington's disease with 140 CAG repeats. J. Comp. Neurol. 465:11–26.

Menalled LB, Zanjani H, MacKenzie L, Koppel A, Carpenter E, Zeitlin S, Chesselet MF (2000) Decrease in striatal enkephalin mRNA in mouse models of Huntington's disease. Exp. Neurol. 162:328–342.

Meredith GE, Wouterlood FG, Pattiselanno A (1990) Hippocampal fibers make synaptic contacts with glutamate decarboxylase-immunoreactive neurons in the rat nucleus accumbens. Brain Res. 513:329–334.

Miller BR, Dorner JL, Bunner KD, Gaither TW, Klein EL, Barton SJ, Rebec G V. (2012) Up-regulation of GLT1 reverses the deficit in cortically evoked striatal ascorbate efflux in the R6/2 mouse model of Huntington's disease. J. Neurochem. 121:629–638.

Miller BR, Dorner JL, Shou M, Sari Y, Barton SJ, Sengelaub DR, Kennedy RT, Rebec G V. (2008) Up-regulation of GLT1 expression increases glutamate uptake and attenuates the Huntington's disease phenotype in the R6/2 mouse. Neuroscience 153:329–337.

Milnerwood AJ, Cummings DM, Dallérac GM, Brown JY, Vatsavayai SC, Hirst MC, Rezaie P, Murphy KP (2006) Early development of aberrant synaptic plasticity in a mouse model of Huntington's disease. Hum. Mol. Genet. 15:1690–1703.

Milnerwood AJ, Gladding CM, Pouladi MA, Kaufman AM, Hines RM, Boyd JD, Ko RWY, Vasuta OC, Graham RK, Hayden MR, Murphy TH, Raymond LA (2010) Early increase in extrasynaptic NMDA receptor signaling and expression contributes to phenotype onset in Huntington's disease mice. Neuron 65:178–190.

Minamimoto T, Kimura M (2002) Participation of the Thalamic CM-Pf Complex in Attentional Orienting. J. Neurophysiol. 87:3090–3101.

Mink JW (1996) The basal ganglia: focused selection and inhibition of competing motor programs. Prog. Neurobiol. 50:381–425.

Mochel F, Durant B, Durr A, Schiffmann R (2011) Altered dopamine and serotonin metabolism in motorically asymptomatic R6/2 mice. PLoS One 6:e18336.

Morris G, Arkadir D, Nevet A, Vaadia E, Bergman H (2004) Coincident but distinct messages of midbrain dopamine and striatal tonically active neurons. Neuron 43:133–143.

Morton AJ, Avanzo L (2011) Executive decision-making in the domestic sheep. PLoS One 6:e15752.

Morton AJ, Glynn D, Leavens W, Zheng Z, Faull RL, Skepper JN, Wight JM (2009) Paradoxical delay in the onset of disease caused by super-long CAG repeat expansions in R6/2 mice. Neurobiol. Dis. 33:331–341.

Morton AJ, Wood NI, Hastings MH, Hurelbrink C, Barker RA, Maywood ES (2005) Disintegration of the sleep-wake cycle and circadian timing in Huntington's disease. J. Neurosci. 25:157–163.

Nagel G, Szellas T, Huhn W, Kateriya S, Adeishvili N, Berthold P, Ollig D, Hegemann P, Bamberg E (2003) Cation-Selective Membrane Channel. PNAS 100:13940–13945.

Nasir J, Floresco SB, O'Kusky JR, Diewert VM, Richman JM, Zeisler J, Borowski A, Marth JD, Phillips AG, Hayden MR (1995) Targeted Disruption of the Huntington's Disease Gene Results in Embryonic Lethality and Behavioral and Morphological Changes in Heterozygotes. Cell 81:811–823.

NicNiocaill B, Haraldsson B, Hansson O, O'Connor WT, Brundin P (2001) Altered striatal amino acid neurotransmitter release monitored using microdialysis in R6/1 Huntington transgenic mice. Eur. J. Neurosci. 13:206–210.

Nithianantharajah J, Hannan AJ (2013) Dysregulation of synaptic proteins, dendritic spine abnormalities and pathological plasticity of synapses as experience-dependent mediators of cognitive and psychiatric symptoms in Huntington's disease. Neuroscience 251:66–74.

Nørremølle A, Sørensen SA, Fenger K, Hasholt L (1995) Correlation between magnitude of CAG repeat length alterations and length of the paternal repeat in paternally inherited Huntington's disease. Clin. Genet. 47:113–117.

Novak MJU, Tabrizi SJ (2010) Huntington's Disease. BMJ 340.

Okamoto S, Pouladi MA, Talantova M, Yao D, Xia P, Ehrnhoefer DE, Zaidi R, Clemente A, Kaul M, Graham RK, Zhang D, Chen H-SV, Tong G, Hayden MR, Lipton SA (2009) Balance between synaptic versus extrasynaptic NMDA receptor activity influences inclusions and neurotoxicity of mutant huntingtin. Nat. Med. 15:1407–1413.

Omrani A, Melone M, Bellesi M, Safiulina V, Aida T, Tanaka K, Cherubini E, Conti F (2009) Up-regulation of GLT-1 severely impairs LTD at mossy fibre--CA3 synapses. J. Physiol. 587:4575–4588.

Ordway JM, Tallaksen-Greene S, Gutekunst CA, Bernstein EM, Cearley JA, Wiener HW, Dure IV LS, Lindsey R, Hersch SM, Jope RS, Albin RL, Detloff PJ (1997) Ectopically expressed CAG repeats cause intranuclear inclusions and a progressive late onset neurological phenotype in the mouse. Cell 91:753–763.

Ortiz AN, Kurth BJ, Osterhaus GL, Johnson MA (2010) Dysregulation of Intracellular Dopamine Stores Revealed in the R6/2 Mouse Striatum. J. Neurochem. 112:755–761.

Palygin O, Lalo U, Verkhratsky A, Pankratov Y (2010) Ionotropic NMDA and P2X1/5 receptors mediate synaptically induced Ca2+ signalling in cortical astrocytes. Cell Calcium 48:225–231.

Papadia S, Hardingham GE (2007) The dichotomy of NMDA receptor signalling. Neuroscientist 13:572–579.

Patel S, Rademacher DJ, Hillard CJ (2003) Differential regulation of the endocannabinoids anandamide and 2-arachidonylglycerol within the limbic forebrain by dopamine receptor activity. J. Pharmacol. Exp. Ther. 306:880–888.

Pearson SJ, Reynolds GP (1994) Neocortical neurotransmitter markers in Huntington's disease. J. Neural Transm. Gen. Sect. 98:197–207.

Penney JB, Young AB (1983) Speculations on the Functional Anatomy of Basal Ganglia Disorders. Annu. Rev. Neurosci. 6:73–94.

Perry TL, Hansen S, Kloster M (1973) Huntington's Chorea. N. Engl. J. Med. 288:337–342.

Perry TL, Hansen S, Wall RA, Gauthier SG (1982) Human CSF GABA concentrations: revised downward for controls, but not decreased in Huntington's chorea. J. Neurochem. 38:766–773.

Petersén A, Chase K, Puschban Z, DiFiglia M, Brundin P, Aronin N (2002)(a) Maintenance of susceptibility to neurodegeneration following intrastriatal injections of quinolinic acid in a new transgenic mouse model of Huntington's disease. Exp. Neurol. 175:297–300.

Petersén A, Puschban Z, Lotharius J, NicNiocaill B, Wiekop P, O'Connor WT, Brundin P (2002)(b) Evidence for dysfunction of the nigrostriatal pathway in the R6/1 line of transgenic Huntington's disease mice. Neurobiol. Dis. 11:134–146.

Pettibone DJ, Pflueger AB, Totaro JA (1984) Tetrabenazine-induced depletion of brain monoamines: mechanism by which desmethylimipramine protects cortical norepinephrine. Eur. J. Pharmacol. 102:431–436.

Plotkin JL, Day M, Peterson JD, Xie Z, Kress GJ, Rafalovich I, Kondapalli J, Gertler TS, Flajolet M, Greengard P, Stavarache M, Kaplitt MG, Rosinski J, Chan CS, Surmeier DJ (2014) Impaired TrkB Receptor Signaling Underlies Corticostriatal Dysfunction in Huntington's Disease. Neuron 83:178–188.

Plotkin JL, Surmeier DJ (2015) Corticostriatal synaptic adaptations in Huntington's disease. Curr. Opin. Neurobiol. 33:53–62.

Pouladi MA, Morton AJ, Hayden MR (2013) Choosing an animal model for the study of Huntington's disease. Nat. Rev. Neurosci. 14:708–721.

Pouladi MA, Stanek LM, Xie Y, Franciosi S, Southwell AL, Deng Y, Butland S, Zhang W, Cheng SH, Shihabuddin LS, Hayden MR (2012) Marked differences in neurochemistry and aggregates despite similar behavioural and neuropathological features of Huntington disease in the full-length BACHD and YAC128 mice. Hum. Mol. Genet. 21:2219–2232.

Raamsdonk JM Van, Murphy Z, Slow EJ, Leavitt BR, Hayden MR (2005) Selective degeneration and nuclear localization of mutant huntingtin in the YAC128 mouse model of Huntington disease. Hum. Mol. Genet. 14:3823–3835.

Rasmussen A, Macias R, Yescas P, Ochoa A, Davila G, Alonso E (2000) Huntington Disease in Children: Genotype-Phenotype Correlation. Neuropediatrics 31:190–194.

Raymond LA, André VM, Cepeda C, Gladding CM, Milnerwood AJ, Levine MS (2011) Pathophysiology of Huntington's disease: time-dependent alterations in synaptic and receptor function. Neuroscience 198:252–273.

Rebec GV, Conroy SK, Barton SJ (2006) Hyperactive striatal neurons in symptomatic Huntington R6/2 mice: Variations with behavioral state and repeated ascorbate treatment. Neuroscience 137:327–336.

Reiner A, Albin RL, Anderson KD, D'Amato CJ, Penney JB, Young AB (1988) Differential Loss of Striatal Projection Neurons in Huntington Disease. PNAS 85:5733–5737.

Reiner A, Jiao Y, Mar N Del, Laverghetta AV, Lei W (2003) Differential morphology of pyramidal tract-type and intratelencephalically projecting-type corticostriatal neurons and their intrastriatal terminals in rats. J. Comp. Neurol. 457:420–440.

Reiner A, Shelby E, Wang H, Demarch Z, Deng Y, Guley NH, Hogg V, Roxburgh R, Tippett LJ, Waldvogel HJ, Faull RLM (2013) Striatal parvalbuminergic neurons are lost in Huntington's disease: Implications for dystonia. Mov. Disord. 28:1691–1699.

Reisine TD, Overstreet D, Gale K, Rossor M, Iversen L, Yamamura HI (1980) Benzodiazepine Receptors: The Effect of GABA on Their Characterisitics in Human Brain and Their Alteration in Huntington's Disease. Brain Res. 199:79–88.

Ross CA, Tabrizi SJ (2011) Huntington's Disease: from Molecular Pathogenesis to Clinical Treatment. Lancet Neurol. 10:83–98.

Rothstein JD, Patel S, Regan MR, Haenggeli C, Huang YH, Bergles DE, Jin L, Dykes Hoberg M, Vidensky S, Chung DS, Toan SV, Bruijn LI, Su Z-Z, Gupta P, Fisher PB (2005) Beta-lactam antibiotics offer neuroprotection by increasing glutamate transporter expression. Nature 433:73–77.

Sadikot AF, Parent A, François C (1992) Efferent connections of the centromedian and parafascicular thalamic nuclei in the squirrel monkey: a PHA-L study of subcortical projections. J. Comp. Neurol. 315:137–159.

Santhakumar V, Jones RT, Mody I (2010) Developmental regulation and neuroprotective effects of striatal tonic GABAA currents. Neuroscience 167:644–655.

Scherzinger E, Sittler A, Schweiger K, Heiser V, Lurz R, Hasenbank R, Bates GP, Lehrach H, Wanker EE (1999) Self-assembly of polyglutamine-containing huntingtin fragments into amyloid-like fibrils: implications for Huntington's disease pathology. PNAS 96:4604–4609.

Schousboe A, Sickmann HM, Bak LK, Schousboe I, Jajo FS, Faek SAA, Waagepetersen HS (2011) Neuron-glia interactions in glutamatergic neurotransmission: Roles of oxidative and glycolytic adenosine triphosphate as energy source. J. Neurosci. Res. 89:1926–1934.

Schwarcz R, Foster AC, French ED, Whetsell WO, Köhler C (1984) Excitotoxic models for neurodegenerative disorders. Life Sci. 35:19–32.

Sedvall G, Karlsson P, Lundin A, Anvret M, Suhara T, Halldin C, Farde L (1994) Dopamine D1 receptor number--a sensitive PET marker for early brain degeneration in Huntington's disease. Eur. Arch. Psychiatry Clin. Neurosci. 243:249–255.

Seneca S, Fagnart D, Keymolen K, Lissens W, Hasaerts D, Debulpaep S, Desprechins B, Liebaers I, Meirleir L De (2004) Early onset Huntington disease: A neuronal degeneration syndrome. Eur. J. Pediatr. 163:717–721.

Shehadeh J, Fernandes HB, Mullins Z, M. M, Graham RK, Leavitt BR, Hayden MR, Raymond LA (2006) Striatal neuronal apoptosis is preferentially enhanced by NMDA receptor activation in YAC transgenic mouse model of Huntington disease. Neurobiol. Dis. 21:392–403.

Shelbourne PF, Killeen N, Hevner RF, Johnston HM, Tecott L, Lewandoski M, Ennis M, Ramirez L, Li Z, Iannicola C, Littman DR, Myers RM (1999) A Huntington's disease CAG expansion at the murine Hdh locus is unstable and associated with behavioural abnormalities in mice. Hum. Mol. Genet. 8:763–774.

Shen W, Hamilton SE, Nathanson NM, Surmeier DJ (2005) Cholinergic suppression of KCNQ channel currents enhances excitability of striatal medium spiny neurons. J. Neurosci. 25:7449–7458.

Shuen JA, Chen M, Gloss B, Calakos N (2008) Drd1a-tdTomato BAC transgenic mice for simultaneous visualization of medium spiny neurons in the direct and indirect pathways of the basal ganglia. J. Neurosci. 28:2681–2685.

Sidibé M, Smith Y (1996) Differential synaptic innervation of striatofugal neurones projecting to the internal or external segments of the globus pallidus by thalamic afferents in the squirrel monkey. J. Comp. Neurol. 365:445–465.

Slow EJ, Raamsdonk JM Van, Rogers D, Coleman SH, Graham RK, Deng Y, Oh R, Bissada N, Hossain SM, Yang YZ, Li X-J, Simpson EM, Gutekunst CA, Leavitt BR, Hayden MR (2003) Selective striatal neuronal loss in a YAC128 mouse model of Huntington disease. Hum. Mol. Genet. 12:1555–1567.

Smeal RM, Keefe KA, Wilcox KS (2008) Differences in Excitatory Transmission Between Thalamic and Cortical Afferents to Single Spiny Efferent Neurons of Rat Dorsal Striatum. Eur. J. Neurosci. 28:2041–2052.

Smith A, Bolam JP (1990) The neural network of the basal ganglia as revealed by the study of synaptic connections of identified neurones. Trends Neurosci. 13:259–265.

Smith R, Brundin P, Li JY (2005) Synaptic dysfunction in Huntington's disease: A new perspective. Cell. Mol. Life Sci. 62:1901–1912.

Smith R, Chung H, Rundquist S, Maat-Schieman MLC, Colgan L, Englund E, Liu YJ, Roos RAC, Faull RLM, Brundin P, Li J-Y (2006) Cholinergic neuronal defect without cell loss in Huntington's disease. Hum. Mol. Genet. 15:3119–3131.

Smith Y, Bennett BD, Bolam JP, Parent A, Sadikot AF (1994) Synaptic relationships between dopaminergic afferents and cortical or thalamic input in the sensorimotor territory of the striatum in monkey. J. Comp. Neurol. 344:1–19.

Smith Y, Raju DV, Pare J-F, Sidibé M (2004) The Thalamostriatal System: a Highly Specific Network of the Basal Ganglia Circuitry. Trends Neurosci. 27:520–527.

Sotrel A, Paskevich PA, Kiely DK, Bird ED, Williams RS, Myers RH (1991) Morphometric analysis of the prefrontal cortex in Huntington's disease. Neurology 41:1117–1123.

Spampanato J, Gu X, Yang XW, Mody I (2008) Progressive synaptic pathology of motor cortical neurons in a BAC transgenic mouse model of Huntington's disease. Neuroscience 157:606–620.

Spokes EG (1980) Neurochemical Alterations in Huntington's Chorea. Brain 103:179–210.

Spokes EG, Garrett NJ, Rossor MN, Iversen LL (1980) Distribution of GABA in post-mortem brain tissue from control, psychotic and Huntington's chorea subjects. J. Neurol. Sci. 48:303–313.

Stack EC, Dedeoglu A, Smith KM, Cormier K, Kubilus JK, Bogdanov M, Matson WR, Yang L, Jenkins BG, Luthi-Carter R, Kowall NW, Hersch SM, Beal MF, Ferrante RJ (2007) Neuroprotective effects of synaptic modulation in Huntington's disease R6/2 mice. J. Neurosci. 27:12908–12915.

Steiner H, Gerfen CR (1999) Enkephalin regulates acute D2 dopamine receptor antagonist-induced immediate-early gene expression in striatal neurons. Neuroscience 88:795–810.

Taverna S, Ilijic E, Surmeier DJ (2008) Recurrent collateral connections of striatal medium spiny neurons are disrupted in models of Parkinson's disease. J. Neurosci. 28:5504–5512.

Telenius H, Almqvist E, Kremer B, Spence N, Squitieri F, Nichol K, Grandell U, Starr E, Benjamin C, Castaldo I (1995) Somatic mosaicism in sperm is associated with intergenerational (CAG)n changes in Huntington disease. Hum. Mol. Genet. 4:189–195.

Telenius H, Kremer B, Goldberg YP, Theilmann J, Andrew SE, Zeisler J, Adam S, Greenberg C, Ives EJ, Clarke LA (1994) Somatic and gonadal mosaicism of the Huntington disease gene CAG repeat in brain and sperm. Nat. Genet. 6:409–414.

Tepper JM, Koós T, Wilson CJ (2004) GABAergic microcircuits in the neostriatum. Trends Neurosci. 27:662–669.

Tepper JM, Tecuapetla F, Koós T, Ibáñez-Sandoval O (2010) Heterogeneity and diversity of striatal GABAergic interneurons. Front. Neuroanat. 4:1–18.

Tepper JM, Wilson CJ, Koós T (2008) Feedforward and feedback inhibition in neostriatal GABAergic spiny neurons. Brain Res. Rev. 58:272–281.

The Huntington's Disease Collaborative Research Group (1993) A Novel Gene Containing a Trinucleotide That Is Expanded and Unstable on Huntington's Disease Chromosomes. Cell 72:971–983.

Thomas EA, Coppola G, Tang B, Kuhn A, Kim S, Geschwind DH, Brown TB, Luthi-Carter R, Ehrlich ME (2011) In vivo cell-autonomous transcriptional abnormalities revealed in mice expressing mutant huntingtin in striatal but not cortical neurons. Hum. Mol. Genet. 20:1049–1060.

Thomas TM, Smith Y, Levey AI, Hersch SM (2000) Cortical inputs to m2-immunoreactive striatal interneurons in rat and monkey. Synapse 37:252–261.

Trotti D, Rossi D, Gjesdal O, Levy LM, Racagni G, Danbolt NC, Volterra A (1996) Peroxynitrite inhibits glutamate transporter subtypes. J. Biol. Chem. 271:5976–5979.

Turmaine M, Raza A, Mahal A, Mangiarini L, Bates GP, Davies SW (2000) Nonapoptotic neurodegeneration in a transgenic mouse model of Huntington's disease. PNAS 97:8093–8097.

Velier J, Kim M, Schwarz C, Kim TW, Sapp E, Chase K, Aronin N, DiFiglia M (1998) Wild-type and mutant huntingtins function in vesicle trafficking in the secretory and endocytic pathways. Exp. Neurol. 152:34–40.

Vetter JM, Jehle T, Heinemeyer J, Franz P, Behrens PF, Jackisch R, Landwehrmeyer GB, Feuerstein TJ (2003) Mice transgenic for exon 1 of Huntington's disease: properties of cholinergic and dopaminergic pre-synaptic function in the striatum. J. Neurochem. 85:1054–1063.

Vicini S, Wang JF, Li JH, Zhu WJ, Wang YH, Luo JH, Wolfe BB, Grayson DR (1998) Functional and Pharmacological Differences Between Recombinant N-methyl-D-Aspartate Receptors. J. Neurophysiol. 79:555–566.

Vincent S, Hökfelt T, Christensson I, Terenius L (1982) Immunohistochemical evidence for a dynorphin immunoreactive striato-nigral pathway. Eur. J. Pharmacol. 85:251–252.

Vonsattel J-P, Myers RH, Stevens TJ, Ferrante RJ, Bird ED, Richardson EP (1985) Neuropathological Classification of Huntington's Disease. J. Neuropathol. Exp. Neurol. 44:559–577.

Waelter S, Boeddrich A, Lurz R, Scherzinger E, Lueder G, Lehrach H, Wanker EE (2001) Accumulation of mutant huntingtin fragments in aggresome-like inclusion bodies as a result of insufficient protein degradation. Mol. Biol. Cell 12:1393–1407.

Walker FO (2007) Huntington's disease. Lancet 369:218–228.

Walker FO, Young AB, Penney JB, Dovorini-Zis K, Shoulson I (1984) Benzodiazepine and GABA receptors in early Huntington's disease. Neurology 34:1237–1240.

Wang N, Gray M, Lu X-H, Cantle JP, Holley SM, Greiner E, Gu X, Shirasaki D, Cepeda C, Li Y, Dong H, Levine MS, Yang XW (2014) Neuronal targets for reducing mutant huntingtin expression to ameliorate disease in a mouse model of Huntington's disease. Nat. Med. 20:536–41.

Weeks RA, Piccini P, Harding AE, Brooks DJ (1996) Striatal D1 and D2 dopamine receptor loss in asymptomatic mutation carriers of Huntington's disease. Ann. Neurol. 40:49–54.

Wheeler VC, Auerbach W, White JK, Srinidhi J, Auerbach A, Ryan A, Duyao MP, Vrbanac V, Weaver M, Gusella JF, Joyner AL, MacDonald ME (1998) Length-dependent gametic CAG repeat instability in the Huntington's disease knock-in mouse. Hum. Mol. Genet. 8:115–122.

Wheeler VC, Persichetti F, McNeil SM, Mysore JS, Mysore SS, MacDonald ME, Myers RH, Gusella JF, Wexler NS (2007) Factors associated with HD CAG repeat instability in Huntington disease. J. Med. Genet. 44:695–701.

Wheeler VC, White JK, Gutekunst CA, Vrbanac V, Weaver M, Li XJ, Li SH, Yi H, Vonsattel J-P, Gusella JF, Hersch S, Auerbach W, Joyner AL, MacDonald ME (2000) Long glutamine tracts cause nuclear localization of a novel form of huntingtin in medium spiny striatal neurons in HdhQ92 and HdhQ111 knock-in mice. Hum. Mol. Genet. 9:503–513.

White JK, Auerbach W, Duyao MP, Vonsattel J-P, Gusella JF, Joyner AL, MacDonald ME (1997) Huntingtin is required for neurogenesis and is not impaired by the Huntington's disease CAG expansion. Nat. Genet. 17:404–410.

Wilson CJ (1993) The Generation of Natural Firing Patterns in Neostriatal Neurons. Prog. Brain Res. 99:277–297.

Wojaczyńska-Stanek K, Adamek D, Marszał E, Hoffman-Zacharska D (2006) Huntington disease in a 9-year-old boy: clinical course and neuropathologic examination. J. Child Neurol. 21:1068–1073.

Wójtowicz AM, Dvorzhak A, Semtner M, Grantyn R (2013) Reduced tonic inhibition in striatal output neurons from Huntington mice due to loss of astrocytic GABA release through GAT-3. Front. Neural Circuits 7:1–12.

Wong PT (1985) Abnormalities in glutamatergic mechanisms in human Huntington's disease. Ann. Acad. Med. Singapore 14:147–152.

Wood JD, MacMillan JC, Harper PS, Lowenstein PR, Jones AL (1996) Partial characterisation of murine huntingtin and apparent variations in the subcellular localisation of huntingtin in human, mouse and rat brain. Hum. Mol. Genet. 5:481–487.

Woodman B, Butler R, Landles C, Lupton MK, Tse J, Hockly E, Moffitt H, Sathasivam K, Bates GP (2007) The HdhQ150/Q150 knock-in mouse model of HD and the R6/2 exon 1 model develop comparable and widespread molecular phenotypes. Brain Res. Bull. 72:83–97.

Wu N-P, Cepeda C, Zhuang X, Levine MS (2007) Altered corticostriatal neurotransmission and modulation in dopamine transporter knock-down mice. J. Neurophysiol. 98:423–432.

Xu ZC, Wilson CJ, Emson PC (1991) Restoration of thalamostriatal projections in rat neostriatal grafts: An electron microscopic analysis. J. Comp. Neurol. 303:22–34.

Yamamoto A, Lucas JJ, Hen R (2000) Reversal of neuropathology and motor dysfunction in a conditional model of Huntington's disease. Cell 101:57–66.

Yang D, Wang CE, Zhao B, Li W, Ouyang Z, Liu Z, Yang H, Fan P, O'Neill A, Gu W, Yi H, Li S-H, Lai L, Li X-J (2010) Expression of Huntington's disease protein results in apoptotic neurons in the brains of cloned transgenic pigs. Hum. Mol. Genet. 19:3983–3994.

Yang S-H, Cheng P-H, Banta H, Piotrowska-Nitsche K, Yang J-J, Cheng ECH, Snyder B, Larkin K, Liu J, Orkin J, Fang Z-H, Smith Y, Bachevalier J, Zola SM, Li S-H, Li X-J, Chan AWS (2008) Towards a transgenic model of Huntington's disease in a non-human primate. Nature 453:921–924.

Yizhar O, Fenno LE, Davidson TJ, Mogri M, Deisseroth K (2011) Primer Optogenetics in Neural Systems. Neuron Prim. 71:9–34.

Young AB, Greenamyre JT, Hollingsworth ZR, Albin RL, D'Amato C, Shoulson I, Penney JB (1988) NMDA receptor losses in putamen from patients with Huntington's disease. Science 241:981–983.

Zemanick MC, Strick PL, Dix RD (1991) Direction of transneuronal transport of herpes simplex virus 1 in the primate motor system is strain-dependent. Proc. Natl. Acad. Sci. U. S. A. 88:8048–8051.

Zeron MM, Fernandes HB, Krebs C, Shehadeh J, Wellington CL, Leavitt BR, Baimbridge KG, Hayden MR, Raymond LA (2004) Potentiation of NMDA receptor-mediated excitotoxicity linked with intrinsic apoptotic pathway in YAC transgenic mouse model of Huntington's disease. Mol. Cell. Neurosci. 25:469–479.

Zeron MM, Hansson O, Chen N, Wellington CL, Leavitt BR, Brundin P, Hayden MR, Raymond LA (2002) Increased sensitivity to N-methyl-D-aspartate receptor-mediated excitotoxicity in a mouse model of Huntington's disease. Neuron 33:849–860.

Zuccato C, Cattaneo E (2009) Brain-derived neurotrophic factor in neurodegenerative diseases. Nat. Rev. Neurol. 5:311–322.

Zuccato C, Ciammola A, Rigamonti D, Leavitt BR, Goffredo D, Conti L, MacDonald ME, Friedlander RM, Silani V, Hayden MR, Timmusk T, Sipione S, Cattaneo E (2001) Loss of huntingtin-mediated BDNF gene transcription in Huntington's disease. Science 293:493–498.

Zucker RS (1989) Short-term Synaptic Plasticity. Annu. Rev. Neurosci. 12:13–31.

Zühlke C, Riess O, Bockel B, Lange H, Thies U (1993) Mitotic stability and meiotic variability of the (CAG)n repeat in the Huntington disease gene. Hum. Mol. Genet. 2:2063–2067.